PD-1 checkpoint inhibition in *Leishmania* infection of primary human cells

Dissertation

zur Erlangung des Grades
Doktor der Naturwissenschaften

am Fachbereich Biologie
der Johannes Gutenberg-Universität Mainz

Christodoulos Filippis

geb. am 17.05.1986 in Samos

Mainz, 2018

Dekan

1. Berichterstatter

2. Berichterstatter

Tag der mündlichen Prüfung

During this time the obtained research data and collaborative studies led to the following publications:

Filippis C, Arens K, Noubissi Nzeteu GA, Reichmann G, Waibler Z, Crauwels P and van Zandbergen G. Nivolumab enhances *in vitro* effector functions of PD-1^{+} T-lymphocytes and *Leishmania*-infected human myeloid cells in a host cell-dependent manner. Front Immunol. 2017; 8:1880. PMID: 29312350

Arens K, **Filippis C**, Kleinfelder H, Goetzee A, Reichmann G, Waibler Z, Crauwels P and van Zandbergen G. Anti-TNFα therapeutics differentially affect *Leishmania* infection of human macrophages. 2017, submitted

Summary

In this study we investigated the impact of Programmed Death-1/Programmed Death-1 ligand (PD-1/PD-L) axis in an *in vitro Leishmania major* (*Lm*) infection model consisting of primary human myeloid and lymphoid cells. Two different PD-1 checkpoint inhibitors (IgG1 and IgG4) were used to modulate the PD-1/PD-L interactions in different *Lm*-specific T-cell assay setups. As read-outs, *Lm*-induced T-cell proliferation and *Lm* infection rate in host cells was assessed. First, PD-1 ligand expression was demonstrated on three different *Lm* host cells, namely pro-inflammatory and anti-inflammatory human monocyte-derived macrophages (hMDM1 and hMDM2) and dendritic cells (hMDDC). PD-1 checkpoint blockade had no significant impact on *Lm*-induced T-cell proliferation or *Lm* infection rate in a co-culture of *Lm*-infected host cells together with autologous peripheral blood lymphocytes (PBLs). Using an approach with pre-cultured leucocytes (RESTORE-Assay by Römer et al. 2011) which mimics tissue-like conditions and renders T-cells more responsive to their cognate antigen, revealed a similar picture. Although PD-1 and its ligands were detectable in this assay, no significant differences in T-cell proliferation due to PD-1 checkpoint blockade were observed.

Because PD-1/PD-L interactions are highly prominent during chronic inflammation and antigen stimulation, we investigated an approach using phytohemagglutinin-pre-stimulated PBLs in a co-culture with infected hMDM1, hMDM2 or hMDDC. In this approach, two different PD-1 checkpoint inhibitors (IgG1 and IgG4) increased T-cell effector functions in a similar manner. As a consequence *Lm* infection decreased, being the most pronounced in hMDDC, compared to hMDM1 and hMDM2. Focusing on hMDDC, effects mediated by PD-1 blockade were shown to be partially TNFα dependent. Moreover, treatment with the therapeutic PD-1 checkpoint inhibitor nivolumab specifically enhanced proliferation of $CD4^+$ T-cells, increased expression of the T_H1-specific transcription factor Tbet, T-cell activation markers and cytolytic effector proteins, which at large might be implicated in enhanced parasite killing. In all, our data describe an important role for the PD-1/PD-L axis upon *Lm* infection using a human primary cell system. These data contribute to a better understanding of the PD-1/PD-L-induced T-cell impairment during infectious disease and its influence on immune effector mechanisms to combat *Lm* infection.

Zusammenfassung

Ziel dieser Studie war die Untersuchung des Programmed Death-1/Programmed Death-1 ligand (PD-1/PD-L) Signalwegs innerhalb eines *in vitro Leishmania major* (*Lm*) Infektionsmodells bestehend aus humanen myeloiden und lymphoiden Zellen. Zwei verschiedene Subklassen von PD-1 Checkpoint Inhibitoren (IgG1 und IgG4) wurden zur Modulation des PD-1/PD-L Signalwegs in verschiedenen Versuchsaufbauten getestet, wobei der Einfluss auf *Lm*-induzierte T-Zellproliferation und Infektionsrate bestimmt wurde.

Zunächst wurde gezeigt, dass die PD-1 Liganden auf drei verschiedenen *Lm* Wirtszellen exprimiert werden, und zwar auf pro- und anti-inflammatorischen humanen Monozyten-abgeleiteten Makrophagen (hMDM1 und hMDM2) sowie auf humanen Monozyten-abgeleiteten dendritischen Zellen (hMDDC). PD-1 Checkpoint Blockade hatte keinen Einfluss auf die *Lm*-induzierte T-Zellproliferation oder die Infektionsrate in einer Kokultur bestehend aus *Lm* Wirtszellen und peripheren Blutlymphozyten (PBLs). Ähnliche Ergebnisse wurden mit einem Versuchsaufbau bestehend aus vorkultivierten Leukozyten erzielt (RESTORE-Assay von Römer et al. 2011). Dabei wurden *in-vitro* gewebeartige Bedingungen geschaffen, die T-Zellen stärker auf Antigenstimulation reagieren lassen. Obwohl PD-1 sowie die zugehörigen Liganden messbar waren, hatte PD-1 Checkpoint Blockade keinen signifikanten Effekt auf die T-Zellproliferation.

Da der PD-1/PD-L Signalweg insbesondere bei chronischer Entzündung und Antigenstimulation eine inhibierende Rolle spielt, entwickelten wir einen Versuchsansatz mit Phytohemagglutinin-vorstimulierten PBLs, welche mit infizierten hMDM1, hMDM2 oder hMDDC kokultiviert wurden. In diesem Versuchsansatz verstärkten die oben genannten PD-1 Checkpoint Inhibitoren (IgG1 und IgG4) T-Zell Effektor-Funktionen in ähnlicher Weise. Dadurch verringerte sich die *Lm* Infektion am stärksten in hMDDC im Vergleich zu hMDM1 und hMDM2. In der hMDDC Kokultur wurde gezeigt, dass die Effekte der PD-1-Blockade teilweise TNFα abhängig sind. Des Weiteren verstärkte der therapeutische IgG4 PD-1 Checkpoint Inhibitor Nivolumab spezifisch die $CD4^+$ T-Zellproliferation, die Expression des T_H1-spezifischen Transkriptionsfaktors Tbet, T-Zell Aktivierungsmarker sowie zytolytische Effektor-Proteine, welche womöglich in der Gesamtheit zur Parasitenabtötung beitragen. Insgesamt

zeigen unsere Ergebnisse, dass der PD-1/PD-L Signalweg bei *Lm* Infektion von primären humanen Zellen eine wichtige Rolle spielt. Diese Daten können zu einem besseren Verständnis der durch PD-1/PD-L-induzierten T-Zellbeeinträchtigung während der humanen Leishmaniose beitragen sowie für die Entwicklung von Immuntherapieansätzen genutzt werden.

Table of content

1 Introduction

1.1 Monoclonal antibodies in Immunotherapy

The use of antibodies for immunotherapy was proposed already a century ago by Paul Ehrlich (Ehrlich, 1906). Almost 70 years later, establishment of the hybridoma technology allowed production of monoclonal antibodies (mAbs) with a certain specificity (Köhler and Milstein, 1975). The efficacy of the first therapeutic mouse mAbs in humans was very limited due to their short half-life and high immunogenicity (Nadler et al., 1980; Ritz and Schlossman, 1982). In the following decades, these stability and immunogenicity issues were strongly reduced by the design of chimeric, humanized and fully-human mAbs (Beck et al., 2010). The first approved chimeric mAb for cancer immunotherapy was Rituximab targeting the tumor antigen CD20 on B-cell lymphoma cells (McLaughlin et al., 1998). Since then, therapeutic mAbs directed against several other targets have been approved for several indications in humans with tremendous success.

Therapeutic antibodies are used for neutralization of soluble factors, for targeted killing of specific cells or for blocking receptor-ligand interactions (**Figure 1**; European Medicines Agency, 2017). To achieve these different mechanisms of action, various factors need to be considered: the design of the antibody depending on the IgG subclass, the target affinity of the Fab part and the Fc glycosylation pattern. Together these structural and kinetic features mainly determine effector functions, target specificity and half-life of a therapeutic antibody. Nimmerjahn and colleagues found that the ratio of Fc-binding affinities to activating or inhibiting Fc gamma receptors (A/I ratio) can be used to determine Fc effector functions of a mAb (Nimmerjahn and Ravetch, 2008). The IgG1 subclass, which has a high A/I ratio, is widely used for the generation of therapeutic antibodies when Fc-mediated effector functions (antibody dependent cellular cytotoxicity, complement dependent cytotoxicity or antibody dependent cellular phagocytosis) are required to kill a targeted cell. For blocking receptor-ligand interactions, IgG4 is the IgG subclass of choice due to its low interaction with activating Fc gamma receptors on several immune cells (Bruhns et al., 2009; Nimmerjahn et al., 2015). Additional glyco-engineering allows further optimization of mAb effector functions, but *in vivo* studies analyzing the effects of these changes are still incomplete or lacking

(Sha et al., 2016). An overview of mAb effector mechanisms is illustrated in Figure 1.

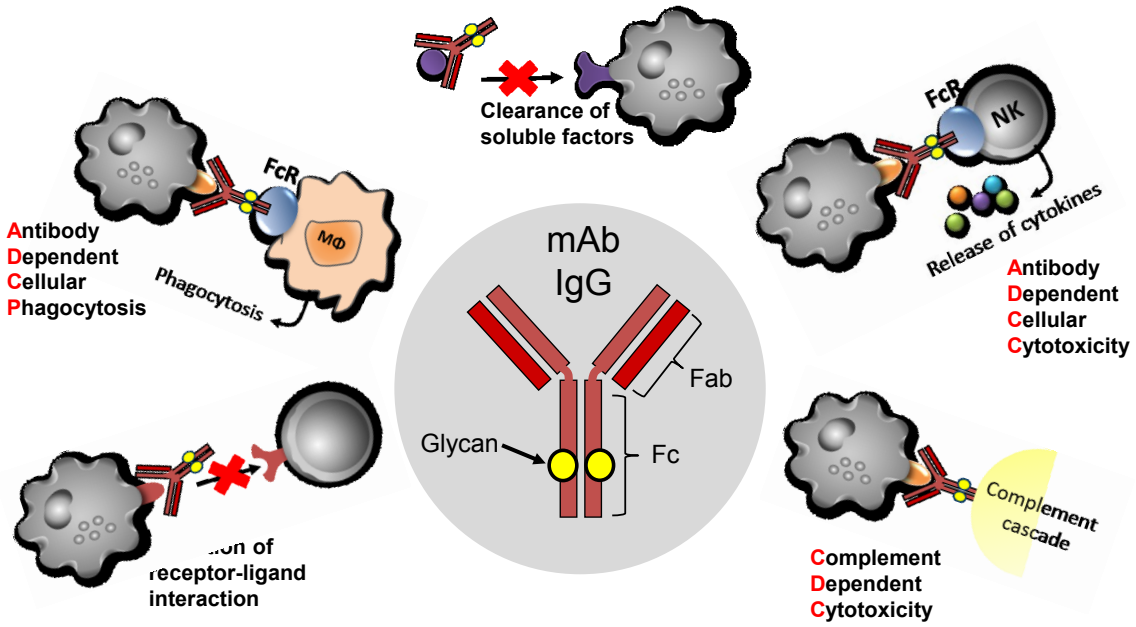

Figure 1: Overview of the different effector mechanisms of therapeutic monoclonal antibodies. Monoclonal antibodies (mAbs) that are used for therapy belong to the immunoglobulin g (IgG) class. The two variable Fab (Fragment antigen binding) parts contain the antigen binding site, whereas the Fc (fragment crystallizable region) part interacts with different Fcγ receptors (FcR) thereby mediating immune effector functions. A mAb targeted cell can be killed e.g. by ADCP (antibody dependent cellular phagocytosis) via phagocytosis by macrophages (Mϕ). In ADCC (antibody dependent cellular cytotoxicity) targeted cells are killed by natural killer cells (NK). In CDC (complement dependent cytotoxicity), the activated complement cascade kills the targeted cell. Additionally therapeutic mAbs are used for blocking of receptor-ligand interactions or neutralization of soluble factors. Fc-effector functions differ between IgG subclasses (IgG1, IgG2, IgG3 and IgG4) and strongly depend on the glycan pattern of the Fc-part.

An important class of monoclonal antibodies which is increasingly used in immunotherapy are the so called immune checkpoint inhibitors. These mAbs target immune checkpoints such as co-stimulatory molecules (CD27, CD40, OX40, GITR, etc.) or co-inhibitory molecules (PD-1, CTLA-4, LAG-3, KIR, etc.) on immune cells e.g. T-cells. By blocking immune checkpoints, the immune response can be boosted (e.g. in cancer therapy) or dampened (e.g. in autoimmune diseases) (Webster, 2014). The first approved IgG4 checkpoint inhibitor ipilimumab from Bristol-Myers Squibb (approved in 2011), which targets CTLA-4, showed very promising results in advanced melanoma patients, although at the expense of strong side effects. In that regard

pembrolizumab and nivolumab, two IgG4 anti-PD-1 mAbs approved in 2015 for therapy of melanoma and other carcinomas, were superior as they were more effective and well-tolerated (Hodi et al., 2010; Topalian et al., 2012). Since then, especially checkpoint inhibitors targeting the PD-1/PD-1 ligand (PD-1/PD-L) axis are developed and approved.

1.2 PD-1/PD-L immune checkpoint

1.2.1 Structure, expression, function and signal transduction

Programmed-Death 1 (PD-1, CD279) was initially identified as an upregulated gene in two murine lymphoid cell lines (2B4.11 and LyD9), which underwent stimulation-induced programmed cell death. Sequence analysis revealed that PD-1 belongs to the immunoglobulin family (Ishida et al., 1992). The 288 amino acid long protein has a molecular weight of 50-55 kDa, contains an immunoreceptor tyrosine-based switch motif (ITSM) plus an immunoreceptor tyrosine-based inhibition motif (ITIM) and is lowly expressed on B-cells, T-cells and myeloid-derived cells. PD-1 expression is increased after T-cell activation (Agata et al., 1996; Boussiotis et al., 2014). The first indicative that PD-1 serves as negative regulator of immune responses arose from PD-1 knockout mice that developed a lupus-like autoimmune disease (Nishimura et al., 1999). Identification of the PD-1 ligands PD-L1 (B7H1, CD274) and PD-L2 (B7DC, CD273), both members of the immune-regulatory B7 family, allowed further functional investigations regarding PD-1/PD-L pathway. Upon interaction of PD-1 with one of its ligands, stimulation-induced T-cell proliferation is inhibited and cytokine release is reduced (Freeman et al., 2000; Latchman et al., 2001). Whereas PD-L2 expression is mostly restricted to professional antigen presenting cells e.g. dendritic cells and macrophages, PD-L1 is broadly expressed on diverse (non-) hematopoietic cells (Okazaki and Honjo, 2006; Keir et al., 2008). PD-L1 has CD80, expressed on antigen presenting cells, as additional binding partner and PD-L2 also binds to the repulsive guidance molecule B (RGMb), which is expressed e.g. on alveolar epithelial cells (Xiao et al., 2014) **(Figure 2)**.

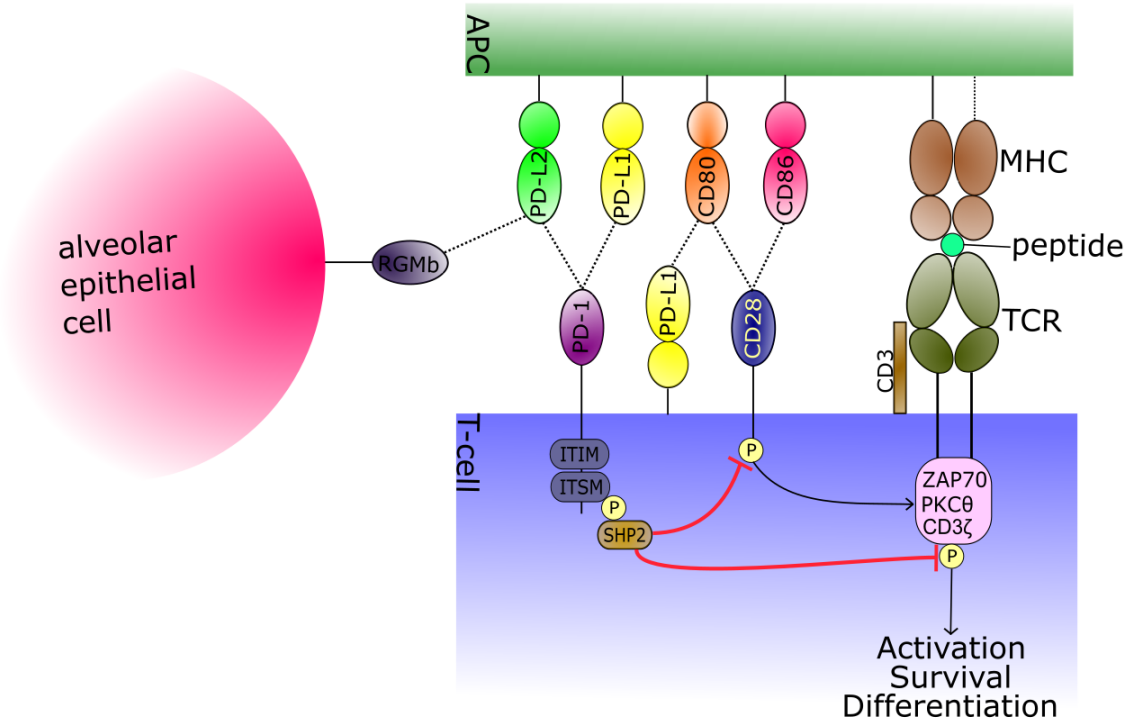

Figure 2: PD-1 signaling in T-cells and possible interactions of the PD-1/PD-L axis. For an adequate activation, T-cells require at least a primary (MHC-peptide-TCR signal) and secondary stimulatory signal (CD28-CD80 or CD28-CD86) mediated by an antigen presenting cell (APC), e.g. a macrophage or dendritic cell. The PD-1/PD-Ligand pathway interferes with these stimulatory signals. Upon interaction of PD-1 with PD-L1 or PD-L2, phosphorylation of the cytoplasmic tail of PD-1 leads to recruitment of SHP2 phosphatases. SHP2 dephosphorylates CD28 and the TCR signaling molecules ZAP70, PKCθ and CD3ζ and thereby inhibits downstream signaling important for T-cell activation, survival or differentiation. PD-L1 additionally competes with CD28 for CD80 binding. PD-L2 can interact with RGMb on alveolar epithelial cells, which is important for respiratory tolerance. **Modified after Freeman (2008), Larsson et al. (2013) and Xiao et al. (2014)**.

To date there is no information regarding differences in signal transduction between the PD-1/PD-L1 and PD-1/PD-L2 interaction, although binding kinetics strongly differ between both PD-1 ligands (Youngnak et al., 2003; Lázár-Molnár et al., 2008; Ghiotto et al., 2010). Engagement of PD-1 on T-cells to either of its ligands results in tyrosine phosphorylation of the cytoplasmic domain and recruitment of the SHP2 phosphatases. The resulting dephosphorylation of the TCR signaling molecules ZAP70, PKCθ and CD3ζ attenuates the TCR/CD28 signaling (Freeman, 2008) (**Figure 2**). Recently Hui and colleagues showed that the SHP2 phosphatase primarily inactivates CD28 and not TCR signaling (Hui et al., 2017). Also there is some evidence for reverse signaling via PD-L1 or PD-L2 (Kuipers et al., 2006; Park et al., 2010; Ishibashi et al., 2015).

Approximately 90% of CD3/CD28 receptor-regulated transcripts are reduced fivefold or more by PD-1/PD-L engagement showing that the PD-1/PD-L pathway is a very effective negative regulator of T-cell activation (Parry et al., 2005; Riley, 2009).

1.2.2 Role in tolerance and autoimmunity

Studies from murine mouse models support the notion that the PD-1/PD-L pathway is an important mediator of immune tolerance (Zamani et al., 2016). During the central tolerance process, PD-1, PD-L1 and to a lesser extent PD-L2 are expressed on cells of the thymus (Brown et al., 2003; Liang et al., 2003). $CD4^-CD8^-$ thymocytes undergoing TCRβ rearrangement increase their PD-1 expression (Nishimura et al., 1996). The resulting PD-1/PD-L1 signaling inhibits positive selection during transition from $CD4^-CD8^-$ to $CD4^+CD8^+$ T-cells (Nishimura et al., 2000). PD-1 knockout mice have a higher number of $CD4^-CD8^-$ T-cells in their peripheral blood, which supports the role of the PD-1/PD-L pathway as important regulator during negative selection (Blank et al., 2003). Besides central tolerance, the PD-1/PD-L pathway plays a critical role in tissue tolerance (Rodig et al., 2003) and peripheral tolerance (Nishimura and Honjo, 2001). Self-reactive T cells that escaped from the thymus are inactivated or deleted via T-cell intrinsic (e.g. anergy or apoptosis) or extrinsic (tolerogenic dendritic cells or regulatory T-cells) mechanisms (Walker and Abbas, 2002). Immature dendritic cells can induce tolerance in $CD8^+$ T-cells via PD-L1 and PD-L2 (Probst et al., 2005). Evidence that the PD-1/PD-L pathway has important tasks in maintaining peripheral tolerance comes from observations in immune-privileged sites like the placenta, which highly expresses PD-L1 (Sharpe et al., 2007; Veras et al., 2017). Blocking the PD-1 or PD-L1 interaction increased the rate of abortions due to enhanced T-cell invasion in the placenta of pregnant mice. Also embryo resorption was increased and litter size reduced, which might be due to lower regulatory T-cell (Treg) numbers (Guleria et al., 2005). With regard to Tregs, PD-L1 was shown to promote the generation of inducible Tregs, thereby suppressing effector T-cells. This favors immune tolerance (Francisco et al., 2009).

Dysregulation of the PD-1 expression and/or its ligands is associated with a vast number of autoimmune diseases (Zamani et al., 2016). Modulation of the PD-1/PD-L axis in murine Type I diabetes yielded conflicting results depending

on the used mouse model and the experimental strategy (Subudhi et al., 2004; Wang et al., 2008; Kadri et al., 2012). A general observation made in several murine autoimmune disease models is that the PD-1/PD-L1 axis delays disease progression and severity and is important for Treg development and function. Interestingly in humans, several single nucleotide polymorphisms (SNP) in the PD-1 gene are associated with a higher prevalence to develop systemic lupus erythematosus, ankylosing spondylitis, rheumatoid arthritis or Type I diabetes (Zamani et al., 2016). The most interesting SNP thereby is PD-1.3A/G, where the binding site for one PD-1 transcription factor namely RUNX1 is disrupted. Corresponding, this SNP correlated with a lower PD-1 expression in systemic lupus erythematosus patients (Kristjansdottir et al., 2010).

1.2.3 Role in infection and cancer

There is accumulating evidence that during chronic infections and cancer the PD-1/PD-L axis plays an important role in the stepwise deterioration of effector T-cell functions (Wherry and Kurachi, 2015). The inhibitory role of the PD-1/PD-L axis during viral infection was extensively investigated in the lymphocytic choriomeningitis virus (LCMV) mouse model. In acute LCMV infection, PD-1 is transiently expressed on virus-specific $CD8^+$ T-cells during the effector phase but rapidly downregulated after infection (Barber et al., 2006). In contrast, during chronic LCMV infection, virus-specific $CD8^+$ T-cells show a sustained expression of PD-1 (and other co-inhibitory molecules) leading to a dysfunctional state called T-cell exhaustion **(see Figure 3)**. This exhaustion occurs in a hierarchical manner, where T-cells gradually lose their effector functions until they undergo apoptosis (Wherry et al., 2007; Blackburn et al., 2009). It became apparent that persistent antigen stimulation is a main driver of T-cell exhaustion. By blocking the PD-1/PD-L interaction, it was demonstrated that effector functions of exhausted T-cells can be partially restored, thereby leading to reduced viral titers (Barber et al., 2006).

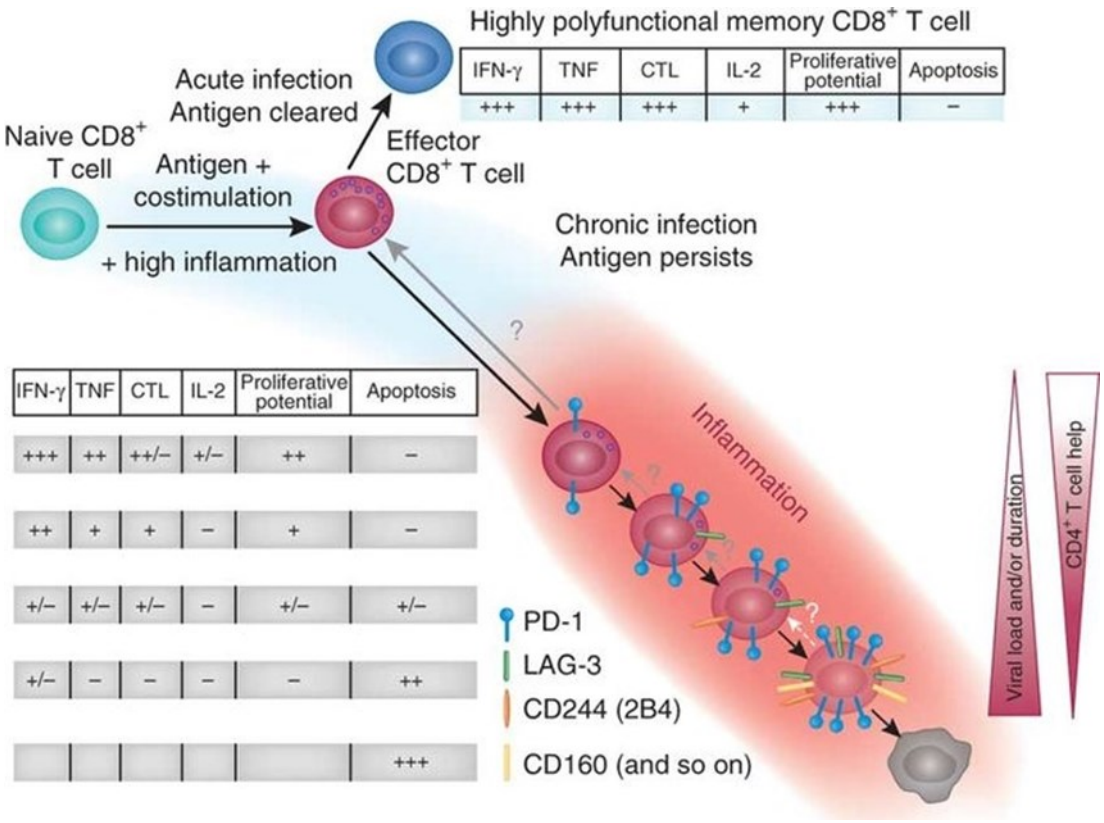

Figure 3: Progressive T-cell exhaustion in chronic LCMV infection.

Acute LCMV infection induces priming of naive T-cells (antigen + co-stimulation + inflammation), which differentiate into LCMV-specific effector T-cells. Clearance of infection and antigen entails that a subset of effector T-cells differentiate into highly polyfunctional and long-living memory T-cells, which are able to rapidly respond by cytokine production and proliferation on reoccurrence of LCMV antigen (top). During chronic infection (bottom), effector T-cells are unable to sufficiently reduce infection or antigen load. As inflammation, viral load and antigen persists, effector T-cells progressively become dysfunctional thereby losing effector functions and other properties. This process termed T-cell exhaustion is accompanied by a progressive increase of several inhibitory receptors (PD-1, LAG-3, 2B4, CD160 and more). Ultimately, virus-specific T-cells can be completely eliminated, if inflammation persists. Severity of T-cell exhaustion correlates with high inhibitory receptor expression, high viral load and loss of $CD4^+$ T-cell help. Activity of each property is illustrated on a scale from high (+++) to low (-); 'CTL' indicates cytotoxic potential. **Adapted from Wherry (2011)**.

Virus-specific exhausted $CD8^+$ T-cells were observed also in HIV (Freeman et al., 2006; Hoffmann et al., 2016), HCV (Radziewicz et al., 2007) or HBV (Ye et al., 2015). Subsequently it became evident that T-cell exhaustion occurs also in chronic infectious diseases caused by bacteria (Shen et al., 2016), fungi (Spec et al., 2016), protozoan parasites (Hernández-Ruiz et al., 2010; Esch et al., 2013; Gautam et al., 2014) and malignancies like cancer (Speiser, 2012).

Especially in cancer the immune evading effects of the PD-1/PD-L1 pathway were intensively studied. More than a decade ago a high PD-L1 expression was demonstrated on several malignant carcinomas, e.g. breast, lung, colon carcinoma or melanoma (Brown et al., 2003; Konishi et al., 2004). Several clinical studies have reported that PD-L1 overexpression correlates with poor prognosis for several tumor types (e.g. renal-cell carcinoma, esophageal cancer, gastric cancer, and others) and reduced tumor infiltrating T-cells (Iwai et al., 2017). Blocking the PD-1/PD-L1 interaction effectively reduced tumor burden in a cancer mouse model (Iwai et al., 2002; Iwai et al., 2005). Also tumor-specific human T-cell effector functions were enhanced *in vitro* by PD-1/PD-L1 blockade (Blank et al., 2006). These and other studies paved the way for design of the therapeutic PD-1/PD-L1 blocking antibodies for immunotherapy of cancer.

1.2.4 PD-1 checkpoint inhibition as therapeutic approach

The anti-PD-1 mAb nivolumab was designed as fully humanized IgG4. The IgG4 subtype minimizes CDC as well as ADCC. Additionally, a serine-to proline substitution at position 228 in the hinge region almost completely ablates ADCC activity towards PD-1^+ T-cells and prevents Fab arm exchange (Wang et al., 2014). First-in-man studies (phase I) with nivolumab started in 2006 in the United States and in 2009 in Japan. Treatment with nivolumab resulted in cumulative response rates between 18 % for non-small cell lung carcinoma (NSCLC) and 28 % in case of melanoma (Iwai et al., 2017). Compared to the standard-of-care chemotherapy with docetaxel, nivolumab was better tolerated, and superior in terms of overall survival, progression free survival, duration of response and response rate in NSCLC or melanoma patients (Nishijima et al., 2017; Ramos-Esquivel et al., 2017). In NSCLC, PD-L1 expression on tumor tissue is a predictive biomarker associated with a higher overall response rate by PD-1/PD-L1 blockade (Mino-Kenudson, 2016).

Nivolumab and pembrolizumab were the first PD-1 checkpoint inhibitors that gained marketing authorization by the FDA (2014) and the EMA (2015). Nivolumab was initially used for the treatment of NSCLC, whereas pembrolizumab was used for metastatic melanoma. Since then, indications for both mAbs are continually expanded. Recently, PD-L1 checkpoint inhibitors, like e.g. atezolizumab, are increasingly approved for immunotherapy because they

are thought to have fewer side effects compared to PD-1 checkpoint inhibitors. As they are designed as IgG1 subclass, they additionally can induce ADCC or CDC against the PD-L1 harboring cancer cell thereby enhancing efficacy. A systematic comparison of PD-L1 and PD-1 checkpoint inhibitors in 5744 NSCLC patients, did not reveal significant differences regarding toxicity or efficacy (Pillai et al., 2017).

To date, there are five therapeutic monoclonal antibodies targeting the PD-1/PD-L axis approved by the FDA and EMA (except durvalumab) for cancer immunotherapy (**Table 1**).

Table 1: Therapeutic monoclonal antibodies targeting the PD-1/PD-L axis approved for cancer immunotherapy.

(European Medicines Agency, 2017; U.S. Food & Drug Administration, 2017).

	Anti-PD-L1			Anti-PD-1	
Name:	Avelumab	Durvalumab	Atezolizumab	Nivolumab	Pembrolizumab
IgG class:	Fully human IgG1,λ	Fully human IgG1, κ	Humanized IgG1, κ	Fully human IgG4, κ	humanized IgG4, κ
Company:	Merck Sharp & Dohme Limited	Astrazeneca UK	Genentech (Roche)	Bristol-Myers Squibb	Merck & Co., Inc.
Approval:	FDA EMA	FDA	FDA EMA	FDA EMA	FDA EMA
Indications:	Metastatic Merkel cell carcinoma	Metastatic urothelial carcinoma	Metastatic non-small cell lung cancer Metastatic urothelial carcinoma	Carcinoma; non-small-cell lung carcinoma; Head and Neck Cancer, renal cell carcinoma Hodgkin's lymphoma melanoma; metastatic urothelial carcinoma	Melanoma, Lung Cancer, Head and Neck Cancer, Classical Hodgkin Lymphoma, Urothelial Carcinoma, Microsatellite Instability-High (MSI-H) Cancer

PD-1/PD-L checkpoint inhibitors clearly have the potential to become blockbuster drugs. This is the reason why several drugs targeting the PD-1/PD-L pathway are still developed or in clinical trials (REGN2810, AMP224, MEDI0680, PDR001, pidilizumab) (Alsaab et al., 2017). Not all of them are IgG4 mAbs; Pidilizumab e.g. is a humanized anti-PD-1 IgG1 mAb. Thus, its Fc-mediated effector functions might differ in comparison to anti-PD-1 IgG4 mAbs. In patient studies slight differences between the two approved anti-PD-1 IgG4 mAbs pembrolizumab and nivolumab were observed. NSCLC patients treated with pembrolizumab had a higher incidence to develop grade 3 adverse events compared to patients treated with nivolumab (Peng et al., 2017). This could be also related to biochemical differences (e.g. glycosylation pattern) of the Fc-part between both antibodies. Tumor mouse model studies

indicate that even low engagement of FcγRs by anti-PD-1 mAbs reduces their anti-tumor efficacy (Dahan et al., 2015). Therefore, comparative studies of PD-1 checkpoint inhibitors are required to evaluate Fc-dependent differences in terms of safety and efficacy.

1.3 Role of macrophages and dendritic cells in T-cell activation

Macrophages (MFs) (Greek: “big eaters”) and dendritic cells (DCs) are a heterogeneous class of immune cells that belong to the mononuclear phagocyte system as part of innate immunity. MFs reside in all tissues of the body and have tissue-specific functions and designations, e.g. Kupffer cells (liver) or microglia (brain and spinal cord). Many MFs are derived from monocytes and are large vacuolar professional antigen-presenting cells which phagocytose and digest cell debris, apoptotic cells, foreign substances, microbes and degenerated cells (Guilliams et al., 2014). Classical activation of monocytes by IFNγ (+LPS), TNFα or GM-CSF leads to differentiation towards pro-inflammatory Type I macrophages (M1). M1 are IL-12^{high}IL-10^{low} cytokine producing cells that are specialized in killing intracellular pathogens by producing microbicidal free radicals such as nitric oxide (NO) or/and reactive oxygen species (ROS). M1 participate in the polarization towards a pro-inflammatory T-helper I immunity (Mantovani et al., 2004; Verreck et al., 2004). In contrast, stimulation of monocytes with IL-4/IL-13, IC/TLR/IL-1R ligand, IL-10 or M-CSF promotes the differentiation program towards anti-inflammatory Type II macrophages (M2). These cells produce IL-10 and have important roles in wound healing, tissue repair and angiogenesis (presumably mediated by arginases). Furthermore M2 participate in the induction of Tregs and the anti-inflammatory T-helper 2 response, thereby favoring a humoral immune response (Mantovani et al., 2004; Verreck et al., 2004; Stechmiller et al., 2005).
Like MFs, DCs come in different flavors and are present in all tissues were they are constantly take up material by phagocytosis and pinocytosis. Upon uptake and processing of e.g. an infectious agent, DCs maturate and travel to the lymph node, where they present the foreign antigens to the cognate T-cells. In contrast to MFs, DCs are up to 100 - 1000-fold more potent in activating naïve and memory T-cells (Chung et al., 2004; Banchereau and Palucka, 2005; Kubach et al., 2005). *In vitro* a pure population of immature DCs can be generated by stimulation of monocytes (or CD34^{+} hematopoietic precursor

cells) with GM-CSF and IL-4 (Sallusto, 1994; Caux, 1996). These monocyte-derived DCs resemble *in vivo* interstitial DCs, which after maturation promote a T-helper 1 response. To date, human monocyte-derived DCs are the only pure source of human DCs which can be produced in GMP quality. Therefore these cells are investigated as cancer vaccines to boost tumor-specific T-cell immunity (Serbina et al., 2003; Banchereau and Palucka, 2005; Hubo et al., 2013).

Macrophages and dendritic cells are both host cells for *Leishmania* parasites. Differentiation and activation of these host cells have important implications for the outcome of leishmaniasis (Liu and Uzonna, 2012).

1.4 Leishmaniasis

1.4.1 Epidemiology and clinical manifestations

The parasitic disease leishmaniasis is still endemic in 97 countries, causing up to 30,000 deaths annually, a number potentially increasing due to climate changes and global warming. However, up to 90% of all new cases occur in just 13 countries, which are Afghanistan, Algeria, Bangladesh, Bolivia, Brazil, Columbia, Ethiopia, India, Iran, Peru, South Sudan, Sudan and Syria (World Health Organization, 2017). To date there are 18 known human pathogenic *Leishmania* strains causing different clinical manifestations of leishmaniasis. Two main clinical manifestations of leishmaniasis can be distinguished, the cutaneous and visceral form. The most common form, cutaneous leishmaniasis (CL), occurs in three different sub-forms: localized cutaneous leishmaniasis (LCL), diffuse cutaneous leishmaniasis (DCL) and mucocutaneous leishmaniasis (MCL). LCL, caused e.g. by *L. major*, leads to skin lesions mainly ulcers on exposed body parts. In contrast to LCL, ulceration is absent in DCL, but multiple slowly progressing nodules on the complete body characterize this disease form, which is caused e.g. by *L. aethiopica*. The mucocutaneous form, caused by e.g. *L. brasiliensis*, attaints and destroys the mucosa in mouth, nose and throat. Visceral leishmaniasis (VL), caused e.g. by *L. donovani*, affects the internal organs and is the most severe form leading to death if untreated (Steverding, 2017).

1.4.2 Transmission and parasite life cycle

Leishmania parasites have a biphasic life cycle, one phase inside the gut of the phlebotomine sand fly and one phase in phagocytes of mammals **(Figure 4)**. Upon blood meal of the infected *Phlebotomus* sand fly, an infectious inoculum containing metacyclic flagellated *Leishmania* promastigotes is transferred to its mammalian host. There the parasites are taken up by different phagocytes (Kaye and Scott, 2011). Shortly after *L. major* infection, polymorphonuclear neutrophil granulocytes (PMNs) are the main infected cell population. By "hiding" inside apoptotic PMNs, the parasites are silently taken up by MFs, without inducing overwhelming inflammation (van Zandbergen et al., 2004).

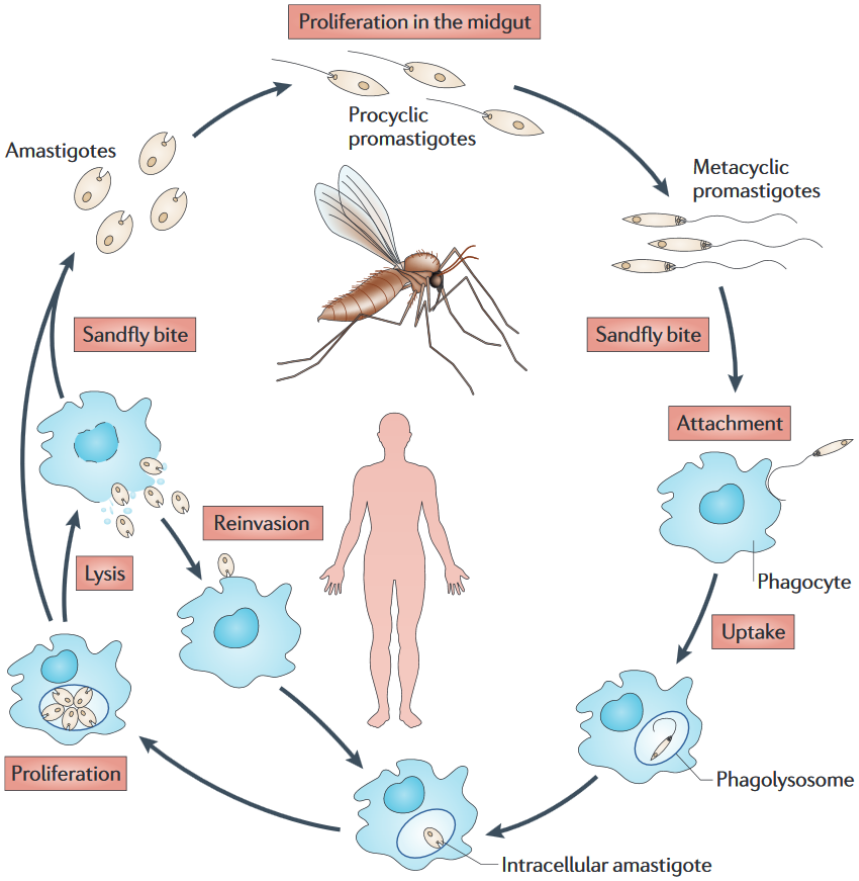

Figure 4: The biphasic life cycle of *Leishmania* parasites.
In the gut of the infected sand fly flagellated procyclic *Leishmania* promastigotes differentiate into infective metacyclic promastigotes. Upon sand fly blood meal these promastigotes are transferred to their mammalian host where they are taken up by phagocytes such as neutrophils, macrophages, monocytes or dendritic cells. Inside the phagocytes they differentiate into the egg-shaped non-flagellated multiplying amastigote form. Amastigotes proliferate until lysis of their host cell. Afterwards they infect new phagocytes or are taken up by the bite of the sand fly, where they transform back into the promastigote form. **Adapted from Kaye and Scott (2011).**

Inside the phagolysosome of the MF, promastigotes transform into the multiplying amastigote form, which is a prerequisite to establish a productive infection. In murine experimental leishmaniasis, DCs also serve as host for *Leishmania* parasites. In contrast to MF, parasite uptake is slower, less efficient and parasite replication as well as amastigote transformation is limited (Stebut and Tenzer, 2017). We showed *in vitro* that *L. major* amastigote development and replication also occurs in human DCs (Crauwels, 2015). Upon cell lysis, amastigotes can either infect new phagocytes or are taken up by the *Phlebotomus* sand fly, where they transform back into the promastigote form (Kaye and Scott, 2011). The *Leishmania* strain, host and other factors determine which clinical manifestation of the disease leishmaniasis occurs.

In this work we used an experimental cutaneous human leishmaniasis cell model consisting of the parasite *L. major* and primary human cells. *In vitro*, *Leishmania* host cells were infected with stationary phase *L. major* promastigotes. The latter are generated *in vitro,* are highly virulent and comprise metacyclic promastigotes, which are also transferred by the bite of the infected sand fly to their mammalian host (Sacks and Perkins, 1984; da Silva and Sacks, 1987).

1.4.3 Therapy and drug resistances

The treatment strategies for leishmaniasis strongly differ depending on the *Leishmania* strain, the clinical presentation, the immune status of the patient, potential co-infections, the place of contagion and the clinician. Old World CL (caused by e.g. *L. major* or *L. tropica*) lesions can heal spontaneously even without therapy, but this can take up to one year and leaves behind ugly scars. Therefore local therapies (thermotherapy, cryotherapy, paromomycin ointment, local infiltration with antimonials) are carried out in mild cases, because they have less systemic toxicity. Complex cases are systemically treated e.g. with azole drugs, miltefosine, antimonials or amphotericin B formulations. New World CL (caused by e.g. *L. brasiliensis* or *L. mexicana*) patients require toxic systemic treatments (mainly pentavalent antimonials), because the disease can spread into the mucosa and lead to severe disfigurement (Monge-Maillo and López-Vélez, 2013a). VL patients also require systemic therapy (e.g. amphotericin B formulations, miltefosine or paromomycin). Because drug

resistance development is especially high in VL, drugs are used in combinations to encourage a cure (Monge-Maillo and López-Vélez, 2013b).

Despite optimal administration of treatments, there is increasing evidence for drug resistance in several *Leishmania* strains. A reason for this is the intensified use of only four main chemotherapeutic drugs: pentavalent antimonials, miltefosine, amphotericin B and paromomycin. Pentavalent antimonials are used for leishmaniasis treatment for almost 80 years. Whereas in the early 20th century, VL cure rates were greater than 90% with this drug, the treatment failure rate for VL reached 65% in India at the end of the century, although the drug dosage was doubled (Hefnawy et al., 2017). The efficacy of miltefosine is constantly decreasing, too. Amphotericin B and paromomycin are still efficient but experimental studies indicate that these drugs could also become ineffective, even in multi-drug approaches (García-Hernández et al., 2012). Therefore alternative treatment options are investigated aside from chemotherapy including (dendritic cell-based) vaccination or immunotherapy targeting immune checkpoints (Bagirova et al., 2016; Kumar et al., 2017).

1.5 Adaptive immunity and T-cell impairment during leishmaniasis

Based on experimental *L. major* mouse models, it is widely accepted that disease susceptibility is associated with IL-10 and IL-4 producing T-helper 2 (T_H2) cells, whereas a strong T-helper 1(T_H1)-mediated IFNγ production promotes healing by inducing leishmanicidal nitric oxide in the *Leishmania*-harboring cells (Sacks and Noben-Trauth, 2002). In human leishmaniasis this T_H1/T_H2 dichotomy does not always hold true and the resulting T-cell response strongly depends on the *Leishmania* strain and the immune status of the host (Baratta-Masini, 2007; Tripathi et al., 2007; Castellano et al., 2009). In addition, *in vitro* data from cutaneous leishmaniasis patients show parasite control to be mediated rather by IFNγ-induced reactive oxygen species (ROS) then by nitric oxide (Novais et al., 2014; Carneiro et al., 2016). As already mentioned, macrophages and dendritic cells, the final host cells of *Leishmania* parasites, play an important role in the initiation of the adaptive immune response. Several *in vitro* studies demonstrated *Leishmania*-naive healthy human donors to possess a natural T-cell response against live parasites, antigen extracts or specific components of different *Leishmania* strains (Kemp et al., 1992; Russo et al., 1998; Jensen et al., 2001; Pompeu et al., 2001; Bourreau et al., 2002;

Ettinger and Wilson, 2008; Crauwels et al., 2015). This early MHC class II dependent T-cell response was shown to dampen *Leishmania* parasite burden in autologous human macrophage/T-cell co-cultures (Crauwels, 2015). The activation of $CD8^+$ and $CD4^+$ T-cells is regulated by various signals such as co-stimulatory molecules, which can either positively or negatively influence T-cell priming. Intracellular protozoan parasites of the genus *Leishmania* or *Trypanosoma* can disturb those signals thereby impairing parasite specific T-cell effector functions. Three mechanisms of T-cell impairment during parasitic diseases are described: T-cell anergy, T-cell exhaustion and T-cell apoptosis (**Figure 5**; Rodrigues et al., 2014).

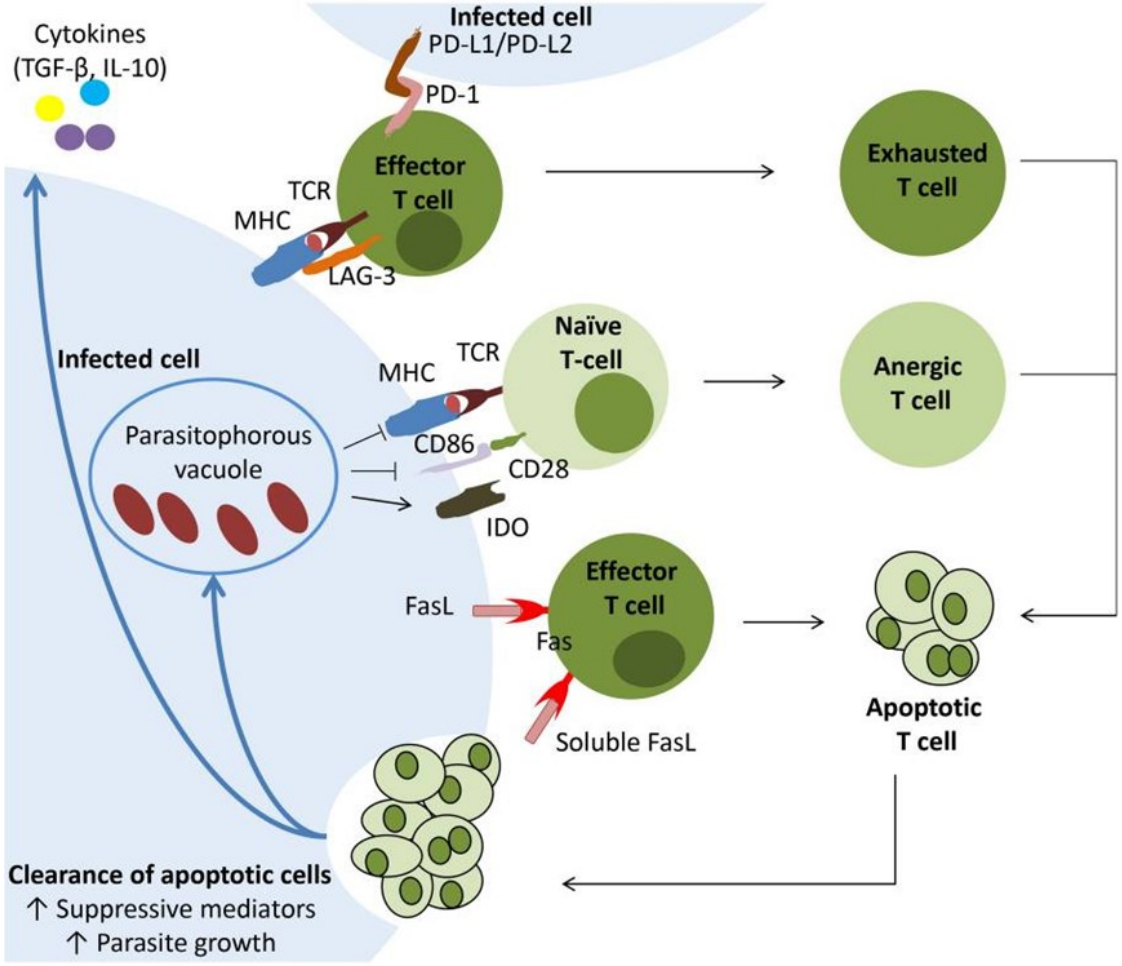

Figure 5: Intracellular protozoan parasites can induce different forms of T-cell dysfunction.

Antigen persistence and inhibitory T-cell receptors (PD-1/PD-L, LAG-3) induce T-cell exhaustion. Parasite-induced inhibition of antigen presentation and co-stimulation, together with tryptophan catabolizing enzymes (as IDO), may render naïve T-cells anergic. Eventually T-cells undergo programmed cell death by FAS/FAS-L interactions or by terminal differentiation. Apoptotic T-cells that are cleared by the (infected) phagocytes, release suppressive mediators that favor parasite survival. **Adapted from Rodrigues et al. (2014).**

T-cell anergy is achieved e.g. by reduced antigen presentation and reduced co-stimulation during the initial priming of naïve T-cells. This results in low T-cell proliferation, defective differentiation, low effector functions and eventually apoptosis. T-cell exhaustion occurs during the effector phase and is induced by e.g. antigen persistence, chronic activation and anti-inflammatory cytokines like IL-10 or TGF-β **(Figure 5)**. Characteristic for this type of impairment is the progressive loss of T-cell effector functions and increased expression of inhibitory receptors like TIM-3, LAG-3 or PD-1 (Rodrigues et al., 2014).

As already mentioned the role of the PD-1/PD-L axis in T-cell exhaustion, a functional impairment of T-cells, is very well studied in the field of cancer and in chronic viral infections (**see chapter 1.2.3**). Recent publications indicate that the PD-1/PD-L pathway may play a similar role during *Leishmania* infection. In the canine and mouse model of VL, PD-1/PD-L-mediated T-cell exhaustion together with an impaired phagocyte function was observed. Blocking the PD-1/PD-L interaction in these models partially rescued effector functions of exhausted T-cells, which resulted in a lower parasite burden (Joshi et al., 2009; Esch et al., 2013). Wild type mice infected with a transgenic *Leishmania* strain inducing chronic cutaneous leishmaniasis showed a high number of exhausted PD-1$^+$CD4$^+$T-cells. PD-1 blockade restored CD4$^+$ T-cell functionality and led to healing (Mou et al., 2013). In splenic aspirates of visceral leishmaniasis patients an anergic/exhausted CD8$^+$ T-cell phenotype plus an augmented expression of PD-1 was found (Gautam et al., 2014). Likewise, CD8$^+$ T-cells of diffuse cutaneous leishmaniasis patients displayed signs of functional exhaustion including PD-1 expression (Hernández-Ruiz et al., 2010). Functional data on the effects of PD-1 checkpoint blockade in human leishmaniasis are scarce. Only Gautam and colleagues analyzed IFNγ levels of splenic aspirates and PBMCs of 3 - 6 VL patients *ex vivo*. In the presence of PD-1/PD-L blocking antibodies, IFNγ release was not significantly altered both in the PBMC or splenic aspirate culture after three days incubation (Gautam et al., 2014). Here, we strove to apply different experimental read-outs and cultivation methods to determine whether PD-1 checkpoint inhibition has an effect in human leishmaniasis.

1.6 Hypothesis and aims

There is increasing evidence from murine and canine leishmaniasis that PD-1/PD-L interactions have a negative impact on disease outcome and partially benefit from a PD-1 checkpoint inhibition approach. To date, there are two PD-1 checkpoint inhibitors of the IgG4 subclass approved for cancer therapy. In human leishmaniasis information regarding the influence of the PD-1/PD-L axis is rare and mostly restricted to data on transcriptional regulation of cytokine and receptor expression. In this study we wanted to clarify whether PD-1/PD-L interactions have functions in *Leishmania major* (*Lm*) infection of primary human cells. Furthermore, we sought to examine whether a PD-1 checkpoint inhibition approach can enhance leishmanicidal immune effector functions. As there are therapeutic PD-1 checkpoint inhibitors of the IgG1 subclass in clinical studies, we aimed to compare IgG1 and IgG4 PD-1 blocking antibodies.

Thus, in this thesis we hypothesize that:

"PD-1/PD-L interactions inhibit effector functions of *Lm*-induced T-cells and PD-1 checkpoint inhibitors reinvigorate those effector functions."

To investigate this hypothesis, we have the following aims **(Figure 6):**

Aim 1: Establish co-culture assays upon *Lm* infection, with T-cell proliferation and parasite load as read-outs. In addition investigate their suitability with regard to modulation of PD-1/PD-L interactions by PD-1 checkpoint blockade.

Aim 2: Investigate whether two different IgG antibody subclasses (IgG1 and IgG4) of PD-1 checkpoint inhibitors modulate T-cell proliferation and parasite load differently.

Aim 3: Identify and evaluate the effects of PD-1 checkpoint blockade on parasite survival and *Lm*-induced T-cell effector functions with regard to different *Lm* host cells as antigen presenting cells.

Aim 4: Furthermore, gain of first mechanistic insights regarding PD-1 checkpoint blockade in *Lm* infection of primary human cells by determination of cytokine release, T-cell phenotype and cytolytic effector molecules.

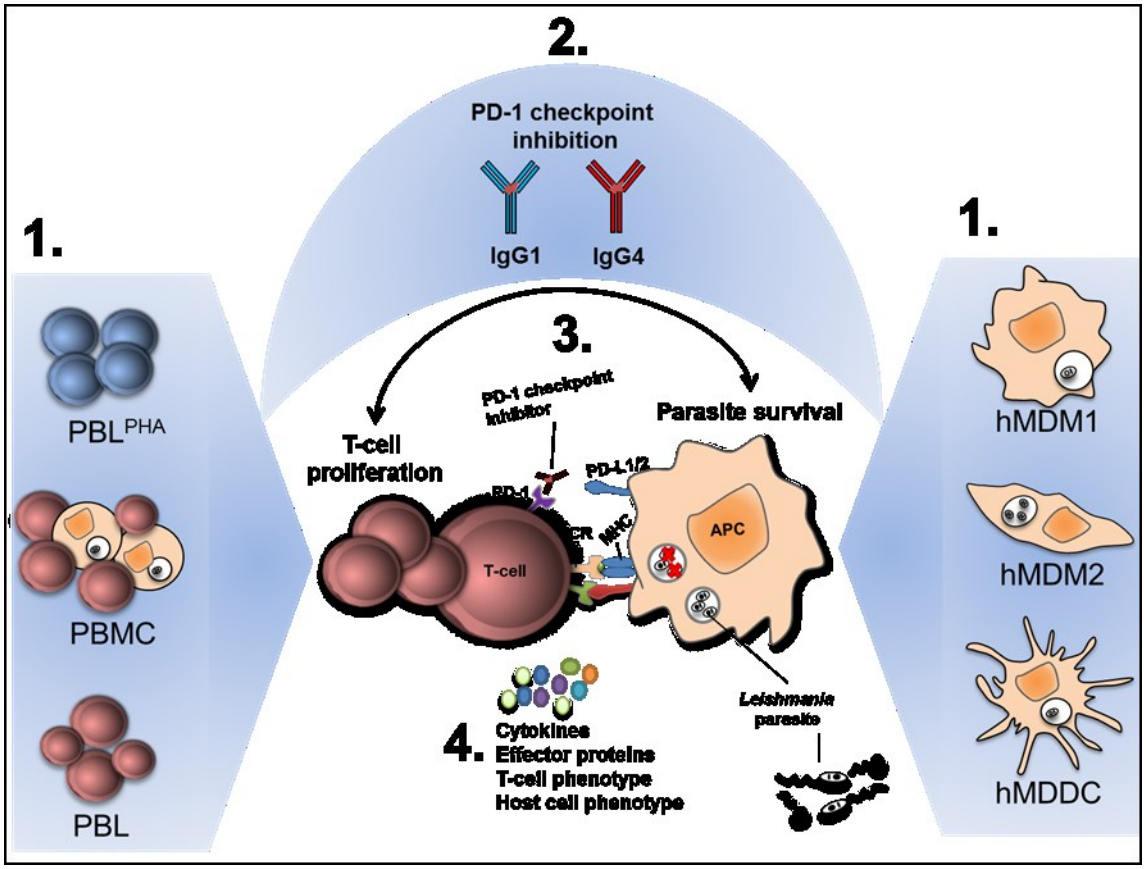

Figure 6: Schematic presentation of the aims and hypothesis of this thesis.

1.) Establish *Lm*-specific T-cell assays with T-cell proliferation and parasite load as read outs. Use and modify protocols from Crauwels (2015; *Lm*-infected pro-inflammatory human monocyte-derived macrophages (hMDM1), anti-inflammatory human monocyte-derived macrophages (hMDM2) or human monocyte-derived dendritic cells (hMDDC) in co-culture with peripheral blood lymphocytes (PBLs) or PHA-pre-stimulated PBLs; $PBLs^{PHA}$) and Römer et al. (2011; low and high density pre-cultivated peripheral blood mononuclear cells (PBMCs) infected with *Lm* parasites). Investigate these assays for their suitability to modulate PD-1/PD-L interactions by PD-1 checkpoint blockade **2.)** Investigate whether two different subclasses (IgG1 and IgG4) of PD-1 checkpoint inhibitors modulate T-cell proliferation and parasite survival differently. **3.)** Explore effects of PD-1 checkpoint blockade on parasite survival and *Lm*-induced T-cell proliferation with regard to different *Lm* host cells as antigen presenting cells **4.)** Furthermore, examine the impact of PD-1 checkpoint blockade on *Lm*-induced cytokine release, cytolytic effector proteins and T-cell/host cell phenotype.

2 Material

2.1 Antibodies

2.1.1 Blocking antibodies

Antibody	Subclass & clone	Source
α-human-PD-1 (nivolumab)	Fully-human IgG4	Bristol-Myers Squibb, New York (USA)
α-human-PD-1	Humanized IgG1	G&P Biosciences, Santa Clara (USA)
α-human-CD28 (TGN1412)	Humanized IgG4 9D7	TeGenero Immuno Therapeutics, Würzburg (GER)
LEAF™ α-human-IFNγ	Mouse IgG1, κ B27	BioLegend, San Diego (USA)
α-human-TNFα (infliximab)	Chimeric IgG1	Mundipharma GmbH, Limburg (GER)
Ultra-LEAF™ α-human-CD40L	Mouse IgG1, κ 24-31	BioLegend, San Diego (USA)
Ultra-LEAF™ Isotype Control	Mouse IgG1, κ MOPC-21	BioLegend, San Diego (USA)
Ultra-LEAF™ Isotype Control	Human IgG1, κ QA16A12	BioLegend, San Diego (USA)

2.1.2 Fluorescently labeled antibodies

Antibody	Subclass & clone	Source
α-human-CD1a (FITC)	Mouse IgG1, κ HI149	BD Pharmingen, Heidelberg (GER)
α-human-CD3 (PB)	Mouse IgG1, κ UCHT1	BD Pharmingen, Heidelberg (GER)
α-human-CD3 (APC)	Mouse IgG1, κ UCHT1	BioLegend, San Diego (USA)
α-human-CD4 (PE)	Mouse IgG1, κ RPA-T4	BD Pharmingen, Heidelberg (GER)
α-human-CD8 (PB)	Mouse IgG1, κ RPA-T8	BD Pharmingen, Heidelberg (GER)
α-human-CD14 (PB)	Mouse IgG1, κ M5E2	BD Pharmingen, Heidelberg (GER)
α-human-CD19 (APC)	Mouse IgG1, κ HIB19	BioLegend, San Diego (USA)
α-human-CD25 (APC)	Mouse IgG1, κ M-A251	BioLegend, San Diego (USA)
α-human-CD28 (PE)	Mouse IgG1, κ CD28.2	BD Pharmingen, Heidelberg (GER)

α-human-CD40 (PE)	Mouse IgG1, κ 5C3	BD Pharmingen, Heidelberg (GER)
α-human-CD56 (PE)	Mouse IgG1, κ HCD56	BioLegend, San Diego (USA)
α-human-CD80 (V450)	Mouse IgG1, κ L307	BD Pharmingen, Heidelberg (GER)
α-human-CD83 (APC)	Mouse IgG1, κ HB15e	BD Pharmingen, Heidelberg (GER)
α-human-CD86 (FITC)	Mouse IgG1, κ 2331 (FUN-1)	BD Pharmingen, Heidelberg (GER)
α-human-CD154 (CD40L) (BV421)	Mouse IgG1, κ TRAP1	BD Pharmingen, Heidelberg (GER)
α-human-CD160 (PE)	Mouse IgM, κ BY55	BioLegend, San Diego (USA)
α-human-CD163 (BV421)	Mouse IgG1, κ GHI/61	BD Pharmingen, Heidelberg (GER)
α-human-CD223 (LAG-3)(PE)	Mouse IgG1, κ T47-530	BD Pharmingen, Heidelberg (GER)
α-human-CD273 (PD-L2) (PE)	Mouse IgG2a, κ 24F.10C12	BioLegend, San Diego (USA)
α-human-CD274 (PD-L1) (PE)	Mouse IgG1, κ MIH1	BD Pharmingen, Heidelberg (GER)
α-human-CD279 (PD-1) (PE)	Mouse IgG1, κ MIH4	BD Pharmingen, Heidelberg (GER)
α-human-HLA-DR (PB)	Mouse IgG2a, κ L243	BioLegend, San Diego (USA)
α-human-FOXP3 (PB)	Mouse IgG1, κ 206D	BioLegend, San Diego (USA)
α-human-Tbet (PB)	Mouse IgG1, κ 4B10	BioLegend, San Diego (USA)
α-human-GATA3 (AF647)	Mouse IgG1, κ L50-823	BD Pharmingen, Heidelberg (GER)
α-human-Perforin (PRF1) (AF647)	Mouse IgG2b, κ dG9	BioLegend, San Diego (USA)
α-human-Granzyme A (GZMA) (AF647)	Mouse IgG1, κ CB9	BioLegend, San Diego (USA)
α-human-Granzyme B (GZMB) (AF647)	Mouse IgG1, κ GB11	BioLegend, San Diego (USA)
α-human-Granulysin (GNLY) (AF647)	Mouse IgG1, κ DH2	BioLegend, San Diego (USA)
α-human-CD244 (2B4) (APC)	Mouse IgG1, κ C1.7	BioLegend, San Diego (USA)
α-human-CD366 (TIM-3) (APC)	Mouse IgG1, κ F38-2E2	BioLegend, San Diego (USA)
α-human IgG (R-PE)	Goat Fab_2 fragment	Dianova GmbH,

	polyclonal	Hamburg (GER)
Isotype Control (PE)	Mouse IgG1, κ MOPC-21	BD Pharmingen, Heidelberg (GER)
Isotype Control (APC)	Mouse IgG1, κ MOPC-21	BD Pharmingen, Heidelberg (GER)
Isotype Control (PE)	Mouse IgM, κ MM-30	BioLegend, San Diego (USA)
Isotype Control (PE)	Mouse IgG2a MOPC-173	BioLegend, San Diego (USA)
Isotype Control (PB)	Mouse IgG1 MOPC-21	BioLegend, San Diego (USA)
Isotype Control (PB)	Mouse IgG2a MOPC-173	BioLegend, San Diego (USA)
Isotype Control (BV421)	Mouse IgG1 MOPC-21	BioLegend, San Diego (USA)
Isotype Control (FITC)	Mouse IgG1 MOPC-21	BD Pharmingen, Heidelberg (GER)
Isotype Control (AF647)	Mouse IgG1 MOPC-21	BioLegend, San Diego (USA)

2.2 Buffer and solutions

Name	Composition
Novy-Nicolle-McNeal blood agar medium	16.6 % Rabbit blood defibrinated 16.6 % 1x PBS 66.2 % Brain Heart Infusion Agar 66.2 U/ml Penicillin 66.2 µg/ml Streptomycin
***Leishmania* medium**	RPMI 1640 Medium 5 % v/v FCS 2 mM L-Glutamine 50 µM β-Mercaptoethanol 100 U/ml Penicillin 100 µg/ml Streptomycin 10 mM HEPES Buffer
Complete medium	RPMI 1640 Medium 10 % v/v FCS 2 mM L-Glutamine 50 µM β-Mercaptoethanol 100 U/ml Penicillin 100 µg/ml Streptomycin 10 mM HEPES Buffer
Cryo-Medium	Complete Medium 40 % v/v FCS 10 % v/v DMSO

Wash-Buffer	1x PBS 5 % v/v Complete Medium
MACS-Buffer pH 7.2	1x PBS 2 mM EDTA 0.5 % w/v BSA
PFA fixation solution	1x PBS 4 % w/v PFA
FACS staining buffer	1x PBS 1 % v/v FCS 1 % v/v Human serum
FACS blocking buffer	1x PBS 10 % v/v FCS 10 % v/v Human serum
Intracellular FACS staining buffer	1x PBS 1 % v/v FCS 1 % v/v Human serum 0.5 % w/v Saponin Sterile filtrated
Intracellular FACS blocking buffer	1x PBS 10 % v/v FCS 10 % v/v Human serum 0.5 % w/v Saponin Sterile filtrated

2.3 Cells

Product	Source
Buffy coat	DRK Blutspendedienst, Frankfurt am Main (GER)
***Leishmania major* wild type**	MHOM/IL/81/FEBNI, originally from a skin biopsy from a patient from Israel. The parasites are from Dr. Frank Ebert , Bernhard Nocht Institute for tropical medicine, Hamburg (GER)
***Leishmania aethiopica* wild type**	MHOM/ET/72/L100 Z14
***Leishmania major* dsRED**	MHOM/IL/81/FEBNI, transfected with the red fluorescent gene dsRED

2.4 Chemicals

Chemicals	Source
ß-Mercaptoethanol	Sigma-Aldrich, Steinheim (GER)
Agarose, LE	Biozym Scientific GmbH, Hessisch Oldendorf (GER)
Ammonium chloride (0.15 M)	Medienküche PEI, Langen (GER)

Aqua distilled	Medienküche PEI, Langen (GER)
Bovine Serum Albumin	Sigma-Aldrich, Steinheim (GER)
CASYton	Roche Innovatis AG, Reutlingen (GER)
Dimethylsulfoxid (DMSO)	Sigma-Aldrich Chemie, Steinheim (GER)
DNA loading buffer (10x)	New England Biolabs, Ipswich (USA)
dNTP: dATP, dCTP, dGTP, dTTP (100mM)	PeqLab, Erlangen (GER)
Ethanol, absolute	VWR, Bruchsal (GER)
FACS Clean	Medienküche PEI, Langen (GER)
FACS Flow (Sheath Solution)	Medienküche PEI, Langen (GER)
FACS Rinse	Medienküche PEI, Langen (GER)
Fetal Calf Serum (FCS)	Sigma-Aldrich Chemie
Glutamine (L-Glutamine)	Biochrom AG, Berlin (GER)
HEPES-Buffer (1 M)	Biochrom AG, Berlin (GER)
Histopaque 1077	PAA, Pasching (AUT)
Human recombinant Interferon γ (IFNγ)	Peprotech®, Rocky Hill (USA)
Human recombinant Interleukine 4 (IL-4)	Thermo fisher scientific, Massachusetts (USA)
Human recombinant Granulocyte Macrophage Colony Stimulation Factor (GM-CSF), Leukine®	Bayer Healthcare Pharmaceutical, Leverkusen (GER)
Human recombinant Macrophage Colony Stimulating Factor (M-CSF)	R&D Systems, Minneapolis (USA)
Human Serum Type AB	Sigma-Aldrich Chemie, Steinheim (GER)
Hygromycin B, solution	Invitrogen, San Diego (USA)
Isopropyl alcohol	Sigma-Aldrich Chemie, Steinheim (GER)
Nuclease free water	Promega Corporation, Madison (USA)
Paraformaldehyde (PFA)	Sigma-Aldrich Chemie, Deisenhof (GER)
Penicillin/ Streptomycin	Biochrom AG, Berlin (GER)
Phosphate buffered saline (1x PBS) wo/ Ca^{2+}, Mg^{2+}; pH 7.1	Medienküche PEI, Langen (GER)
Phosphate buffered saline (1x PBS) wo/ Ca^{2+}, Mg^{2+}; pH 7.4	Medienküche PEI, Langen (GER)
Purified phytohemagglutinin (PHA)	Thermo fisher scientific, Massachusetts (USA)
Rabbit Blood, defibrinated	Elocin-Lab GmbH, Gladbeck (GER)
RNase AWAY	VWR, Darmstadt (GER)
Roswell Park Memorial Institute	Sigma-Aldrich Chemie, Steinheim

(RPMI) 1640 Medium	Biowest, Nuaillé (FRA)
Saponin from Quillaja bark	Sigma-Aldrich Chemie, Steinheim (GER)
Sodium Azide	Sigma-Aldrich Chemie, Deisenhof (GER)
Tween 20	Sigma-Aldrich Chemie, Steinheim (GER)

2.5 Enzymes

Name	Source
Taq Polymerase	New England Biolabs, Ipswich (USA)

2.6 Instruments

Name	Source
Analytical balance KB BA 100	Sartorius, Göttingen (DE)
BIOLiner Buckets (75003670; 75003668)	Thermo Scientific, Dreieich (GER)
CASY Modell TT	Roche Innovatis AG, Reutlingen (GER)
Centrifuge Heraeus Megafuge 40R	Thermo Scientific , Dreieich (GER)
Centrifuges 5430 and 5430R	Eppendorf, Hamburg (GER)
CO_2-Incubator Forma Series II Water Jacket	Thermo Scientific, Marietta (US)
CO2-Incubator, Heraeus Auto Zero	Thermo Scientific, Dreieich (GER)
Flow cytometer LSR II Special Order Research Product	Becton Dickinson, Heidelberg (GER)
Freezer (-20°C, 4°C)	Bosch, Stuttgart (GER)
Freezer Innova® U725-G (-80°C)	Eppendorf, Hamburg (GER)
Laminar flow workbench MSC-Advantage	Thermo Scientific, Dreieich (GER)
LightCycler® 480 System	Roche Applied Science, Mannheim (GER)
Microscope Axio Vert.A1	Carl Zeiss, Jena (GER)
Microscope Primo Star	Carl Zeiss, Jena (GER)
Multichannel Pipette (Research® plus)	Eppendorf, Hamburg (GER)
Multichannel Pipette BrandTech Transferpette® S-8 (0,5µl-100µl, 200µl, 300µl)	Universal medical Inc, Norwood (USA)
Multichannel Pipette electronic (Research® pro)	Eppendorf, Hamburg (GER)
NanoDrop 2000c	PeqLab, Erlangen (GER)
Nalgene™ Mr. Frosty	Thermo Scientific, Dreieich (DE)

Freezing Container	
Nitrogen container "Chronos"	Messer, Bad Soden (DE)
Neubauer improved cell counting chamber (depth 0.1 mm and 0.02 mm)	VWR International, Darmstadt (GER)
Personal Cycler	Biometra, Göttingen (GER)
Pipette controller (accu-jet® pro)	BRAND, Wertheim (GER)
Pipettes (Research® plus: 0,5-10 µl, 10-100 µl, 20-200 µl, 100-1000 µl)	Eppendorf, Hamburg (GER)
Power Supply PowerPac™ 200/2.0	Bio-Rad, München (GER)
Thermomixer comfort (1.5 ml)	Eppendorf, Hamburg (DE)
Thermomixer 5437 (1.5 ml)	Eppendorf, Hamburg (DE)
UV-Transilluminator GenoView	VWR International, Darmstadt (GER)
Vortex mixer VV3	VWR International, Darmstadt (GER)
Water bath	Köttermann VWR International, Darmstadt (GER)

2.7 Marker and Dyes

Name	Source
Annexin-V-FITC Kit	Miltenyi Biotec, Bergisch Gladbach (GER)
5(6)-Carboxyfluorescein diacetate N-succinimidyl ester	Sigma Aldrich Chemie, Steinheim (GER)
CellTrace™ Far Red Cell Proliferation Kit	Thermo Fisher Scientific, Waltham (USA)
1 kb DNA Ladder	New England Biolabs, Ipswich (USA)
100 bp DNA Ladder	Promega, Madison (USA)
Ethidium bromide	Merck, Darmstadt (GER)
Propidium iodide	Sigma Aldrich Chemie, Steinheim (GER)

2.8 Ready to use Kits

Name	Source
$CD14^+$ Micro Beads Human	Miltenyi Biotec, Bergisch Gladbach (GER)
$CD4^+$ Micro Beads Human	Miltenyi Biotec, Bergisch Gladbach (GER)
$CD8^+$ Micro Beads Human	Miltenyi Biotec, Bergisch Gladbach (GER)
ImProm-II Reverse Transcription System	Promega, Mannheim (GER)
MESA Blue qPCR MasterMix Plus	Eurogentec, Köln (GER)

for SYBR	
RNeasy Plus Mini kit	Qiagen, Hilden (GER)
DuoSet® ELISA Development System (human TNFα) Catalog Number DY210	R&D Systems, Minneapolis (USA)
DuoSet® ELISA Development System (human IL-10) Catalog Number DY217B	R&D Systems, Minneapolis (USA)
DuoSet® ELISA Development System (human IFNγ) Catalog Number DY285	R&D Systems, Minneapolis (USA)
eBioscience™ Foxp3/Transcription Factor Staining Buffer Set	Thermo Fisher Scientific, Waltham (USA)

2.9 Laboratory supplies

Name	Source
Cell culture plates (6, 24, 96 well)	Sarstedt, Nürnbrecht (GER)
Cell culture flasks with filter (25 cm^2, 75 cm^2)	Greiner Bio-One, Frickenhausen (GER) BD labware Becton Dickinson GmbH, Heidelberg (GER)
Cell scraper	Sarstedt, Nümbrecht (GER)
Centrifuge tubes (15 ml; 50 ml)	Greiner Bio-One, Frickenhausen (GER)
Cryo tubes (2 ml)	Sigma Aldrich Chemie, Steinheim (GER)
FACS tubes (5ml)	BD labware Becton Dickinson GmbH, Heidelberg (GER)
FACS tubes (2ml)	Micronic, Lelystad (NL)
Light Cycler 96-well plates with foil, white	Roche Applied Science, Darmstadt (GER)
MACS LS columns	Miltenyi Biotec, Bergisch Gladbach (GER)
MACS Chill 15 Rack	Miltenyi Biotec, Bergisch Gladbach (GER)
MACS MultiStand	Miltenyi Biotec, Bergisch Gladbach (GER)
Manufix-sensitive disposal gloves	B. Braun Melsungen AG, Melsungen (GER)
Microcentrifuge tubes (1.5 ml, 2 ml)	Eppendorf, Hamburg (GER)
MidiMACS Magnet	Miltenyi Biotec,

	Bergisch Gladbach (GER)
Nitril gloves	Ansell Healthcare, Brussels (CH)
PCR Tube Multiply® Pro (0.2 ml)	Sarstedt, Nümbrecht (GER)
Petri dish (94 mm x 16 mm)	Greiner Bio-One, Frickenhausen (GER)
Pipette tips (1-10 µl, 10-200 µl, 100-1000 µl)	Eppendorf, Hamburg (GER)
Scott Brand Multifold Paper Towels	Kimberly Clark, Texas (USA)
Serological pipettes, sterile (2 ml, 5 ml, 10 ml, 25 ml)	Greiner Bio-One, Frickenhausen (GER)

2.10 Oligonucleotides

Primers	produced by Eurofins MWG Operon, Ebersberg (GER)
PD-L1 D1 (forward)	5-TGGCATTTGCTGAACGCATTT-3
PD-L1 D2 (reverse)	5-TGCAGCCAGGTCTAATTGTTTT-3
PD-L2 H1 (forward)	5-ACCCTGGAATGCAACTTTGAC-3
PD-L2 H2 (reverse)	5-AAGTGGCTCTTTCACGGTGTG-3
GAPDH (forward)	5-GAGTCAACGGATTTGGTCGT-3
GAPDH (reverse)	5-TTGATTTTGGAGGGATCTCG-3

2.11 Software

Name	Source
BD Diva software v8.0.1	Becton Dickinson, Heidelberg (DE)
FlowJo 7.6.5	FLOWJO, LLC Data analysis Software, Ashland (USA)
Graph Pad Prism 7	GraphPad Software, Inc., La Jolla (USA)
Magellan™ Data Analysis Software für F50 V7.0	Tecan Group Ltd., Männedorf (CH)
Microsoft® Office 2010	Microsoft, Redmont (USA)
Inkscape	Open Source Software
Citavi 5	Swiss Academic Software, Wädenswil (CH)

3 Methods

3.1 Cultivation of human primary cells and *Leishmania* parasites

Human primary myeloid and lymphoid cells were cultivated in complete medium at 37 °C, 5 % CO_2. *Leishmania major* (*Lm*) and *Leishmania aethiopica* (*Lae*) wild type were thawed and cultivated in *Leishmania* medium at 27 °C , 5 % CO_2 in 96-well flat shaped plates containing diagonally casted Novy-Nicolle-McNeal blood agar medium (1×10^6 live parasites/100 µl per well). For cultivation of the transgenic *Leishmania major* dsRED (*Lm* dsRED) strain, 20 µg/ml Hygromycin was added to the *Leishmania* medium to keep selection pressure high towards dsRED positive parasites. For infection experiments only stationary phase (d6-8) parasites were used as they resemble the infectious inoculum which is transferred to the host by the infected sand fly bite (van Zandbergen et al., 2006). All experiments were carried out under a laminar flow bench to assure aseptic conditions. All cells were cultivated in a humidified incubator.

3.2 Cell culture methods

3.2.1 Isolation of peripheral blood mononuclear cells from buffy coat

Human peripheral blood mononuclear cells (PBMCs) were isolated from buffy coats purchased at the DRK-Blutspendedienst Hessen GmbH. The buffy coats were donated by healthy adults without known exposure to *Leishmania* parasites. The buffy coat (~30 ml) was diluted with pre-warmed PBS (20-37°C) to a final volume of 100 ml. Subsequently 15 ml of pre-warmed leukocyte separation medium 1077 (LSM) was pipetted at the bottom of four 50 ml tubes. 25 ml of buffy coat dilution was carefully layered on each 50 ml tube without perturbing the LSM phase. Afterwards the cells were centrifuged at 573xg for 30 min without brake. The interphase containing the PBMCs plus the plasma on top was evenly distributed into six new 50 ml tubes and up to 50 ml Wash-Buffer was added. Cells were centrifuged at 1084xg for 8 min. The supernatant was discarded and the pellet was resuspended. Per 50 ml tube, 50 ml Wash-Buffer was added to dilute residual LSM in the cell pellet. The cells were centrifuged at 573xg for 8 min. Again, supernatants were discarded and the cell pellets were resuspended. By using Wash-Buffer, the cells were pooled from six into four 50 ml tubes followed by a centrifugation step at 143xg for 8 min. This step is required to remove thrombocytes, which are mostly in the supernatant

due to their lower density compared to leukocytes. The supernatants were discarded and the cell pellets were resuspended each in 10 ml 4 °C cold 0.15M ammonium chloride solution for 10 - 15 min. This step lyses erythrocytes, which are more sensitive to osmotic stress compared to leukocytes. The lysis was stopped by adding up to 50 ml Wash-Buffer to the four 50 ml tubes. After centrifugation (143xg, 8 min), the supernatant was discarded and the cells were resuspended and pooled in one 50 ml tube using Wash-Buffer. Subsequently cells were washed by resuspension, centrifugation (143xg, 8 min) and Wash-Buffer as long as the supernatant was turbid.

The PBMC cell pellet was resuspended either in complete medium (for plastic adherence or the modified RESTORE assay) or MACS-Buffer (for magnetic cell separation). 10 µl of PBMC cell suspension was either diluted in 10 ml CASYton or counted directly using a Neubauer improved cell counting chamber (0.1 mm). The diluted cells were counted by the Casy cell counter using the appropriate counting program for PBMCs. The counted PBMCs are further processed in chapter 3.2.2, 3.2.3 or 3.2.5.

3.2.2 Plastic adherence

The cell concentration was adjusted to 8 - 10 × 10^6 PBMC/ml using complete medium plus 1 % v/v human serum. 5 ml (25 cm^2) or 15 ml (75 cm^2) of cell suspension was pipetted into a cell culture flask followed by an incubation step at 37 °C for 1.5 h. During this time monocytes became adherent to the plastic surface of the flask. The non-adherent fraction was saved in a 50 ml falcon and was further used in chapter 3.2.6 and 3.2.7. To remove residual non-adherent cells, the monocytes were gently washed twice by using 4 ml (25 cm^2) or 12 ml (75 cm^2) Wash-Buffer per flask. Monocytes were differentiated in chapter 3.2.4.

3.2.3 Magnetic Cell Separation (MACS)

All MACS steps were performed at 4°C. PBMCs from Chapter 3.2.1 (or $PBLs^{PHA}$) were resuspended in up to 50 ml of MACS-Buffer and centrifuged at 323xg for 8 min. The supernatant was discarded. Cells were resuspended in 95 MACS-Buffer/10×10^6 cells and 5 µl of CD14 beads/10×10^6 cells ($PBLs^{PHA}$: CD4 or CD8 beads/10×10^6 cells). The cells were incubated in the fridge for 15 min and were shaken from time to time. Subsequently up to 50 ml MACS-Buffer was added to the bead-labeled cells. After centrifugation (323xg, 8 min) the

supernatant was decanted, the pellet was resuspended in 3 ml MACS-Buffer and the cell suspension was kept on ice until use. Afterwards the LS column was equilibrated in the magnetic field of the Midi-MACS-Separator by adding two times 5 ml MACS-Buffer on top of the column. The flow though was discarded. Subsequently the bead-labeled cells were added onto the equilibrated LS-column and the flow-through was saved ($CD14^-$ PBLs; further processed in chapter 3.2.6 or 3.2.7) in a 50 ml tube or discarded ($CD4^-$ and $CD8^-$ $PBLs^{PHA}$). To remove residual $CD14^-$ PBLs (or $CD4^-$/$CD8^-$ $PBLs^{PHA)}$, the column was washed three times with 3 ml MACS-Buffer and the flow trough was discarded. Subsequently the LS column containing the $CD14^+$ monocytes ($PBLs^{PHA}$: $CD4^+$ or $CD8^+$ $PBLs^{PHA}$) was removed from the magnetic field and placed onto a 15 ml tube and cells were eluted using 5 ml of MACS-Buffer and a plunger. 10 µl $CD14^+$ monocyte ($PBLs^{PHA}$: $CD4^+$ or $CD8^+$ $PBLs^{PHA}$) suspension was diluted in 10 ml CASYton and monocytes (or PBLs) were counted using the CASY cell counter. The required amount of monocytes (or PBLs) was centrifuged (323xg/8 min) and, after decanting the supernatant, the pellet was further processed in chapter 3.2.4 ($PBLs^{PHA}$: 3.2.10).

3.2.4 Generation of primary human macrophages and dendritic cells

Monocytes ($CD14^+$ MACS or plastic adherence) were differentiated in complete medium (5ml, 25cm^2 flask; 15 ml, 75 cm^2 flask; 3 - 4 × 10^6 cells/2.5 ml in one well of a 6-well plate) supplemented with either 10 ng/mL GM-CSF into pro-inflammatory human monocyte-derived macrophages Type 1 (hMDM1) or 30 ng/mL M-CSF into anti-inflammatory human monocyte-derived macrophages Type 2 (hMDM2). Cells were incubated over a period of 5-7d at 37°C, 5% CO_2. For the generation of human monocyte-derived dendritic cells (hMDDC), $CD14^+$ MACS isolated monocytes were incubated in complete medium (1.5 × 10^6 cells/2 ml in one well of a 6-well plate) supplemented with 5 ng/mL GM-CSF and 10 ng/mL IL-4 over a period of 3d at 37°C, 5% CO_2. On day three cytokines were replenished by adding 1 ml CM supplemented with 15 ng/ml GM-CSF and 30 ng/ml IL-4. After further incubation for 2d at 37 °C, 5% CO_2, hMDM1, hMDM2 and hMDDC were further processed in chapter 3.2.9 and 3.2.10.

3.2.5 Modified RESTORE assay

The RESTORE (RESetting T cells to Original Reactivity) assay was originally established by Römer and colleagues (Römer et al., 2011). In this assay PBMCs are pre-cultured under high density (10 × 10^6 PBMCs/ml) for 2 days before use. During this pre-culture step, which mimics tissue like conditions, T-cells in the PBMCs become more sensitive for antigen-specific activation compared to low density cultivated T-cells. This *in vitro* assay was the first to reflect the cytokine storm inducing effects of the superagonistic antibody TGN1412 (Römer et al., 2011). We modified this assay to assess *Leishmania* infection and T-cell proliferation under low and high density pre-culture in presence and absence of PD-1 checkpoint inhibitors.

Freshly isolated PBMCs (see 3.2.1) were labeled with the cell proliferation dye 5(6)-Carboxyfluorescein diacetate N-succinimidyl ester (CFSE) as described in 3.3.1. 10 µl CFSE-labeled PBMCs were diluted in 10 ml CASYton and cell concentration was determined by CASY cell counter. PBMC concentration was adjusted to 1 x 10^6 cells/ml (low density culture, LD) and 10 x 10^6 cells/ml (high density culture, HD), respectively. Per well of a 24-well plate, 1 ml of LD PBMCs or HD PBMCs was added followed by a cultivation for 48h at 37 °C, 5 % CO_2.

Subsequently LD PBMC or HD PBMCs were resuspended with a 1 ml pipette and transferred into cold 15 ml tubes. The wells were washed once with cold complete medium and residual cells were pipetted into the respective 15 ml tubes. The cells were counted by the Casy cell counter as described above but the PBMC cell numbers (**Figure 7A**) and the monocyte cell numbers (**Figure 7B**) were determined separately for each donor.

Stationary phase *L. major* (*Lm*) dsRED (d6-d8, passage 2-8) were counted in a Neubauer improved cell counting chamber (0.02 mm). Life and dead parasites were taken into account for the calculation of the cell number. 1 × 10^6 monocytes/100 µl CM were co-cultivated with 20 × 10^6 Lm dsRED/10 µl CM in a 1.5 ml reaction tube. Infection took place for 45 min at 37 °C, 5% CO_2. Afterwards 1 ml CM was added to the reaction tube, cells were centrifuged at 68xg for 8 min and the supernatant was removed using a 1 ml pipette. This washing step was repeated with higher centrifugal force (106xg). These two washing steps remove most of the extracellular parasites.

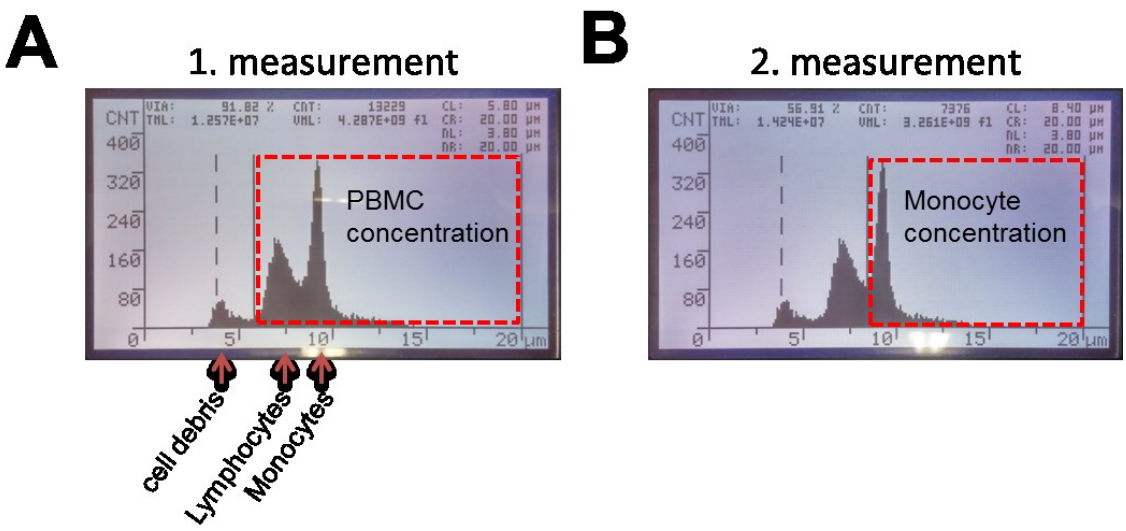

Figure 7: Determination of monocyte and PBMC concentration using the CASY cell counter.

(A) For the calculation of the PBMC concentration all cells between 6 and 20 µm (lymphocytes and monocytes) were taken into account. (B) For the calculation of the monocyte concentration all cells from the right peak between 9 and 20 µm (monocytes and possibly a few activated lymphocytes) were taken into account. The y-axis shows the cell counts and the x-axis the cell diameter (µm).

Subsequently cell concentration was adjusted to 1 x 10^6 monocytes/ml using CM. To calculate how many PBMCs are in the reaction tube, a correction factor was calculated:

Example: 1 x 10^6 monocytes/ml in 1.5 ml reaction tube
9.82 x 10^6 PBMCs/ml ÷ 3.45 x 10^6 monocytes/ml = 2.85
1 x 10^6 monocytes/ml x 2.85 = 2.85 PBMCs/ml

Per well of a 96-U-well shaped plate 0.2 x 10^6 PBMCs/200 µl CM were added. For the positive control 6 LD and 6 HD wells were prepared. Half of the wells were treated with 10µg/ml TGN1412 antibody. TGN1412 should only induce T-cell proliferation when cells were high density pre-cultured. PD-1 checkpoint inhibitors were used at a final concentration of 0.625 µg/ml. Subsequently cells were incubated at 37°C, 5 % CO_2 for 5d. Afterwards cells were immunostained (see 3.3.2) or directly analyzed by flow cytometry (see 3.3.3).

3.2.6 Phytohemagglutinin (PHA) stimulation of peripheral blood lymphocytes

The $CD14^-$ or non-adherent fraction (peripheral blood lymphocytes, PBLs) was centrifuged (323xg, 8 min) and the supernatant discarded. The cell concentration was adjusted to $1x10^6$ cells/mL using CM supplemented with 0.5µg/mL phytohemagglutinin (PHA). Per well of a 6-well plate, 5 ml of cell suspension was added and cells were incubated for 6d at 37°C, 5 % CO_2. The resulting PHA-pre-stimulated PBLs were referred to as $PBLs^{PHA}$. The cells were either immunostained (see chapter 3.3.2) for flow cytometric analysis or used for co-culture experiments (see chapter 3.2.10).

3.2.7 Freezing of peripheral blood lymphocytes

The $CD14^-$ or non-adherent fraction (PBLs) was centrifuged at 323xg for 8 min. The supernatant was decanted. The cell pellet was resuspended in 1800 µl Cryo-Medium. The cell suspension was evenly aliquoted in two cryo tubes. Per cryo tube, 100 µl dimethyl sulfoxide (DMSO) was added on top. DMSO and the cell suspension were mixed by inverting the cryo tubes. Cells were slowly frozen (-1 °C/min) in the -80 °C freezer by using a Nalgene™ Mr. Frosty Freezing Container containing isopropyl alcohol. The frozen cells were stored at -80 °C until use.

3.2.8 Thawing of peripheral blood lymphocytes

An aliquot of frozen PBMCs was thawed in the water bath at 37 °C. As soon as the PBMC suspension was ice crystal free, the cells were slowly pipetted in a 15 ml tube containing 7 ml of warm CM. After centrifugation (323xg, 8 min) the supernatant was decanted and the cells were resuspended in 14 ml CM. 10 µl of cell suspension was diluted in 10 ml CASYton and the cell concentration was determined by the CASY cell counter. The cells were further processed in chapter 3.2.10

3.2.9 Infection of macrophages or dendritic cells with *Leishmania* parasites

On day of harvest, adherent hMDM1 and hMDM2 (from chapter 3.2.4) were incubated on ice for 30 min. Subsequently cells were scraped of the plastic layer by using a cell scraper. Immature hMDDC do not adhere. Thus, the first

two steps are neglectable. Hereafter the cells were resuspended with a serological pipette and transferred into a 50 ml tube. The plastic flasks or plate surfaces were washed once with cold PBS (pH 7.1) to dissolve residual macrophages or dendritic cells. The PBS cell suspension was transferred into the mentioned 50 ml tube. In case of macrophages, the plastic surface was microscopically checked whether all adherent cells were scraped off. If not, the scraping and resuspension steps were repeated. After centrifugation of the cell suspension (323xg, 8 min) the supernatant was discarded and, depending on the pellet size, macrophages/dendritic cells were resuspended in 1 - 4 ml CM. The cell suspension was diluted 1:1000 in CASYton solution and the cell concentration was measured using the CASY cell counter. For each condition, at least 0.2 × 10^6 cells were prepared. For T-cell proliferation assays, cells were fluorescently labeled as described in chapter 3.3.1 prior to *Leishmania* infection. The cell concentration was adjusted to 0.4 × 10^6 cells/ml with CM. Subsequently reaction tubes were prepared (1 ml cell suspension in 1.5 ml reaction tube) and cells were incubated at 37 °C until use.

For infection of hMDM1, hMDM2 or hMDDC, stationary phase parasites (d6-d8 culture, passage 2-8) were used. *Leishmania* parasites were diluted in CM (1:11) and 5 µl parasite suspension was pipetted into a Neubauer improved counting chamber (0.02 mm). The *Leishmania* cell concentration was determined considering both live and dead parasites and the chamber factor. The required amount of parasites was centrifuged (2400xg, 8 min), the supernatant was decanted and the *Leishmania* cell concentration was adjusted to 40 × 10^6 cells/ml. Subsequently macrophages or dendritic cells were infected at a multiplicity of infection (MOI) of 10 (4 × 10^6 *Leishmania* parasites/100 µl CM were added to 0.4 × 10^6 hMDM1, hMDM2 or hMDDC/1 ml CM). The non-infected controls just received 100 µl CM. Reaction tubes were inverted and incubation took place for 24h at 37 °C, 5 % CO_2.

Subsequently (non-) infected hMDM or hMDDCs were centrifuged (209xg, 8 min) and the supernatants were removed carefully by using a 1 ml pipette without taking up the loose cell pellet. Per reaction tube, 1 ml of CM was added and the previous steps were repeated. Cell concentration was adjusted again to 0.4 × 10^6 /ml by adding 1 ml CM per reaction tube. The cells were further used in co-culture together with PBLs or $PBLs^{PHA}$ (chapter 3.2.10), immunostained

for flow cytometric analysis (chapter 3.3.2) or used for RNA-Isolation (chapter 3.4.1).

3.2.10 Co-cultivation of *Leishmania*-infected cells with autologous peripheral blood lymphocytes

(Non-)fluorescently labeled (Non-)infected hMDM or hMDDC (see chapter 3.2.9) were seeded in 96-U-well plates. Per well, 20000 hMDM or hMDDC/50µL CM were seeded and stored at 37°C, 5%CO_2 until use. Subsequently cell concentration of autologous PBLs (see chapter 3.2.8) or $PBLs^{PHA}$ (see chapter 3.2.6) was determined by the Casy cell counter as described. For one experiment $CD4^+$ or $CD8^+$ $PBLs^{PHA}$ were separated using MACS isolation (see chapter 3.2.3). In case that T-cell proliferation had to be assessed, PBLs or ($CD4^+$ or $CD8^+$) $PBLs^{PHA}$ were fluorescently labeled (described in chapter 3.3.1). The cell concentration was adjusted to 1 × 10^6 cells/ml with CM. To each well containing 20000 hMDM or hMDDC, 0.1 × 10^6 PBLs or ($CD4^+$ or $CD8^+$) $PBLs^{PHA}$/100 µl CM were added on top. As a control, PBLs or ($CD4^+$ or $CD8^+$) $PBLs^{PHA}$ were seeded separately. For some experiments also hMDM and hMDDC were seeded separately. In both cases the missing volume in the wells was replaced by CM. PD-1 blocking antibodies (IgG1 and IgG4) and corresponding Isotype controls were used at a final concentration of 0.625 µg/ml unless otherwise specified. Blocking antibodies for neutralization of IFNγ, TNFα or CD40L plus their corresponding isotype controls were used at a final concentration of 20 µg/ml. The cells were incubated at 37 °C, 5 % CO_2 for 5 - 7d. Supernatants were frozen at -80 °C for cytokine analysis (see chapter 3.3.4). Cells were immunostained (see chapter 3.3.2) or directly analyzed via flow cytometry (see chapter 3.3.3).

3.3 Immunological methods

3.3.1 Fluorescent labeling of cells using cell proliferation dyes

Fluorescent labeling of cells with proliferation dyes allows analyzing T-cell proliferation. With each cell division the fluorescence intensity is halved, which can be measured via flow cytometry. In our studies we used two dyes with different excitation/emission spectra: 5(6)-Carboxyfluorescein diacetate N-succinimidyl ester (CFDA-SE) and the CellTrace™ Far Red Cell Proliferation Kit. The first-mentioned CFDA-SE is cell-permeable and non-fluorescent. Inside

the cell esterases remove the diacetate residues. The resulting 6-Carboxyfluorescein N-succinimidyl ester (CFSE) is fluorescent. By covalently binding to primary amine residues, CFSE remains relatively stable inside the cell (Parish, 1999). Data on the chemical structure of the CellTrace™ Far Red dye is not available.

CFSE staining protocol

Up to 10 × 10^6 cells were centrifuged (323xg, 8 min) in a 15 ml tube and the supernatant was decanted. The pellet was resuspended in 2 ml CM. CFSE was reconstituted with DMSO and adjusted to a stock concentration of 10 mM. 1 µl of the CFSE stock solution was diluted in 500 µl CM followed by vortexing. 500 µl CFSE dilution were added to the cell suspension (2 ml) followed by mixing (final concentration: 4 µM CFSE). After 10 min incubation at 37 °C, 5 % CO_2, the CFSE staining reaction was stopped by adding 5 ml CM. Subsequently the cells were centrifuged (323xg, 8 min) and the supernatant was decanted. Hereafter cell concentration was adjusted for the intended use (see chapter 3.2.9 or 3.2.10)

CellTrace™ Far Red protocol

Up to 10 × 10^6 cells were pipetted into a 15 ml tube and filled up with PBS (pH 7.1). After centrifugation (323xg, 8 min) the supernatant was decanted. The pellet was resuspended in 500 µl PBS (pH 7.1). CellTrace™ Far Red powder was reconstituted with DMSO and adjusted to a stock concentration of 1 mM. 1 µl of the CellTrace™ Far Red stock solution was diluted in 500 µl PBS (pH 7.1) followed by vortexing. 500 µl CellTrace™ Far Red dilution were added to the cell suspension (500 µl) followed by mixing (final concentration: 1 µM CellTrace™ Far Red). After 20 min incubation at 37 °C, 5 % CO_2, the CellTrace™ Far Red reaction was stopped by adding 5 ml CM. Subsequently the cells were incubated for 5 min at room temperature and centrifuged (323xg, 8 min). The supernatant was decanted and cell concentration was adjusted for the intended use (see chapter 3.2.9 or 3.2.10)

3.3.2 Immunostaining of samples

To analyze expression of cell surface molecules or intracellular proteins via flow cytometric analysis, cells are incubated with fluorescently labeled antibodies

targeting the desired cell molecules. As fluorescent dyes are available with different excitation and emission spectra, expression of several molecules can be analyzed simultaneously on a cell. Additionally cells can be permeabilized with different detergents prior immunostaining, which enables analysis of intracellular and intranuclear components.

Surface immunostaining

For fluorescent labeling of surface molecules at least 0.2 × 10^6 cells (in case of co-cultures hMDM or hMDDC) were transferred per well into a VEE shaped 96-well plate. All steps were performed at 4°C. Cells were centrifuged at 439xg for 4 min. The supernatant was removed by carefully knocking off the 96-well plate on paper towels. The cells were resuspended in 100 µl blocking buffer/well followed by incubation for 15 min. Cells were centrifuged (439xg for 4 min) and the supernatant was removed as described. Residual blocking buffer was diluted by resuspending the cells in 100 µl FACS-buffer/well followed by centrifugation (439xg for 4 min). Afterwards cells were incubated in 100 µl primary antibody solution for 30 min. The used antibody concentrations are indicated in Table 2.

Table 2: Amounts of antibodies that were used for primary antibody labeling of surface proteins.

Fluorochrome	Specificity	Antibody per 0.2 × 10^6 cells/100 µl FACS-Buffer
PE	Anti-Human CD274	4 µl
PE	Anti-Human CD273	1 µl
PE	Anti-Human CD279	4 µl
APC	Anti-Human CD3	1 µl
Pacific Blue	Anti-Human CD3	1 µl
APC	Anti-Human TIM-3	1 µl
APC	Anti-Human 2B4	1 µl
PE	Anti-Human LAG-3	1 µl
PE	Anti-Human CD160	1 µl
V450	Anti-Human CD80	2 µl
APC	Anti-Human CD83	4 µl
FITC	Anti-Human CD86	4 µl
PE	Anti-Human CD40	1 µl
FITC	Anti-Human CD1a	4 µl
PE	Anti-Human CD4	1 µl
APC	Anti-Human CD19	1 µl
PE	Anti-human CD56	1 µl
APC	Anti-Human CD25	1 µl

Pacific Blue	Anti-Human CD14	1 µl
Pacific Blue	Anti-Human HLA-DR	1 µl
Pacific Blue	Anti-Human CD8	1 µl
BV421	Anti-Human CD163	1 µl
Unlabeled	Anti-Human CD279 (nivolumab)	0.5 µl

Subsequently cells were centrifuged (439xg for 4 min) and the supernatant was removed as described. Unbound primary antibodies were removed by resuspending the cells in 100 µl FACS-buffer/well followed by centrifugation (439xg for 4 min). After removing the supernatants, cells were transferred into a FACS-tube (2 ml) for flow cytometric analysis (see chapter 3.3.3). In case the unlabeled primary antibody nivolumab was used as primary antibody, cells additionally were incubated for 30 min with the secondary RPE-labeled Fab_2 fragment (1:200; Dianova) which targets the Fc-part of nivolumab. After removing unbound Fab_2 fragments by washing with FACS-Buffer, cells were prepared for flow cytometric analysis. In the particular case of nivolumab, human serum in the FACS-Buffer and Blocking-Buffer was replaced by BSA. The reason is that human IgG in the serum would cause unspecific binding of the Fab_2 fragment.

Intracellular immunostaining

For fluorescent labeling of intracellular proteins at least 0.2×10^6 cells (in case of co-cultures hMDM or hMDDC) were transferred per well into a VEE shaped 96-well plate. All steps were performed at 4°C. Cells were centrifuged at 439xg for 4 min. The supernatant was removed by carefully knocking off the 96-well plate on paper towels. The cells were fixed in 100 µl 4% PFA solution/well for 10 min. The fixed cells were centrifuged (439xg for 4 min) and the supernatant was removed as described. Afterwards the cells were resuspended in 100 µl intracellular Blocking-Buffer/well followed by an incubation of 10 min. After renewed centrifugation (439xg for 4 min) and removal of supernatants, the cells were resuspended in 100 ml intracellular FACS-Buffer/well. Hereafter cells were again centrifuged (439xg for 4 min) and, after removal of supernatants, incubated for 30 min in primary antibody solution. The used antibody concentrations are indicated in Table 3.

Table 3: Amounts of antibodies, which were used for labeling of intracellular proteins.

Fluorochrome	Specificity	Antibody per 0.2 × 10^6 cells/100 µl intracellular FACS-Buffer
APC	Anti-Human Perforin	2 µl
Alexa Fluor 647	Anti-Human Granulysin	2 µl
Alexa Fluor 647	Anti-Human Granzyme B	2 µl
Alexa Fluor 647	Anti-Human Granzyme A	2 µl

Subsequently cells were centrifuged (439xg for 4 min) and the supernatant was removed as described. Unbound antibodies were removed by resuspending the cells in 100 µl intracellular FACS-buffer/well followed by centrifugation (439xg for 4 min). After removing the supernatants, cells were resuspended in 100 µl FACS-Buffer/well and transferred into a FACS-tube (2 ml) for flow cytometric analysis (see chapter 3.3.3).

Intranuclear immunostaining

For fluorescent labeling of intranuclear transcription factors at least 0.2 × 10^6 cells (in case of co-cultures hMDM or hMDDC) were transferred per well into a VEE shaped 96-well plate. All steps were performed at 4°C. For the immunostaining procedure we used the eBioscience™ Foxp3 / Transcription Factor Staining Buffer Set and the default protocol which was provided by the manufacturer. The used antibody concentrations are indicated in Table 4.

Table 4: Amounts of antibodies, which were used for labeling of intranuclear transcription factors.

Fluorochrome	Specificity	Antibody per 0.2 × 10^6 cells/100 µl FACS-Buffer
Pacific Blue	Anti-Human Tbet	1 µl
Alexa 647	Anti-Human GATA3	4 µl
Pacific Blue	Anti-Human FOXP3	1 µl

3.3.3 Flow cytometry

Flow cytometry was used to analyze expression of cell surface markers, intracellular proteins, intranuclear transcription factors, *Lm* infection rate and cell proliferation. As instrument, a BD LSRII Special Order Research Product with

four excitation lasers (405nm, 488nm, 561nm, 640nm) was used. The settings for each cell type were adjusted using the FACS DIVA software. FlowJo was used for analysis of the flow cytometric data.

3.3.4 ELISA

To determine specific cytokines in the supernatants of the cell culture assays, we used TNFα, IFNγ or IL-10 specific sandwich ELISA's from R&D systems according to the manufacturer's protocols.

3.4 Nucleic acid methods

To quantify the mRNA levels of hMDM1, hMDM2 or hMDDC in presence or absence of *Lm* infection relative to the housekeeping gene GAPDH, we performed the following methods.

3.4.1 RNA-Isolation

At least 0.3 × 10^6 (Non)-infected hMDM1, hMDM2 or hMDDC (see chapter 3.2.9) were pelleted (515xg, 8 min, 4°C). The supernatants were decanted, and the cell pellet was resuspended in cold PBS pH 7.1 and centrifuged again (515xg, 8 min, 4°C). To isolate RNA the Qiagen RNeasy Plus Mini Kit was used according to the manufacturer's protocol. Residual DNA in the isolated RNA was digested using 10U recombinant DNAase (Roche) and 40U RNase Out™ Ribonuclease Inhibitor (Invitrogen) for 20 min at 37°C. DNAase was heat-inactivated for 10 min at 75°C. Hereafter purity and RNA concentration was measured using the NanoDrop 2000C according to the manufacturer's protocol. RNA was further used in chapter 3.4.2 or 3.4.3.

3.4.2 Polymerase chain reaction (PCR)

To quantify mRNA levels correctly, the isolated RNA had to be free of genomic DNA. To check for genomic DNA, the following GAPDH PCR was pipetted and performed using the Biometra Personal Cycler:

Table 5: Composition of the GAPDH PCR.

Component	final	50 µl
10x NEB Taq-Buffer	1x	5 µl
dNTPs (2mM each)	200 µM	5 µl
GAPDH (forward) (10 µM)	0,2 µM	1 µl
GAPDH (reverse) (10 µM)	0,2 µM	1 µl
NEB Taq-Polymerase (5000 U/ml)	1,25 U	0,25 µl
cDNA [or 100ng RNA]	< 1000 ng	2 µl
RNase-free H_2O		35,75 µl

Table 6: Thermocycling conditions of the GAPDH PCR.

Programme	Temp (°C)	Time	Cycles
Initial Denaturing	95	30 sec	
Denaturing	95	30 sec	
Annealing	60	30 sec	29x
Elongation	68	30 sec	
Final Elongation	68	10 min	
Cooling	4	∞	

cDNA (GAPDH positive) was used as positive control template and H_2O as negative control template. During the PCR, a 1% w/v agarose gel was prepared by heating up 1g agarose together with 100 ml 1x TAE buffer in the microwave. The clear fluid agarose solution was mixed with 2 µl ethidium bromide and poured into a gel tray with a well comb in place. The solidified gel was placed into the gel box and covered completely with 1x TAE-Buffer. PCR products (50 µl) were mixed with 5.5 µl 10x DNA Loading Buffer. Per sample, 10 µl was loaded into the pocket of each lane. In the first two lanes 5µl of a molecular weight ladder (1 kb and 100bp DNA ladder) was added. Gel electrophoresis took place at 100V for 45 min. PCR products were visualized by an UV transilluminator. When no band was observed in the samples at the level of the GAPDH band (positive control), the RNA was used for cDNA synthesis. Otherwise, DNA digestion was repeated.

3.4.3 cDNA synthesis

We used the Promega™ ImProm-II™ Reverse Transcription System to transcribe RNA into more stable cDNA. 100 ng RNA was mixed with 0.5 µg random primers in H_2O (final volume 5 µl) in PCR tubes (0.2 ml). The tubes were heated to 70 °C for 5 min followed by a cooling step (4 °C for 5 min). The tubes were spinned down and the ingredients for the reverse transcriptase reaction were added:

Table 7: Ingredients of the reverse transcriptase reaction.

Component	Volume
RNase-free H_2O	6.5 µl
5x Reaction Buffer	4 µl
Magnesiumchloride	2 µl
dNTPs Mix	1 µl
RNasin Inhibitor	0.5 µl
Reverse Transcriptase	1 µl

Afterwards cDNA was synthesized in the Biometra Personal Cycler using the following thermocycler program:

Table 8: Thermocycling conditions for cDNA synthesis.

Programme	Temp (°C)	Time
Primerannealing	25	5 min
First-strand synthesis	42	60 min
Inactivation of reverse transcriptase	70	15 min
	4	∞

cDNA concentration was determined using the NanoDrop 2000C and cDNA was stored at -20 °C until use (see chapter 3.4.4).

3.4.4 Quantitative real-time polymerase chain reaction (qRT-PCR)

To assess the mRNA levels of PD-L1, PD-L2 relative in (Non-)infected hMDM1, hMDM2 or hMDDC relative to the reference gene GAPDH we used the MESA Blue qPCR MasterMix Plus for SYBR plus the LightCycler® 480 system (Roche). The components for the qRT-PCR were pipetted into a Light Cycler 96-well plate:

Table 9: Components for the qRT-PCR.

Component	Volume
RNase-free H_2O	6 µl
Primer forward (10 µM)	1 µl
Primer reverse (10 µM)	1 µl
MESA Blue qPCR MasterMix Plus	10 µl
cDNA	2 µl

Samples were prepared in duplicates for each primer pair (target genes: PD-L1 and PD-L2; housekeeping gene: GAPDH; for primer sequence go to chapter 2.10). Additionally a control was added, were cDNA was replaced by H_2O. The Light Cycler 96-well plate was shortly spinned down, sealed with a clear foil and qRT-PCR was performed using the following Light Cycler programme:

Table 10: Light Cycler programme.

Programme	Temp (°C)	Time	°C/s
Activation	95	10 min	4.4
Amplification (45 Cycles)			
Denaturation	95	10 sec	4.4
Annealing	60	10 sec	2.2
Elongation	72	15 sec	4.4
Final Elongation	85	10 sec	4.4
Melting Curve	60-99	continuous	0.11
Cooling	40	20 min	2.2

The absolute Crossing point (CP) values were determined in the Light Cycler software using the Absolute quantification/2nd derivate max algorithm. Relative gene expression was calculated using the $2^{-\Delta\Delta CT}$ threshold cycle method (CT) (Livak and Schmittgen, 2001). GAPDH was used as housekeeping gene. The level of gene expression was determined relative to that of uninfected cells for the indicated time point.

3.5 Statistical analysis

Samples were tested for normal Gaussian distribution using D'Agostino-Pearson omnibus normality test. In case of normally distributed paired samples a parametric paired t test was performed. Otherwise, the Wilcoxon signed-rank test was used. For Gaussian distributed unpaired samples the unpaired t test with Welch's correction was used. All calculations were done using Graph-Pad Prism version 7. A value of $P<.05$ was considered statistically significant. Pearson's r correlations were also calculated by Graph-Pad Prism version 7. $r \geq 0.7$ indicates a positive correlation; $r \leq -0.7$ indicates an inverse correlation.

4 Results

4.1 PD-1 ligands were inducible on hMDM1, hMDM2 and hMDDC upon IFNγ stimulation

PD-L1 is expressed on a variety of cells whereas PD-L2 expression is mostly restricted to myeloid cells (Francisco et al., 2010). Both PD-1 ligands have been reported to be strongly induced upon IFNγ stimulation on different cancer cell lines and macrophages or dendritic cells (Yamazaki et al., 2002; Flies and Chen, 2007). To examine the suitability of our chosen PD-L1 and PD-L2 antibody clones for flow cytometric detection, we tested the induction of PD-1 ligands on monocyte-derived macrophages and dendritic cells. Therefore we generated $CD14^+CD163^-$ pro-inflammatory macrophages (hMDM1), $CD14^+CD163^+$ anti-inflammatory macrophages (hMDM2) or $CD1a^+CD14^-$ dendritic cells (hMDDC) as described (Crauwels, 2015). Subsequently we stimulated all cell types for 24h with 100 U/ml of recombinant IFNγ. Hereafter we immunostained PD-L1 and PD-L2 and analyzed the cells by flow cytometry **(Figure 8)**. The representative histograms illustrate, that PD-L1 and PD-L2 expression is increased on hMDM1, hMDM2 and hMDDC after IFNγ stimulation compared to the unstimulated controls **(Figure 8A)**. For quantification, the relative fluorescence intensity (RFI) was measured as the ratio of the mean fluorescence intensity of specific markers and the mean fluorescence intensity of isotype controls. By analyzing the cells of three donors, we detected low basal levels of PD-L1 on hMDM1 (mean RFI±SD: 1.88 ± 0.94) and hMDM2 (mean RFI±SD: 1.28 ± 0.53). Basal expression of PD-L1 on hMDDC (mean RFI±SD: 6.39 ± 2.16) tended to be higher compared to hMDM1 and hMDM2. IFNγ stimulation strongly induced PD-L1 expression on hMDM1 (mean RFI±SD: 6.44 ± 3.05), hMDM2 (mean RFI±SD: 17.15 ± 9.13) and hMDDC (mean RFI±SD: 22.28 ± 9.47) compared to the unstimulated control **(Figure 8B)**. Similarly, PD-L2 was little expressed on hMDM1 (mean RFI±SD: 3.06 ± 1.22), hMDM2 (mean RFI±SD: 1.90 ± 0.644) and hMDDC (mean RFI±SD: 8.23 ± 7.90). Analogous to PD-L1, IFNγ stimulation increased PD-L2 expression on hMDM1 (mean RFI±SD: 20.37 ± 28.06), hMDM2 (mean RFI±SD: 11.16 ± 7.83) and hMDDC (mean RFI±SD: 30.84 ± 30.96).

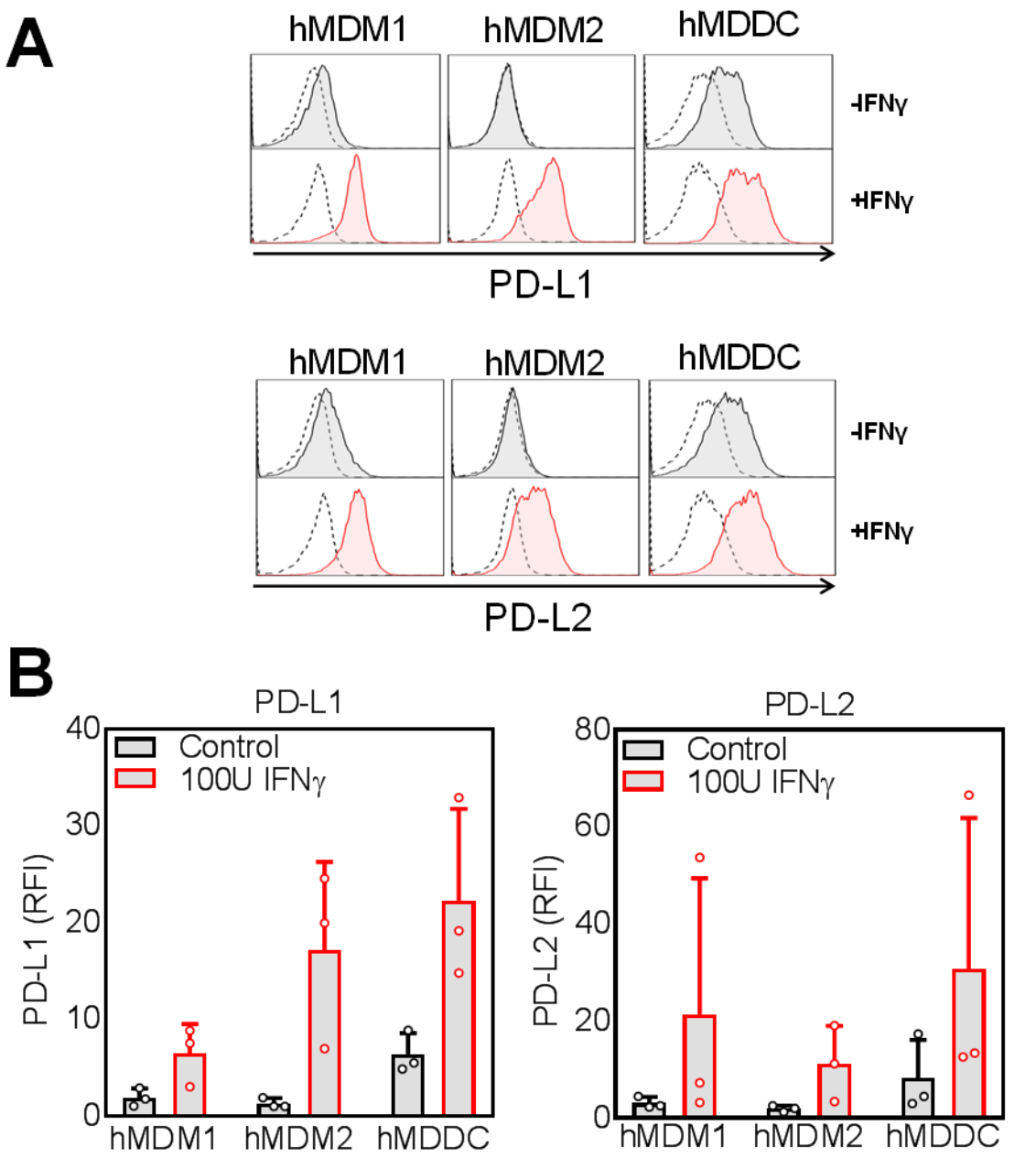

Figure 8: PD-1 ligand expression increased upon IFNγ stimulation.

hMDM1, hMDM2 or hMDDC were cultivated in presence or absence of 100 U/ml recombinant IFNγ for 24h at 37 °C, 5% CO_2. Subsequently, cells were harvested, immunostained (PD-L1; PD-L2) and analyzed by flow cytometry. hMDM1, hMDM2 and hMDDC were gated via their FSC/SSC properties. **(A)** Representative histograms of PD-L1 and PD-L2 expression on hMDM1, hMDM2 and hMDDC in presence (red histogram) or absence (black histogram) of IFNγ. The black dotted line displays the signal of the isotype control. **(B)** Data is presented as mean ± SD RFI (ratio of the mean fluorescence intensity of specific markers to the mean fluorescence intensity of isotype controls). Two independent experiments were performed (N = 3).

With this experiment, we proofed the performance of our detection antibodies. In the next step, we used these antibodies to analyze whether *Leishmania* infection of macrophages or dendritic cells affects the surface expression of PD-1 ligands on these phagocytes.

4.2 *Leishmania major* infection differently modulated PD-1 ligand expression on hMDM1, hMDM2 and hMDDC.

To assess whether PD-1/PD-Ligand (PD-1/PD-L) interactions can influence *Leishmania major* (*Lm*) infection of human myeloid cells, we first examined mRNA and surface protein expression of PD-L1 and PD-L2 on *Lm*-infected hMDM1, hMDM2 and hMDDC. We analyzed all three host cell types, as their individual roles in human *Lm* disease are insufficiently clarified. 24h after infection, RNA was isolated from the infected cells, cDNA was generated and a quantitative real time PCR (qRT-PCR) was performed. Data was normalized to GAPDH, which is a housekeeping gene of macrophages and dendritic cells. QRT-PCR results revealed significantly more PD-L1 mRNA after *Lm* infection in hMDM1 (5.81±2.47 fold), hMDM2 (11.17±1.85 fold) and hMDDC (3.27±1.85 fold) relative to the uninfected control **(Figure 9A)**. PD-L2 mRNA levels were also significantly increased after *Lm* infection in hMDM1 (4.39±2.63 fold), hMDM2 (5.33±3.29 fold) and hMDDC (3.09±1.54 fold) relative to the uninfected control **(Figure 9A)**. Because mRNA levels often do not correlate with protein levels, we additionally quantified the cell surface protein density of both PD-L1 and PD-L2 by flow cytometry. Low levels of PD-L1 were detected on hMDM1 (RFI: 1.42±0.28) and hMDM2 (RFI: 1.21±0.23) **(Figure 9B)**. After *Lm* infection, expression of both ligands significantly increased (hMDM1: RFI: 2.01±1.09 and hMDM2: RFI: 1.78±0.41, respectively). Interestingly, basal surface expression of PD-L1 on hMDDC (RFI: 2.13±0.37) was higher compared to hMDM1 or hMDM2, which however did not increase upon *Lm* infection (RFI: 2.33±0.36). Focusing on PD-L2 expression, a low basal surface expression was observed on hMDM1 (RFI: 1.91±0.88), hMDM2 (RFI: 1.90±0.74) and hMDDC (RFI: 3.27±2.36). During *Lm* infection, PD-L2 surface expression significantly increased on hMDM1 (RFI: 2.78±1.44). However, surface expression levels of PD-L2 on hMDM2 and hMDDC did not differ in presence or absence of *Lm* infection **(Figure 9B)**.

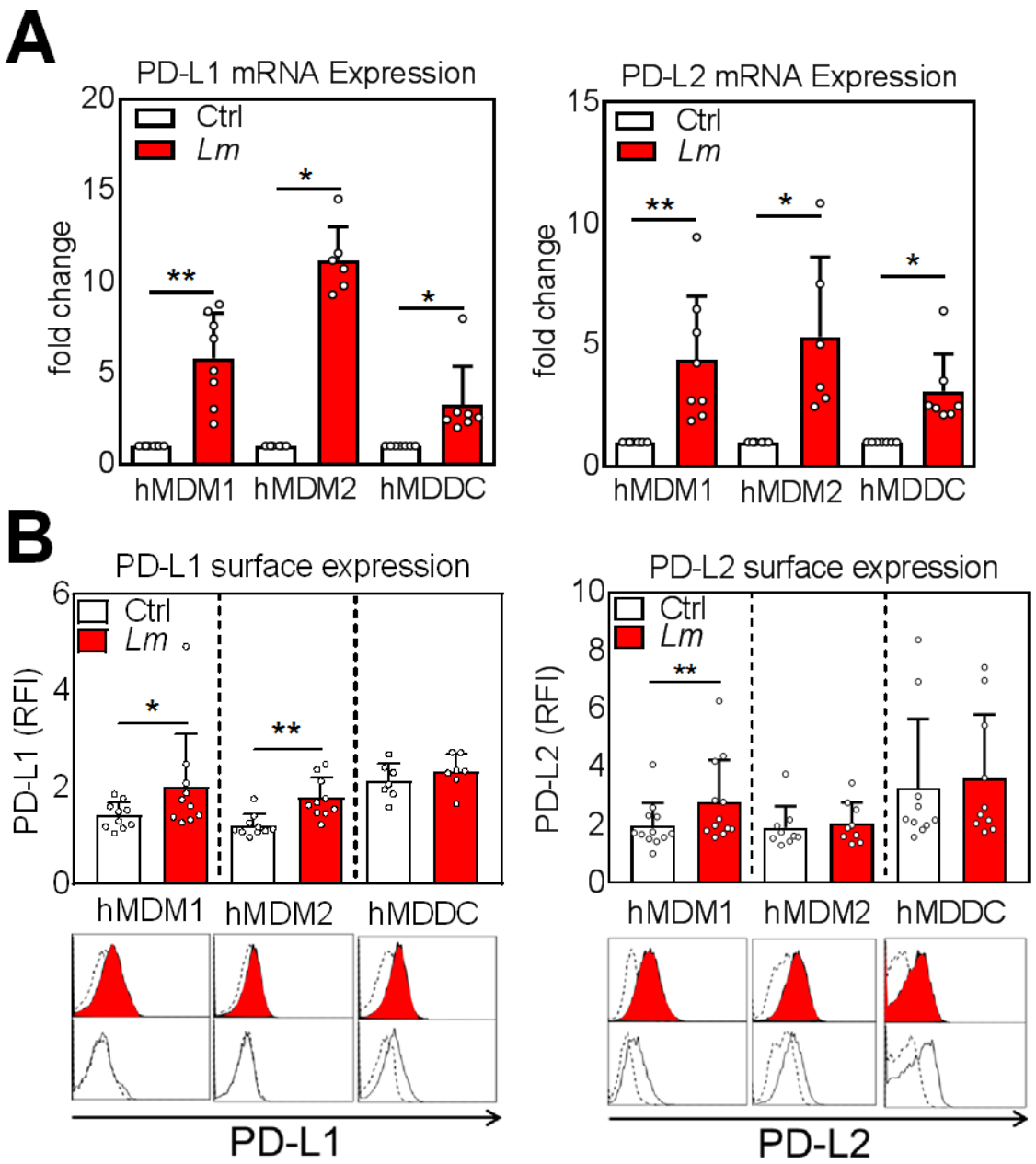

Figure 9: PD-L1/PD-L2 expression on hMDM and hMDDC after *Lm* infection.

hMDM1, hMDM2 or hMDDC were infected with *Lm* for 24h (MOI10). **(A)** RNA-Isolation, cDNA synthesis and qRT-PCR using Light Cycler 480 were carried out as described in the methods chapter. Data is presented as mean fold change ± SD. Statistics were calculated by Wilcoxon matched-pairs signed rank test, $P<0.05$ is considered statistically significant (*$P<0.05$; **$P<0.01$). At least, three independent experiments were performed (N = 6 - 8). **(B)** PD-L1 or PD-L2 surface expression levels were determined by flow cytometry. hMDM and hMDDC were gated using their FSC/SSC properties. Data is presented as mean ± SD RFI (ratio of the mean fluorescence intensity of specific markers to the mean fluorescence intensity of isotype controls). Representative histograms for a surface marker staining of PD-L1 and PD-L2 on infected (red filled histogram) or non-infected (black non-filled histogram) hMDMs or hMDDC, compared to the respective isotype control (black dashed line). Statistics were calculated by Wilcoxon matched-pairs signed rank test, $P<0.05$ is considered statistically significant (*$P<0.05$; **$P<0.01$). At least three independent experiments were performed (N =7-9).

Taken together, we showed that PD-L1 and PD-L2 are expressed on all three host cell types and synthesis of PD-L1 and PD-L2 mRNA is upregulated upon *Lm* infection. In contrast, elevation of PD-L1 and PD-L2 protein surface expression after *Lm* infection was not observed for all host cell types.

4.3 *Leishmania* strain specific PD-L1 expression on infected macrophages

Next, we asked whether the surface expression of the PD-1 ligands differ when using different *Leishmania* strains. Thus, we infected hMDM1, hMDM2 and hMDDC with *Lm* or with *Leishmania aethiopica* (*Lae*). *Lae* causes diffuse cutaneous leishmaniasis which can become chronic, whereas *Lm* causes acute cutaneous leishmaniasis that is self-healing in most cases (Mandell and Douglas; van Griensven et al., 2016). Analyzing the cells of three donors, levels of PD-L1 on *Lm*-infected hMDM1 (mean RFI±SD: 3.17 ± 1.54) tended to be higher compared to *Lae*-infected hMDM1 (mean RFI±SD: 1.68 ± 0.46) **(Figure 10A)**. The same was true for hMDM2 (*Lm*-infected: 1.87 ± 0.46; *Lae*-infected: 1.14 ± 0.10) and hMDDC (*Lm*-infected: 2.60 ± 0.21; *Lae*-infected: 2.13 ± 0.50).

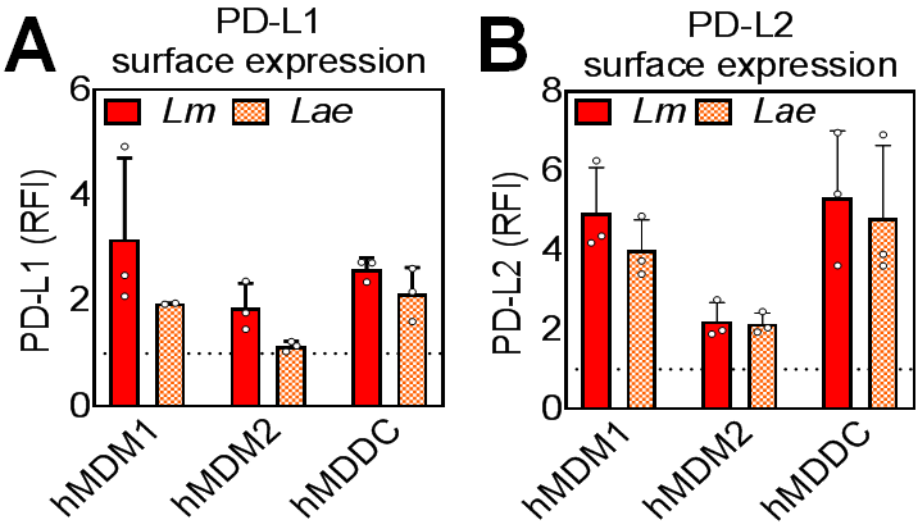

Figure 10: *Lm* infection induced higher PD-L1 expression on macrophages than *Lae* infection.

hMDM1, hMDM2 or hMDDC were either infected with *Lm* or *Lae* for 24h (MOI10) at 37 °C 5% CO_2. **(A)** PD-L1 or **(B)** PD-L2 surface expression levels were determined via flow cytometry. hMDM and hMDDC were gated using their FSC/SSC properties. Data is presented as mean ± SD RFI. Two independent experiments were performed (N = 3).

PD-L2 expression was also higher on *Lm*-infected hMDM1 (mean RFI±SD: 4.94 ± 1.15) by trend compared to *Lae*-infected hMDM1 (mean RFI±SD: 4.00 ± 0.77) **(Figure 10B)**. hMDM2 (*Lm*-infected: 2.21 ± 0.48; *Lae*-infected: 2.15 ± 0.27) and hMDDC (*Lm*-infected: 5.34 ± 1.68; *Lae*-infected: 4.81 ± 1.83) did not differ in their PD-L2 expression upon infection with *Lm* or *Lae*. Due to generally higher expression of PD-1 ligands on all three host cell types after *Lm* infection, we decided to continue our further experiments with the *Lm* strain.

4.4 A host cell:PBLs ratio of 1:5 was optimal for determination of *Lm*-induced lymphocyte proliferation

Several research groups including ours previously showed that there is a *Leishmania*-specific T-cell response *in vitro* when using leukocytes of *Leishmania*-naïve blood donors (Kemp et al., 1992; Russo et al., 1998; Pompeu et al., 2001; Bourreau et al., 2002; Sassi et al., 2005; Ettinger and Wilson, 2008; Crauwels et al., 2015). To analyze this early *Lm*-induced T-cell response with regard to PD-1/PD-L interactions, we applied a co-culture assay that has been established in our laboratory (Crauwels, 2015) where fluorescently labeled (non-)infected hMDM (or hMDDC) had been co-cultivated with fluorescently labeled autologous peripheral blood lymphocytes (PBLs) in a ratio of host cell:PBLs equals 1:5.

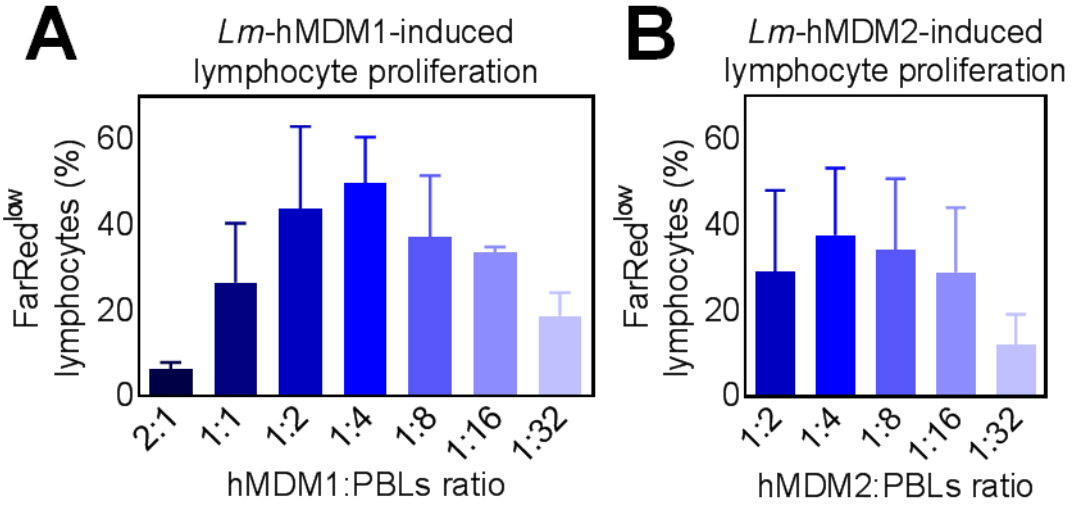

Figure 11: The impact of different hMDM:PBLs ratios on *Lm*-induced lymphocyte proliferation.

FarRed-labeled autologous PBLs were co-cultivated with **(A)** *Lm*-infected hMDM1 or **(B)** hMDM2 at different ratios (as indicated in the figure). After five days, cells were harvested and analyzed by flow cytometry. Lymphocytes were gated via their FSC/SSC properties. Lymphocyte proliferation was assessed by gating on the FarRed^{low} cells. Data is presented as

mean percentage of the FarRed^{low} lymphocytes ± SD. At least two independent experiments were performed (N = 3 - 5).

To investigate whether this ratio is optimal for assessment of lymphocyte proliferation, we exemplarily tested several other hMDM1:PBLs and hMDM2:PBLs ratios **(Figure 11)**. Both, for hMDM1 **(Figure 11A)** and hMDM2 **(Figure 11B)**, a hMDM:PBLs ratio of 1:4 induced the highest T-cell proliferation. Due to this data we did not alter the initial assay setup and proceeded with a hMDM:PBLs ratio of 1:5 for the following experiments.

4.5 PD-1 expression on T-cells was increased after co-incubation with *Lm*-infected host cells

Next, we investigated whether *Lm*-infected hMDM1, hMDM2 or hMDDC have an effect on PD-1 expression of T-cells. To this end, we co-cultivated autologous PBLs, mainly consisting of T-cells, together with one of the three different *Lm*-infected host cell types for 5 - 7 days at 37 °C and 5% CO_2 and determined the PD-1$^+$CD3$^+$T-cells by flow cytometric analysis **(Figure 12)**.
The representative dot blot indicates that only a fraction of the T-cells in the co-cultures was PD-1$^+$ **(Figure 12A)**. Compared to the uninfected control, a significantly higher percentage of PD-1$^+$T-cells was detected in the *Lm*-infected hMDM1 co-culture (10.17±7.90 %; 22.23±7.80 %) **(Figure 12B)**, *Lm*-infected hMDM2 co-culture (8.70±4.19 %; 17.22±7.98 %) **(Figure 12C)** and *Lm*-infected hMDDC co-culture (9.24±2.76 %; 21.75±1.99 %) **(Figure 12D)**. The different *Lm*-infected host cells increased the percentage of PD-1$^+$ T-cells to a similar degree. In all, we found that *Lm*-infected host cells induced PD-1$^+$ T-cells. Together with the determined PD-1 ligand expression on *Lm* host cells, these preliminary data encouraged us to investigate the impact of PD-1 checkpoint inhibition in *Leishmania* infection of primary human cells.

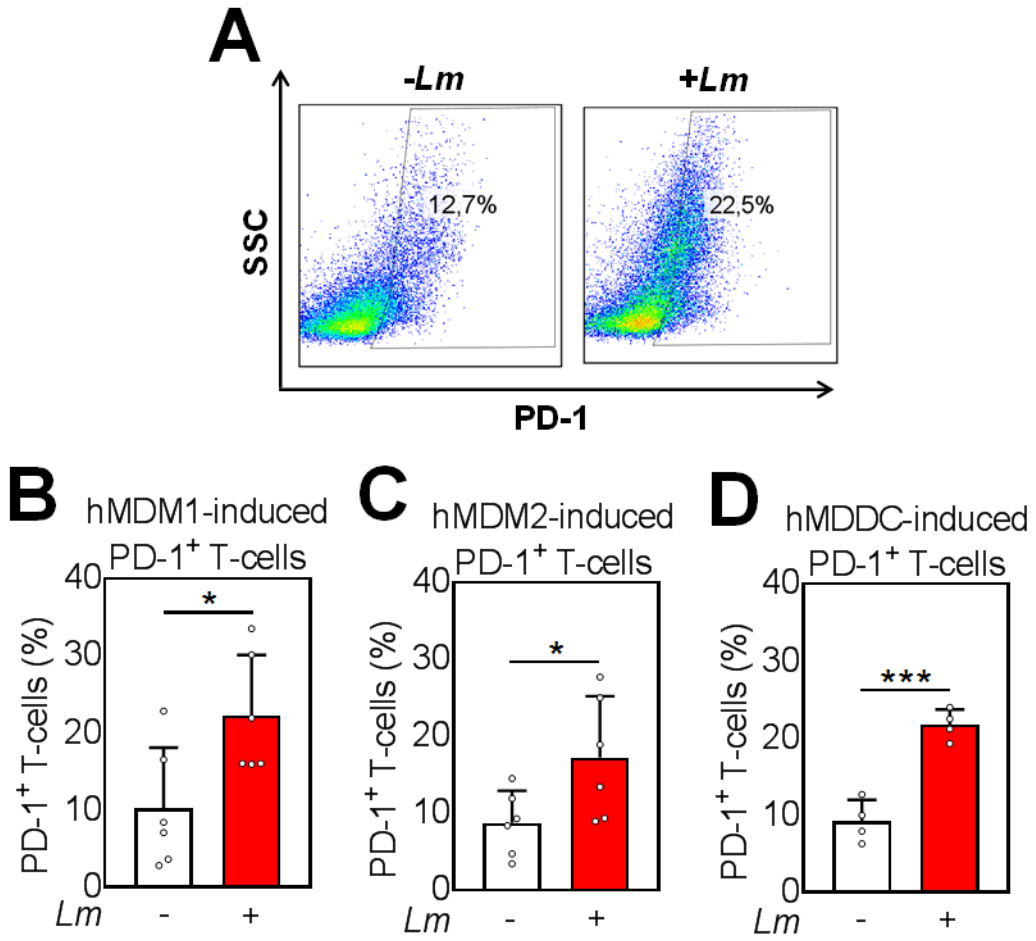

Figure 12: Increased number of PD-1$^+$ T-cells after autologous co-culture with *Lm*-infected hMDM or hMDDC.

Lm-infected hMDM1, hMDM2 or hMDDC were co-cultivated with autologous PBLs for 5 - 7d at 37 °C, 5%CO_2. Afterwards, cells were harvested, immunostained (PD-1, CD3) and analyzed by flow cytometry. T-cells were gated via their FSC/SSC properties and the T-cell marker CD3. **(A)** Representative dot blot showing the percentage of PD-1$^+$ T-cells in the infected (+*Lm*) and non-infected sample (-*Lm*). Gating was determined by referring to the isotype control. **(B, C, D)** Data is presented as mean percentage of PD-1$^+$ T-cells ± SD. At least two independent experiments were performed (N = 4 - 6). Statistics were calculated by a parametric paired t test, $P<0.05$ is considered statistically significant (*$P<0.05$; ***$P<0.001$).

4.6 PD-1/PD-L blockade did not affect *Lm* infection rate and T-cell proliferation in an *in vitro* model mimicking the early T-cell response

First, to assess T-cell proliferation in a co-culture of autologous PBLs with *Lm*-infected host cells, all cells were labeled with a proliferation dye (CFSE or Far Red). On the day of flow cytometric analysis, proliferating T-cells were gated by their FSC/SSC properties, the T-cell marker CD3 and CFSE or FarRed^{low} **(Figure 13A)**. The host cells were infected with a fluorescent transgenic dsRED strain of *Lm*, which is detectable by flow cytometry. To determine infection rate,

host cells were gated first via their FSC/SSC properties, second by proliferation dye^{high} and third on the dsRED^{+} cells **(Figure 13B)**.

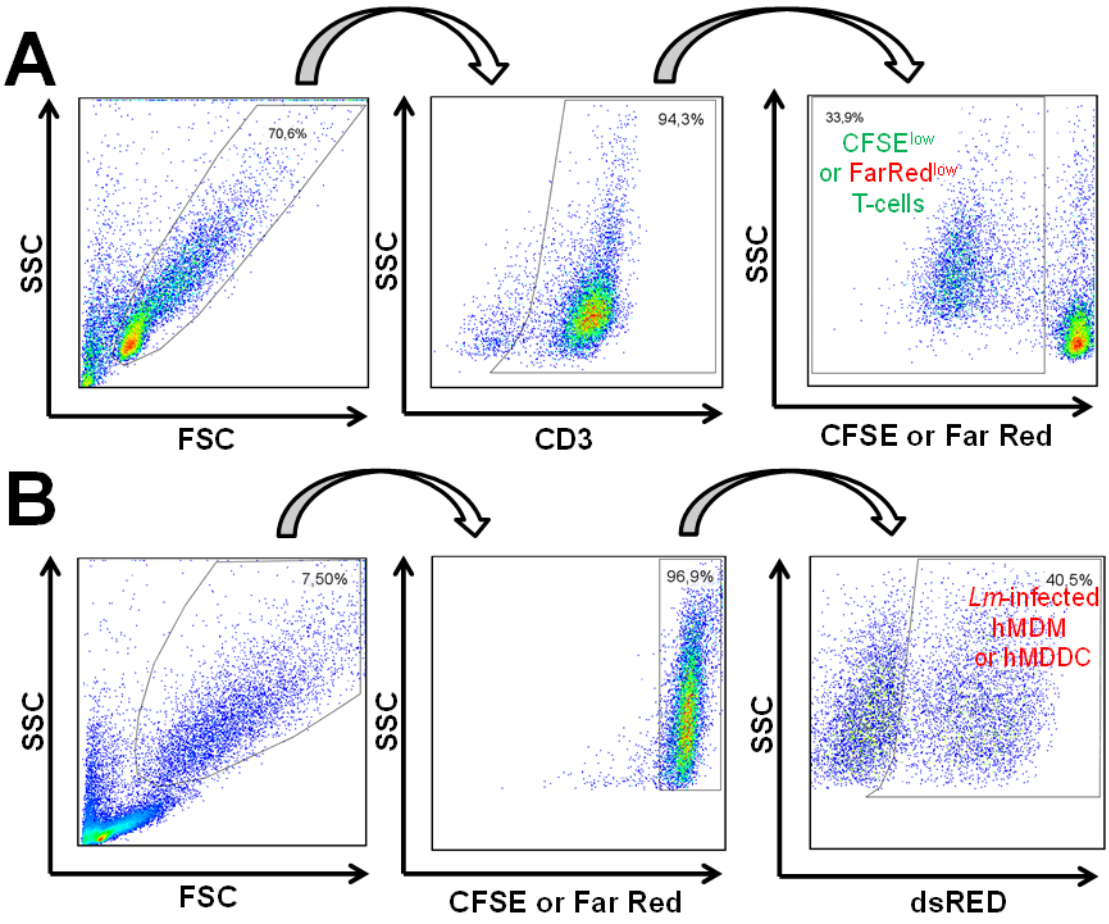

Figure 13: Gating strategy for flow cytometric analysis of T-cell proliferation and *Lm* infection rate.

(A) Lymphocytes were gated via their FSC/SSC properties. Among the lymphocyte population all T-cells were gated for their CD3 positivity. Among all T-cells, only the proliferation dye^{low} cells were considered, which represent T-cells that underwent cell division. **(B)** hMDM and hMDDC were gated via their FSC/SSC properties. Among the hMDM or hMDDC population, proliferation dye^{low} lymphocytes were removed by gating only on the proliferation dye^{high} cells. From these cells only the dsRED^{+} cells were considered, which represent the percentage of *Lm*-infected cells or the *Lm* infection rate.

In a control experiment we proofed that the proliferation dyes CFSE and Far Red yield similar results **(Figure 14)**. Next, to modulate the PD-1/PD-L interaction, we made use of two blocking antibodies: a humanized IgG1 anti-PD-1 monoclonal antibody (αPD-1 IgG1; G&P Biosciences, research grade) and the therapeutically used fully-human IgG4 anti-PD-1 monoclonal antibody nivolumab (αPD-1 IgG4; Bristol-Myers Squibb, GMP grade). Prior to their

application in the co-culture experiments, both antibodies were titrated for optimal performance and to minimize off-target effects.

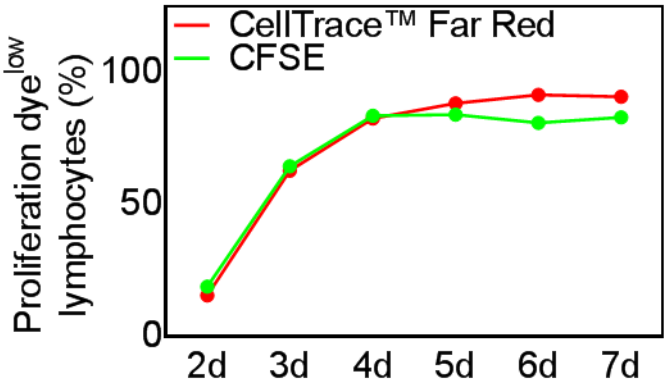

Figure 14: CFSE and CellTrace™ Far Red yield similar results with respect to T-cell proliferation.

PBLs of one donor were labeled either with CFSE or Far Red. Hereafter PBLs were stimulated with 0.5µg/ml phytohemagglutinin (PHA) at 37°C, 5%CO_2 for 7d. From day 2 on, cells were analyzed by flow cytometry. Proliferating lymphocytes were gated via their FSC/SSC properties and proliferation dye^{low}.

As positive control we stimulated PBLs of one donor with phytohemagglutinin for 3d at 37°C, 5% CO_2. After this period, almost all lymphocytes were PD-1^+. Then we incubated 0.2 × 10^6 PHA-stimulated PBLs with six different concentrations of either of the blocking antibodies (10^{-4} - 10^1 µg/ml) in 200 µl CM. After washing away unbound anti-PD-1 antibodies, we labeled the PD-1 bound blocking antibodies by using a PE-labeled secondary Fab_2 fragment against human IgG. Flow cytometric analysis revealed that PD-1 receptors were saturated, when using a blocking antibody concentration between 0.1 and 1 µg/ml, as there was no further increase in fluorescence with higher concentrations **(Figure 15A and B)**. For blocking experiments we used a concentration between 0.1 - 1 µg/ml. Due to practical reasons the final blocking concentration was 0.625 µg/ml. Initial experiments were done using the αPD-1 IgG1.

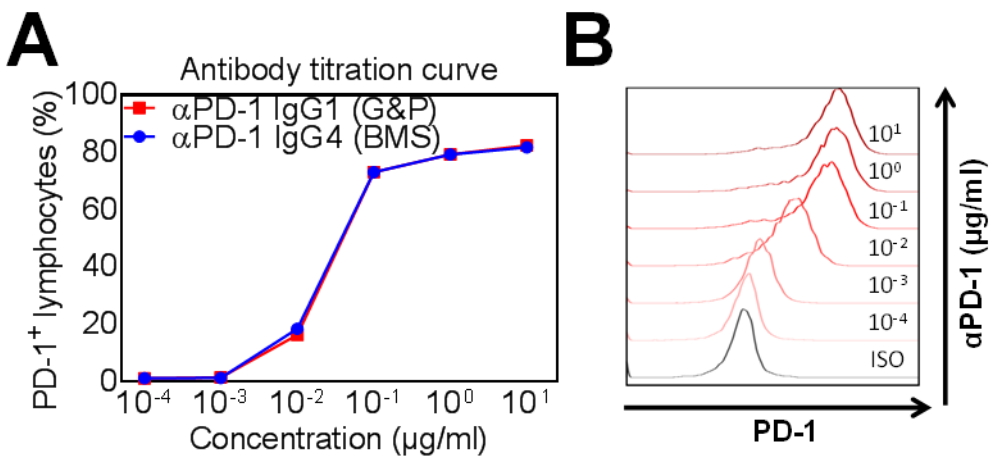

Figure 15: Titration of a humanized IgG1 and a fully human IgG4 anti-PD-1 blocking antibody.

(A, B) PBLs of one donor were stimulated with 0.5 µg/ml phytohemagglutinin (PHA) for 3d at 37°C, 5%CO_2 to induce the maximal expression of PD-1 on lymphocytes. Hereafter 0.2 × 10^6 PHA-stimulated PBLs were resuspended in 200 µl CM and blocked at the indicated concentrations either with a humanized IgG1 anti-PD-1 monoclonal antibody (αPD-1 IgG1; G&P Biosciences, research grade) or the fully-human IgG4 anti-PD-1 monoclonal antibody nivolumab (αPD-1 IgG4; Bristol-Myers Squibb, GMP grade) for 30 min at 37 °C. Non-bound blocking antibody was removed by washing and PD-1 bound antibodies were stained with a secondary PE-labeled Fab_2 fragment targeting the Fc part of human IgG as described in methods. Cells were analyzed by flow cytometry. PD-1^+ lymphocytes were gated via their FSC/SSC properties and PE.

First, we investigated whether PD-1 blockade has an impact on *Lm* infection rate of hMDM1, hMDM2 and hMDDC in the absence of PBLs **(Figure 16A)**. As PD-1 was not detectable on any of the three host cell types in preliminary experiments **(data not shown)**, we did not expect to see an effect related to PD-1 blockade, but maybe due to Fc gamma receptor (FcγR) engagement. No significant differences were observed regarding the *Lm* infection rate of hMDM1, hMDM2 or hMDDC in presence or absence of αPD-1 IgG1 **(Figure 16A)**. Next, we analyzed whether PD-1 blockade has an effect on *Lm*-induced T-cell proliferation and *Lm* infection rate in the autologous co-culture **(Figure 16B)**.

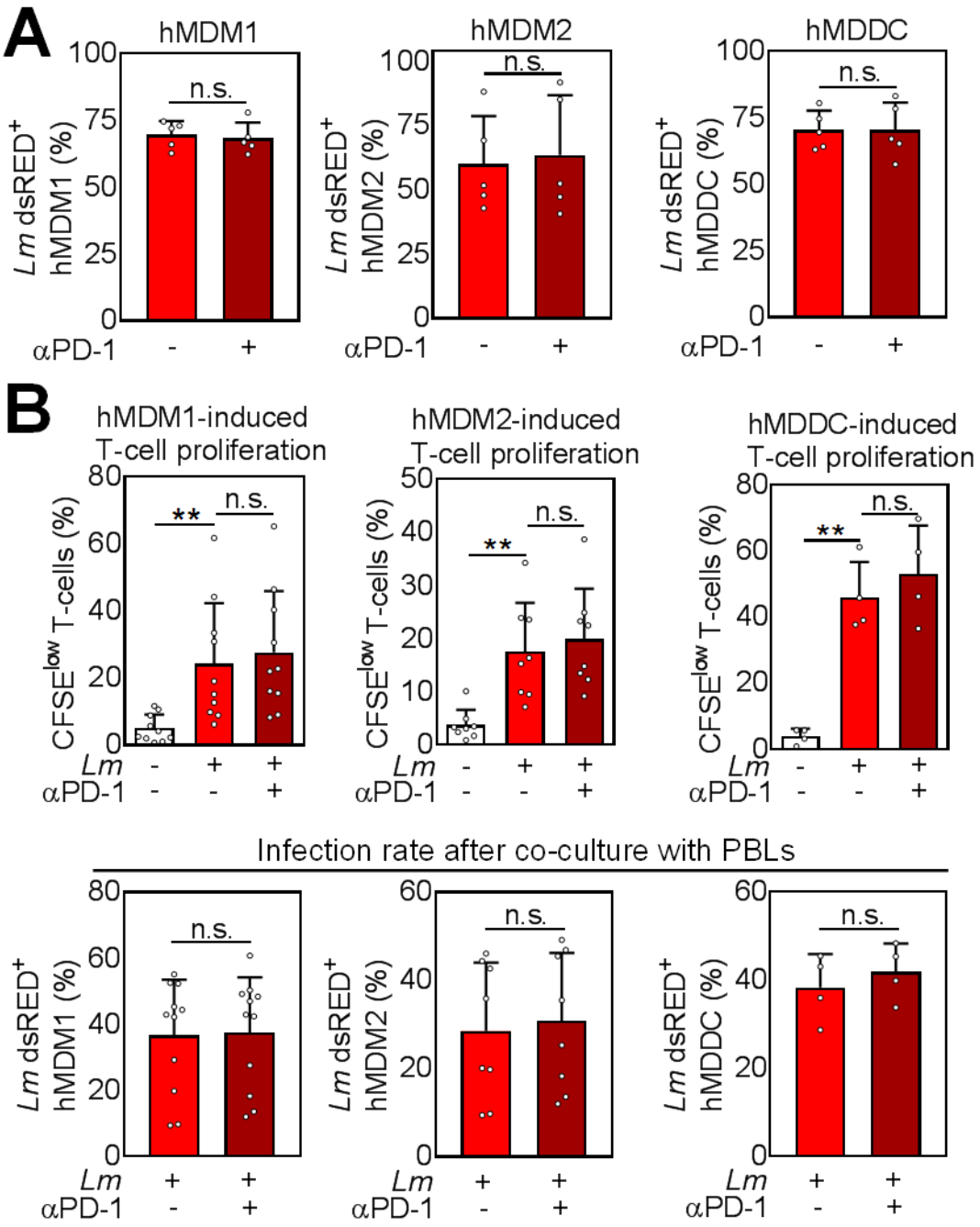

Figure 16: PD-1 blockade has no impact on *Lm* infection rate or T-cell proliferation.

(A) (Non-)*Lm* dsRED-infected hMDM1, hMDM2 or hMDDC were blocked with 0.625 µg/ml αPD-1 (IgG1) followed by an incubation for 5d at 37°C. **(B)** (Non-)*Lm* dsRED-infected hMDM1, hMDM2 or hMDDC were co-cultivated with CFSE-labeled autologous PBLs and blocked with 0.625 µg/ml αPD-1 (IgG1) followed by an incubation for 5d at 37°C. *Lm* infection rate and T-cell proliferation was measured as depicted in the gating strategy by flow cytometry **(Figure 13)**. Statistics were calculated by a parametric paired t test, $P<0.05$ is considered statistically significant (*$P<0.05$; **$P<0.01$; n.s.: not significant). At least two independent experiments were performed (N = 4 - 10).

Compared to the non-infected control, *Lm*-infected hMDM1 significantly induced T-cell proliferation (5.00±4.06 %, 24.23 ±18.07%). PD-1 blockade did not significantly alter proliferation rate of T-cells in the *Lm*-infected hMDM1 co-culture (27.63±18.21%). In analogy, *Lm*-infected hMDM2 or *Lm*-infected hMDDC significantly induced T-cell proliferation compared to the non-infected control (hMDM2: 17.51±9.22%, 3.74±2.85%; hMDDC: 45.88±10.74%, 3.83±2.32%). Here as well, PD-1 blockade did not significantly alter T-cell proliferation (hMDM2: 19.9±9.53%; hMDDC: 53.00±14.62%). A similar picture emerged, when analyzing the infection rate of the host cells in the three co-cultures. *Lm*-infection rate in the hMDM1 (37.50±16.72%, 36.64±16.86%), hMDM2 (30.79±15.45%, 28.53±15.49%) and hMDDC (41.88±6.43%, 38.33±7.58%) co-culture was not significantly different in the presence of PD-1 blockade compared to infection alone **(Figure 16B)**. Even though we showed that PD-1 and its ligands are higher expressed in our *in vitro* model after *Lm* infection, we concluded that those surface proteins are still too low expressed to observe a significant effect of PD-1 blockade. Excessive amounts of activating signals during T-cell priming could have masked PD-1/PD-L-mediated inhibitory signals.

In the here presented *in vitro* model, we used primary human cells of *Leishmania*-naïve blood donors. Hence, this model mimics the early interaction of (naïve) T-cells with *Lm*-infected cells (Rogers and Titus, 2004). During the early priming phase of T-cell activation PD-1/PD-L interactions are not very prominent (Ribas, 2012). Thus, we continued with a different assay setup.

4.7 High density pre-culture of PBMCs increased *Lm*-induced T-cell proliferation

Previously published studies about mouse models demonstrated that naïve T-cells very quickly lose their sensitivity to foreign antigen in the periphery once they left the cell-dense thymus. On the other hand, naïve T-cells in close contact to self-MHC presenting cells gain a pre-activated state, resulting in a more rapid response after foreign antigen encounter (Garbi et al., 2010). Römer and colleagues established an *in vitro* assay, where PBMCs are pre-cultured for a short time under high density conditions. During this pre-culture step, T-cells regain properties that they had in the lymph node or in cell-dense areas (Römer et al., 2011). This so called “RESTORE” assay, was the first *in vitro* assay that

reflected the fatal side effects that occurred during the clinical trial with the superagonistic TGN1412 monoclonal antibody (Suntharalingam et al., 2006). We sought to modify this "RESTORE" assay in order to analyze the effects of PD-1 checkpoint inhibitors on *Lm* infection. Hence, CFSE-labeled PBMCs were cultivated for 2d at 37 °C at low (LD, 1 × 10^6 PBMCs/ml) and high (HD, 10 × 10^6 PBMCs/ml) density. To check whether T-cells regained a pre-activated state during HD culture, we used TGN1412 treatment of T-cells as positive control. This antibody should only induce T-cell proliferation in the HD culture and not in the LD culture, which was the case, indeed **(Figure 17A)**.

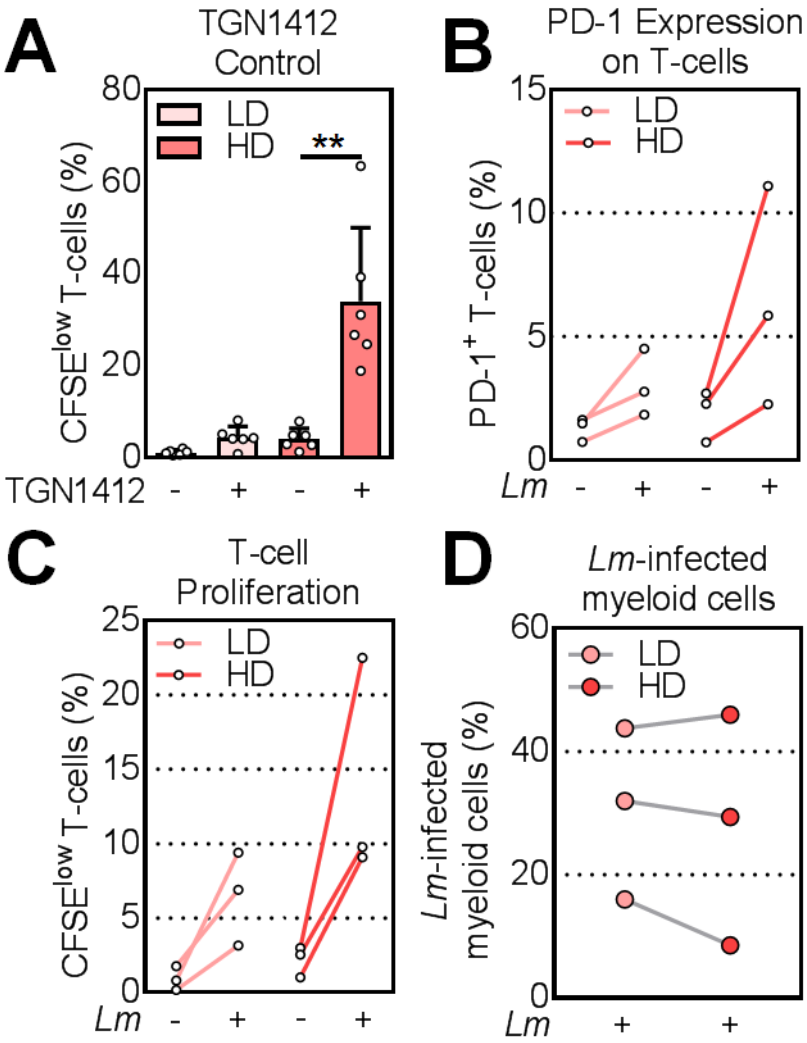

Figure 17: High density pre-culture of PBMCs tended to increase *Lm*-induced T-cell responses.

CFSE-labeled PBMCs were pre-cultivated for 2d at low (LD, 1 × 10^6 PBMCs/ml) or high (HD, 10 × 10^6 PBMCs/ml) density. Hereafter, PBMCs were further cultivated (1 × 10^6 PBMCs/ml) **(A)** together with 10µg/ml TGN1412 **(B,C,D)** or infected with *Lm* dsRED as described in the methods chapter. After 5d at 37°C, 5%CO_2, cells were immunostained (CD3, PD-1) and analyzed by flow cytometry. **(A, B, C)** T-cells were gated via their FSC/SSC properties and

CD3. **(B)** PD-1^{+} T-cells were additionally gated via the PD-1 marker. **(A,C)** T-cell proliferation was assessed by gating on the CFSE^{low} T-cells. **(D)** Myeloid cells were gated via their FSC/SSC properties. *Lm*-infection rate of these cells was measured by gating on the *Lm* dsRED^{+} cells. Data is presented as **(A)** mean ± SD (%) or **(B,C,D)** donor-specific percentage in presence or absence of *Lm* infection connected by a line. Statistics were calculated using a parametric paired t test (**=p<0.01). At least two independent experiments were performed (N = 3 - 6).

Next, we investigated expression of PD-1 in the LD and HD culture in the presence or absence of *Lm* infection. Analyzing cells from three donors, we found an increased PD-1 expression in the *Lm*-infected LD culture compared to the uninfected control. This effect was even more pronounced in the *Lm*-infected HD culture **(Figure 17B)**. Subsequently, we analyzed T-cell proliferation in the same three donors and found T-cell proliferation to be increased after *Lm*-infection in the LD and HD culture, with an, again, more distinct increase in the HD culture **(Figure 17C)**. In two of the three donors, *Lm* infection rate was slightly lower in the HD culture compared to the LD culture, whereas the opposite was observed for the third donor **(Figure 17D).** We showed that the "RESTORE" assay works in principle to investigate effects of *Lm* infection on adaptive immunity and that there are some differences regarding PD-1 expression on T-cells.

4.8 Pro-inflammatory myeloid cell phenotype after high density pre-culture

During culture of HD and LD PBMCs, monocytes can, in principle, differentiate into *Lm* host cells such as macrophages or dendritic cells. To determine the phenotype of the *Lm* host cells 5 days after/without infection, we tested for surface expression of macrophage- and dendritic cell-specific markers including PD-L1 and PD-L2 **(Figure 18)**. HLA-DR (or MHCII) was highly expressed on myeloid cells but did not significantly differ in the four conditions. The dendritic cell-specific marker CD1a was consistently not expressed in any of the four conditions. The hMDM2 specific marker CD163 was significantly lower expressed in the HD culture (24.73±15.67%) compared to the LD culture (67.30±16.57%) indicating a more pro-inflammatory milieu in the HD culture. Compared to the respective non-infected control, CD163 expression was reduced in the *Lm*-infected LD (20.94±13.35%) and HD (2.83±1.33%) culture. CD14 (macrophage and monocyte marker) was highly expressed but not

significantly different using LD (85.73±5.76%) or HD (82.57±10.76%) pre-cultured cells. In the presence of *Lm* infection, CD14 expression tended to be reduced in the LD (58.87±11.51%) and HD (35.77±19.28%) culture compared to the non-infected control.

Then, we investigated whether surface PD-L1 and PD-L2 is expressed on the myeloid cells, using LD or HD pre-cultured cells. PD-L1 expression in the LD (31.78±35.04%) and HD (27.07±30.56%) culture in the absence of infection was comparable. *Lm* infection increased PD-L1 expression to a similar extent both on LD (62.87±5.29%) and HD (59.47±2.57%) pre-cultured myeloid cells. PD-L2 expression was comparably high both in the (non-)infected LD (72.07±14.45%; 56.40±24.28%) and (non-)infected HD (66.70±6.80%; 63.40±6.50%) culture.

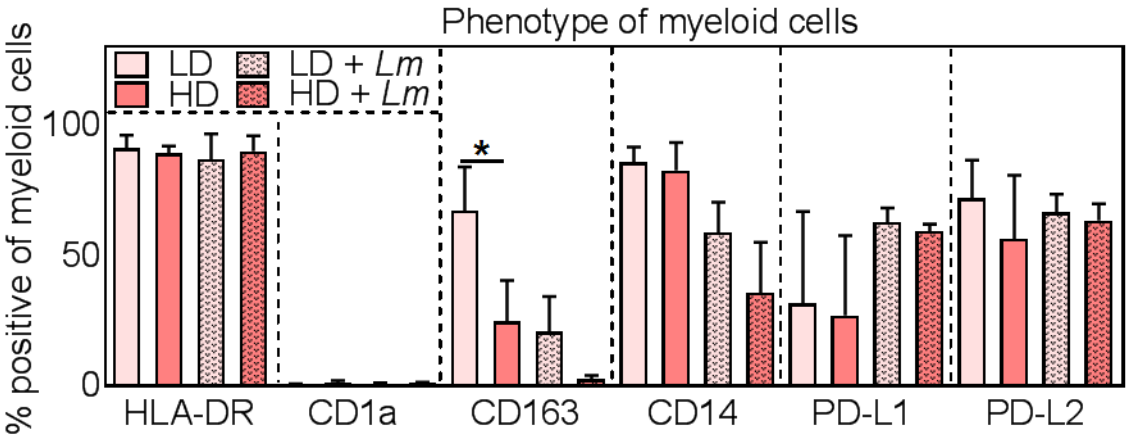

Figure 18: Phenotype of myeloid cells in the LD and HD culture in presence and absence of infection.

CFSE-labeled PBMCs were pre-cultivated for 2d at low (LD, 1 × 10^6 PBMCs/ml) or high (HD, 10 × 10^6 PBMCs/ml) density. Hereafter, PBMCs were infected with *Lm* as described in the methods chapter and were further cultivated (1 × 10^6 PBMCs/ml). After 5d at 37°C, 5%CO_2, cells were immunostained for the indicated targets and analyzed by flow cytometry. Myeloid cells were first gated via their FSC/SSC properties and subsequently by their specific marker. Data is presented as mean percentage ± SD. Statistics were calculated using a parametric paired t test (**=p<0.01). At least two independent experiments were performed (N = 3).

To conclude, HD pre-culture reduced the surface marker CD163 on myeloid cells which is specific for hMDM2 but also a surrogate marker for inflammation (Etzerodt and Moestrup, 2013). This suggests HD pre-cultured cells to be more pro-inflammatory compared to LD pre-cultured cells. Furthermore, *Lm* infection reduced macrophage specific surface markers such as CD14 and CD163. This might be due to inflammation-induced shedding of these molecules (Bazil and

Strominger, 1991; Etzerodt et al., 2010). Irrespective of the pre-culture, PD-L1 tended to be increased after *Lm* infection. Although PD-1 is very lowly expressed on T-cells both in the LD or HD assay, we blocked the PD-1/PD-L interaction and investigated whether this has an impact on T-cell proliferation or *Lm* infection rate.

4.9 PD-1/PD-L blockade did not affect *Lm*-induced T-cell proliferation in low and high pre-cultured PBMCs

To investigate whether PD-1/PD-L interactions have an impact on *Lm* infection rate or *Lm*-induced T-cell proliferation in this assay setup, we blocked PD-1 with the therapeutic IgG4 anti-PD-1 nivolumab **(Figure 19)**. This antibody is designed to only weakly interact with FcγRs and thus, we did not block with an isotype control. *Lm* infection significantly induced T-cell proliferation in the LD culture (7.38±3.43; 0.88±0.41) compared to the non-infected control **(Figure 19A)**. PD-1 blockade did not increase *Lm*-induced T-cell proliferation (8.97±4.68).

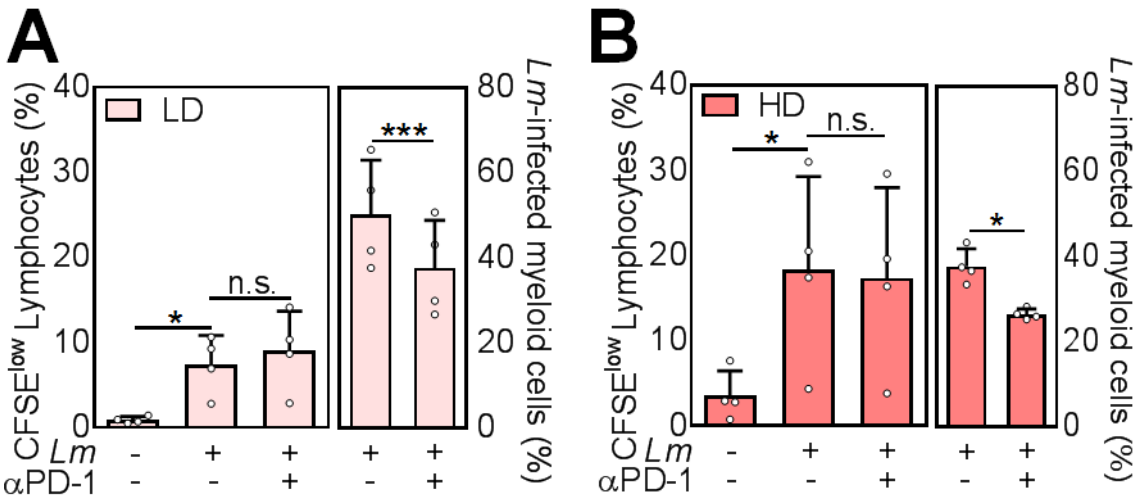

Figure 19: PD-1 blockade unexpectedly reduced *Lm* infection rate but without affecting *Lm*-induced T-cell proliferation.

CFSE-labeled PBMCs were pre-cultivated for 2d at **(A)** low (LD, 1 × 10^6 PBMCs/ml) or **(B)** high (HD, 10 × 10^6 PBMCs/ml) density. Hereafter, PBMCs were infected with *Lm* dsRED as described in the methods chapter and further cultivated in presence or absence of 0.625µg/ml αPD-1 (IgG4) (1 × 10^6 PBMCs/ml). After 5d at 37°C, 5%CO_2, cells were immunostained (CD3) and analyzed by flow cytometry. T-cells were gated via their FSC/SSC properties and CD3. For T-cell proliferation only $CFSE^{low}$ T-cells were considered. Myeloid cells were first gated via their FSC/SSC properties and subsequently *Lm* infection rate was assessed by dsRED. Data is presented as mean percentage ± SD. Statistics were calculated using a parametric paired t test (**=p<0.01). Two independent experiments were performed (N = 4).

Unexpectedly, *Lm* infection rate significantly decreased in the presence of the anti-PD-1 antibody (37.6±11.25; 50.15±12.84) compared to infection alone. A similar result was observed when using HD pre-cultured cells **(Figure 19B)**. PD-1 blockade did not significantly change *Lm*-induced T-cell proliferation (17.35±10.64; 18.32±10.97) in the HD culture, but again *Lm* infection rate was significantly reduced in the presence of αPD-1 (26.45±1.28; 37.70±4.13) compared to infection alone.

Irrespective of the LD or HD culture conditions, PD-1 blockade had no significant effect on *Lm*-induced T-cell proliferation. Surprisingly, *Lm* infection rate of myeloid cells was significantly reduced in the presence of PD-1 checkpoint inhibitors, which could not be linked to enhanced T-cell proliferation. The latter was also the reason, why this observation and the "RESTORE" assay were not further studied. Instead, we proceeded with a much more promising assay, where we used pre-stimulated PBLs, to study the effects of PD-1 checkpoint inhibition in *Lm* infection.

4.10 Phytohemagglutinin (PHA) treatment mimicked T-cell exhaustion as determined by surface expression of various marker proteins

In the chronic lymphocytic choriomeningitis virus (LCMV) mouse model, persistent antigen stimulation leads to T-cell exhaustion, which is characterized by a stepwise upregulation of several inhibitory molecules like PD-1, PD-L1, 2B4, LAG-3, TIM-3 and CD160 (Blattman et al., 2009; Wherry and Kurachi, 2015). To mimic exhausted T-cells in an *in vitro* assay, we stimulated PBLs with phytohemagglutinin (PHA) for 6d prior co-cultivation with *Lm*-infected host cells. PHA stimulation has been reported to lead to an expansion of functionally impaired T-cells (Duarte et al., 2002). After six days of PHA stimulation, we observed that most of the B-cells and NK-cells were overgrown by T-cells shown by the significant increase of CD3 positivity (96.3%±1.58%), compared to the unstimulated control (80.9%±5.59%) (**Figure 20)**. To assure that the T-cells were not functionally impaired by senescence which is characterized by downregulation or loss of CD28, we additionally analyzed the expression of this co-stimulatory molecule. CD28 expression tended to be higher in PHA-stimulated T-cells (RFI: 15.65±10.06) compared to the untreated control (RFI: 12.7±5.81) (**Figure 20**). Therefore, we excluded T-cell senescence. Next, we investigated surface expression of several T-cell exhaustion markers on T-cells

of PHA-pre-stimulated PBLs (PBLs^{PHA}). Compared to the unstimulated control, PHA-pre-stimulated T-cells expressed the co-inhibitory molecules PD-1 (RFI: 1.87±0.55; 7.41±2.50), PD-L1 (RFI: 4.09±1.42; 7.52±2.18), 2B4 (RFI: 4.27±1.71; 9.70±3.71), LAG-3 (RFI: 1.66±0.34; 2.95±0.35) and TIM-3 (RFI: 1.47±0.16; 28.73±18.65) to a significantly higher degree (**Figure 20**). CD160 expression was not affected by PHA stimulation (RFI: 1.17±0.07; 1.45±0.56) (**Figure 20)**. Due to the high expression of several inhibitory molecules, we considered T-cells of PBLs^{PHA} to resemble exhausted T-cells. In the next step we investigated the functionality of PBLs^{PHA} in comparison to PBLs in autologous co-cultures with *Lm*-infected hMDM1.

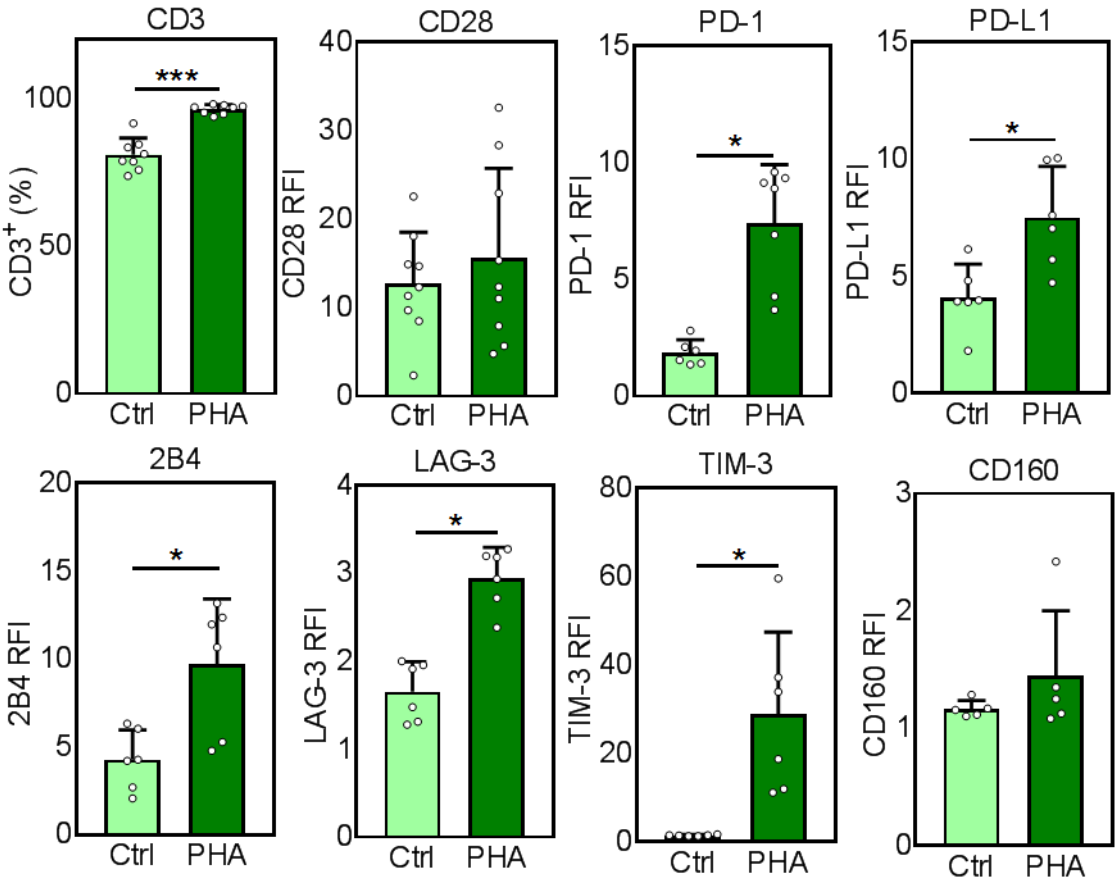

Figure 20: Expression of T-cell exhaustion marker after PHA-stimulation of PBLs.

PBLs were incubated for 6d with/without PHA (0.5 µg/mL) and expression levels of the indicated surface molecules were determined via flow cytometry. T-cells were gated via their FSC/SSC properties and CD3. Data is presented as RFI (ratio of the mean fluorescence intensity of specific markers to the mean fluorescence intensity of isotype controls) or percentage of CD3$^+$ cells. Statistics were calculated using the parametric paired t-test (CD3, CD28) or Wilcoxon matched-pairs signed rank test; P<0.05 is considered statistically significant (*P<0.05; **P<0.01). At least three independent experiments were performed (N = 6 - 9).

4.11 PHA-pre-stimulated T-cells proliferated less upon *Lm* antigen encounter and parasite survival was increased

To examine, whether T-cells of PBLs^{PHA} are indeed functionally impaired, we exemplarily compared them to PBLs in autologous *Lm*-infected hMDM1. In the *Lm*-infected hMDM1:PBLs co-culture there was a strong and significant increase in T-cell proliferation (41.98±14.77%) compared to the uninfected control (3.59±1.29%), whereas T-cell proliferation in the *Lm*-infected hMDM1:PBLs^{PHA} co-culture was significantly decreased (9.50±8.49%) **(Figure 21A)**. Though, compared to the non-infected hMDM1:PBLs^{PHA} control (3.94±3.50%), *Lm*-induced T-cell proliferation in the hMDM1:PBLs^{PHA} co-culture was significantly higher.

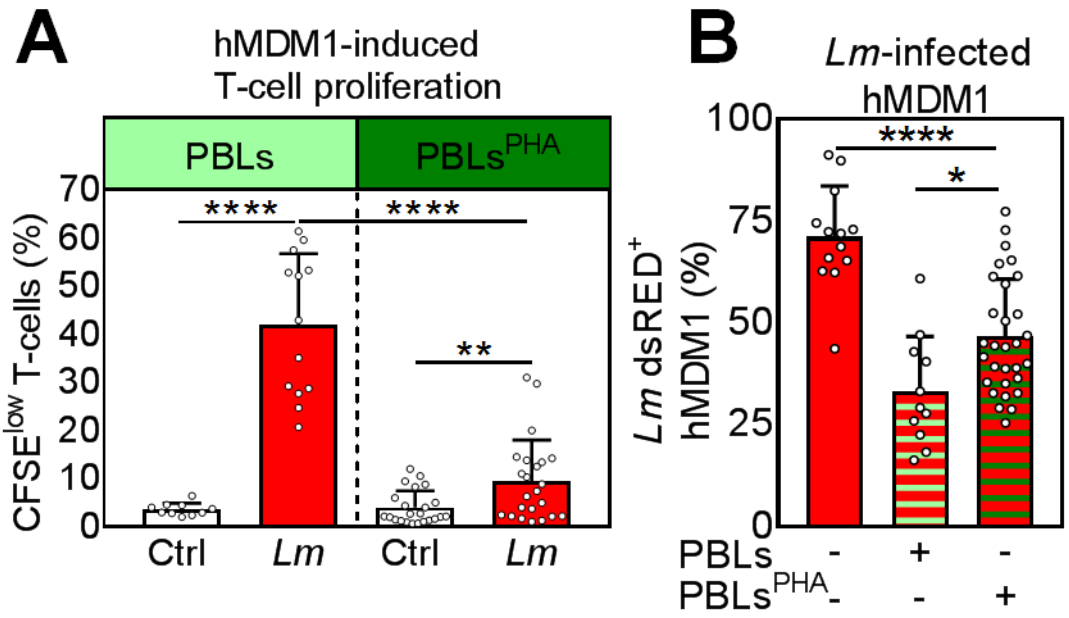

Figure 21: PHA-pre-stimulated T-cells are less responsive to *Lm* antigen encounter.
hMDM1 were incubated with or without *Lm* dsRED (MOI 10) for 24h. After washing extracellular parasites away, hMDM1 were co-cultivated with CFSE-labeled autologous PBLs or PBLs^{PHA} for 5d. **(A)** CFSE^{low} T-cell proliferation and **(B)** *Lm* infection rate (%) were analyzed by flow cytometry as described. P < 0.05 is considered statistically significant (parametric unpaired t-test with Welch's correction, * = P < 0.05; ** = P < 0.01, **** = P < 0.0001). At least five independent experiments were performed (N = 11 - 34).

This indicates PHA-pre-stimulated T-cells to be functionally impaired with residual effector functions. *Lm* infection rate of hMDM1 was significantly dampened in the co-culture with PBLs^{PHA} compared to hMDM1 alone (46.63±14.13%; 71.12±12.49%). However, parasite survival in the presence of PBLs was reduced to a significantly higher degree (33.15±13.52%) compared to

PBLs^{PHA}. This functional data suggests, T-cells of PBLs^{PHA} to be impaired in their response to *Lm*-infected hMDM1. To examine whether effector functions of these cells can be restored by PD-1 checkpoint inhibition, we used PBLs^{PHA} in the following co-culture experiments (PBLs^{PHA} assay).

4.12 IgG1 and IgG4 subclasses of PD-1 blocking antibodies yielded similar results with regard to *Lm* infection and T-cell proliferation

Therapeutic anti-PD-1 blocking antibodies like nivolumab or pembrolizumab are designed as human IgG4 subclass to minimize Fc provoked ADCC or CDC. In contrast, human IgG1 antibodies strongly interact with FcγRs on several cells and thus, can induce ADCC and CDC, leading to an increased cell death of the antibody-targeted cell (Vidarsson et al., 2014). We were interested whether we can measure differences between the humanized anti-PD-1 IgG1 (G&P Biosciences, research grade) and the fully-human IgG4 (BMS nivolumab, GMP grade) blocking antibody in terms of *Lm* infection rate and T-cell proliferation by using our newly established PBLs^{PHA} assay. In comparison to hMDDC, the three FcγRs CD16, CD32 and CD64 are higher expressed on hMDM1 and hMDM2 (**data not shown**). Therefore, we chose to infect hMDM1 or hMDM2 with *Lm* to co-cultivate them together with CFSE-labeled PBLs^{PHA}. PD-1/PD-L interactions were blocked using either the humanized IgG1 or the fully-human IgG4 anti-PD-1 antibody. After incubation for 5d at 37°C, 5% CO_2, T-cell proliferation and *Lm* infection rate were measured **(Figure 22A and B)**. In the absence of infection, hMDM1-induced T-cell proliferation was slightly increased after PD-1 blockade (IgG1: 4.68±3.51%; IgG4: 5.27±3.00%) compared to the untreated sample (2.33±1.84%). *Lm*-infected hMDM1 induced also a slight increase in T-cell proliferation (4.76±1.96%) **(Figure 22A)**. PD-1 blockade significantly increased *Lm*-induced T-cell proliferation (IgG1: 20.41±11.02%; IgG4: 20.29±12.07%). By implication, *Lm* infection rate was significantly reduced in the PD-1-blocked infected sample (IgG1: 31.68±18.83%; IgG4: 31.36±18.62%) compared to infection alone (40.55±23.19%). When we performed the same co-culture experiment with *Lm*-infected hMDM2, we observed a similar pattern as for the *Lm*-infected hMDM1 co-culture, except that *Lm* infection rate was generally higher and PD-1 blockade-induced T-cell proliferation tended to be lower **(Figure 22B).** In both experiments, no

significant IgG subclass-specific effects on T-cell proliferation or *Lm* infection rate were observed.

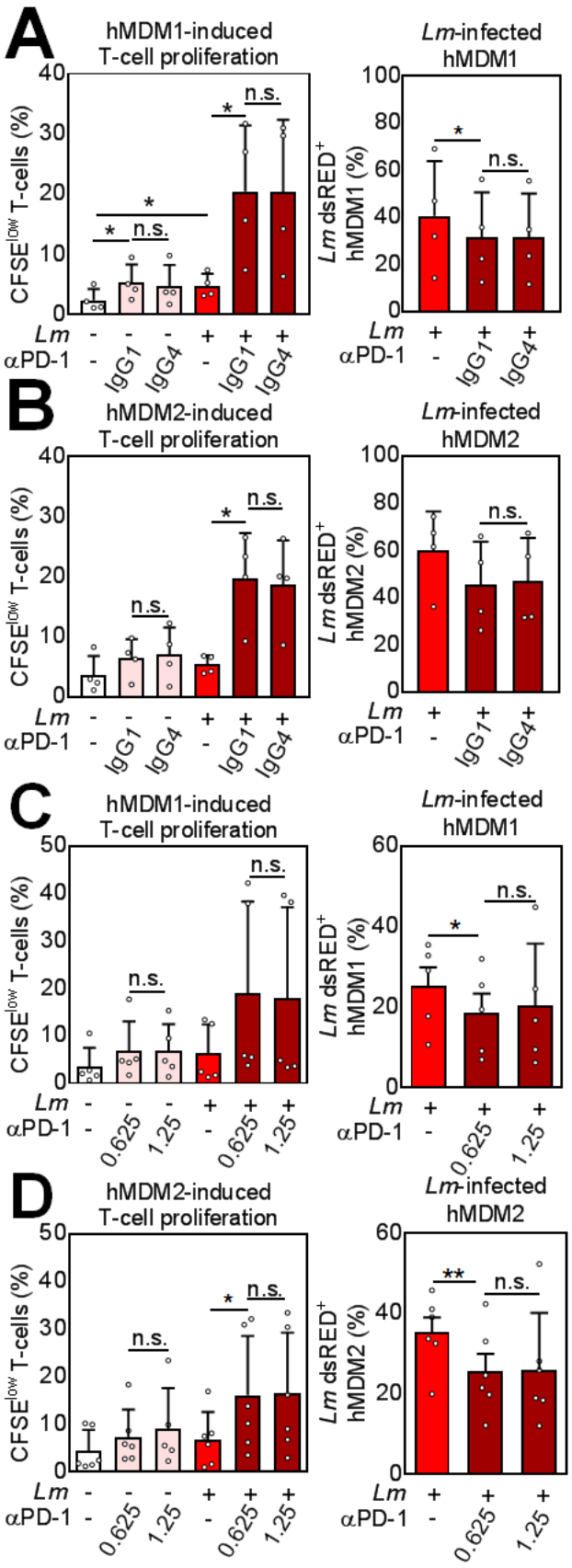

Figure 22: PD-1 blockade increases *Lm*-induced T-cell proliferation and reduced parasite survival to a similar extend when using IgG1 or IgG4 blocking antibodies.

(A, C) hMDM1 or **(B, D)** hMDM2 were incubated with/without *Lm* dsRED (MOI 10) for 24h. After washing extracellular parasites away, infected cells were co-cultivated with CFSE-labeled autologous $PBLs^{PHA}$ and **(A, B)** two different subclasses of αPD-1 (IgG1, G&P Biosciences; IgG4, BMS nivolumab; 0.625 µg/ml) or **(C, D)** two different blocking concentrations of αPD-1 (IgG4, BMS nivolumab; 0.625 or 1.25 µg/ml) for 5d. **(A, C)** $CFSE^{low}$ T-cell proliferation and **(B, D)** *Lm* infection rate (%) were analyzed by flow cytometry as described. $P < 0.05$ is considered statistically significant (parametric paired t-test, * = $P < 0.05$; ** = $P < 0.01$, n.s. = not significant). At least two independent experiments were performed (N = 4 - 5).

Thus, we decided to use only the IgG4 anti-PD-1 blocking antibody nivolumab in the following experiments, because it is more relevant in terms of therapy. Additionally, we tested a higher concentration (1.25µg/ml) of the IgG4 anti-PD-1 antibody using the previous approach **(Figure 22C, D)**. The higher blocking concentration did not significantly change *Lm*-induced T-cell proliferation and *Lm* infection rate compared to the lower concentration (0.625µg/ml), both in the hMDM1 and the hMDM2 co-culture **(Figure 22C, D)**. Thus, we continued using 0.625µg/ml as final anti-PD-1 blocking concentration in follow-up experiments.

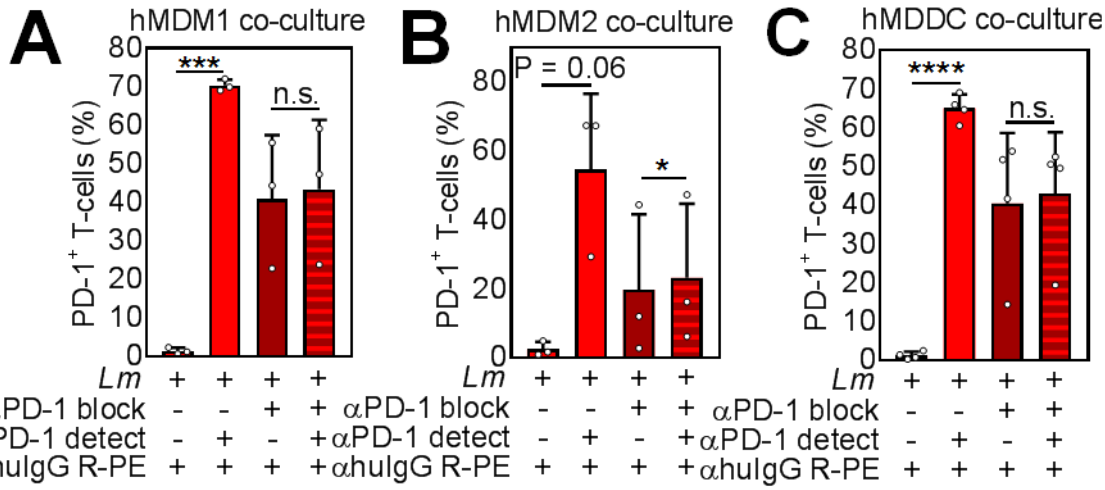

Figure 23: PD-1 receptor is still blocked after 5d co-culture.

(A) hMDM1, **(B)** hMDM2 or **(C)** hMDDC were incubated with *Lm* (MOI 10) for 24h. After washing away extracellular parasites, infected cells were co-cultivated with autologous $PBLs^{PHA}$ and nivolumab (αPD-1 block). After 5d, cells were harvested and T-cells were analyzed by flow cytometry (Gating via FSC/SSC properties + CD3). PD-1 was detected using human IgG4 nivolumab (αPD-1 detect) plus an anti-human IgG PE-labeled Fab_2 fragment (Dianova®; αhuIgG R-PE). The Fab_2 fragment alone detected nivolumab (αPD-1 block) that was added at the beginning of the co-culture experiment. Further addition of nivolumab (αPD-1 detect) at the

detection time point did not increase PD-1 positivity in the PD-1-blocked samples (αPD-1 block). Two independent experiments were performed (N = 3 - 4). Data is presented as mean ± SD.

Before we investigated effects of PD-1 checkpoint inhibition in the $PBLs^{PHA}$ assay in more detail, we studied whether the PD-1 receptor is blocked by the IgG4 anti-PD-1 blocking antibody throughout the whole co-culture experiment **(Figure 23)**. To detect the blocking anti-PD-1 antibody on the T-cells, we used a PE-labeled secondary Fab_2 fragment targeting the Fc part of human IgG (αhuIgG R-PE). *Lm*-infected hMDM1, hMDM2 or hMDDC were co-cultivated with $PBLs^{PHA}$ in presence and absence of an anti-PD-1 antibody (αPD-1 block). After 5d at 37 °C, 5%CO_2 cells were harvested and immunostained. Either only secondary detection antibody was added (αhuIgG R-PE) or anti-PD-1 antibody (αPD-1 detect) plus secondary detection antibody **(Figure 23)**. When using secondary antibody only (αhuIgG R-PE), no signal specific to PD-1 was detected in the *Lm*-infected samples. Prior addition of anti-PD-1 blocking antibody as primary antibody for detection (αPD-1 detect) revealed a high percentage of $PD\text{-}1^+$ T-cells in the *Lm*-infected hMDM1 (70.40±1.54%), hMDM2 (54.77±21.77%) and hMDDC (65.10±3.52%) co-culture. When blocking PD-1 at the start point of the co-culture (αPD-1 block), the secondary detection antibody (αhuIgG R-PE) bound "αPD-1 block" on the surface of T-cells. Compared the corresponding untreated infected sample, slightly less $PD\text{-}1^+$ T-cells were detected in the αPD-1-treated *Lm*-infected hMDM1 (40.93±16.57%), hMDM2 (19.83±21.86%) and hMDDC (40.48±18.19%) co-cultures. By adding additional "αPD-1 detect" on the day of cell harvest, the percentage of $PD\text{-}1^+$ T-cells did not significantly increase in the αPD-1-treated *Lm*-infected hMDM1 (43.47±17.96%) and hMDDC (43.03±15.80%) co-cultures **(Figure 23A and C)**. An exception formed the αPD-1-treated *Lm*-infected hMDM2 co-culture, where a modest but significant increase of $PD\text{-}1^+$ T-cells after additional αPD-1 detect was measured (23.31±21.46%) **(Figure 23B)**. This data shows that the PD-1 receptor is blocked throughout the 5d of co-culture at 37°C, when using a final blocking concentration of 0.625 µg/ml.

4.13 PD-1/PD-L blockade-induced T-cell proliferation and *Lm* infection rate were dependent on the initial host cell phenotype

So far, we showed that T-cell effector functions of PBLs^{PHA} can be reinvigorated by the therapeutic IgG4 anti-PD-1 antibody nivolumab which had a significant impact on *Lm* infection rate in hMDM1 co-cultures and to a lesser extent in hMDM2 co-cultures. Next we investigated which impact the initially used *Lm* host cell phenotype (hMDM1, hMDM2, hMDDC) has on PD-1 blockade-mediated effects. Therefore, we compared hMDM1, hMDM2 and hMDDC as *Lm* host cells in co-cultures with autologous PBLs^{PHA}. PD-1 blockade already slightly increased T-cell proliferation in co-cultures with non-infected hMDM1 (9.77%±5.09%, 4.63%±3.33%) (**Figure 24A**). *Lm*-infected hMDM1 significantly increased T-cell proliferation (12.32%±9.49%) in the co-culture, compared to the uninfected control. PD-1 blockade strongly enhanced *Lm*-induced T-cell proliferation (25.96%±15.07%).

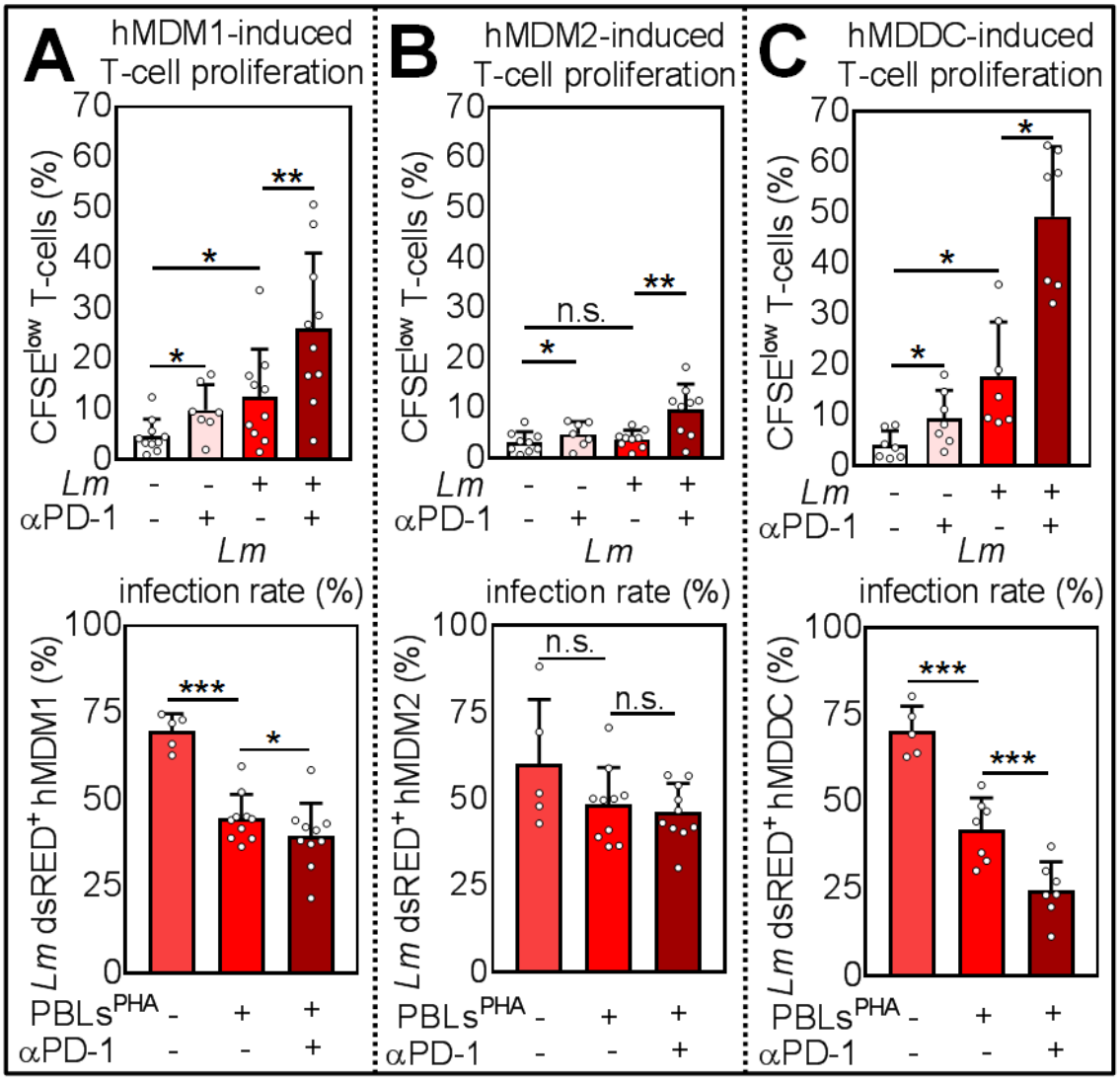

Figure 24: Host cell phenotype-dependent T-cell proliferation, parasite killing and cytokine release upon PD-1 blockade.

(A,B,C) CFSE-labeled autologous $PBLs^{PHA}$ were co-cultivated with *Lm*-infected host cells and blocked with nivolumab (αPD-1). After five days, cells were harvested and analyzed by flow cytometry (hMDM/hMDDC gated via their FSC/SSC properties, T-cells additionally via CD3). Data is presented as mean percentage of $CFSE^{low}$ proliferating T-cells ± SD or *Lm* dsRED-infected hMDM or hMDDC ± SD, respectively. For statistics, a parametric paired t-test was performed, P<0.05 is considered statistically significant, *P<0.05, **P<0.01, ***P<0.001, ****P<0.0001). At least three independent experiments were performed (N = 6 - 14).

Concomitantly, we observed a significant reduction in *Lm* infection in the sample co-cultivated with $PBLs^{PHA}$ (44.62%±6.87%) compared to infected hMDM1 only (69.66%±5.07%), which was reduced to a stronger extent upon PD-1 blockade (39.47%±9.48%) (**Figure 24A**). In the hMDM2 co-cultures, T-cell proliferation was slightly increased in the PD-1 blocked uninfected sample (4.82%±2.47%) in comparison to the *Lm*-infected (3.84%±1.74%) or uninfected sample (3.21%±2.05%) (**Figure 24B**). The ladder two samples did not significantly differ between each other. However, PD-1 blockade enhanced T-cell proliferation significantly in the infected sample (14.48%±12.49%) (**Figure 24B**). Consistently, *Lm* infection rate of hMDM2 in the presence of $PBLs^{PHA}$ was not significantly decreased (48.30%±10.78%) compared to infected hMDM2 only (60.00%±18.64%). Surprisingly, no significant effect on *Lm* infection could be detected when PD-1 was blocked (46.07%±8.43%), even though T-cell proliferation was increased (**Figure 24B**). Compared to hMDM1 and hMDM2, *Lm*-infected hMDDC induced the highest T-cell proliferation in the $PBLs^{PHA}$ co-culture (17.71%±10.73%) and enhanced T-cell proliferation the most after PD-1 blockade (49.30%±13.81%) (**Figure 24C**). Consequently, less *Lm*-infected hMDDCs were observed in the presence of $PBLs^{PHA}$ (42.02%±9.17%) and PD-1 blockade dampened the infection rate of hMDDC the most (24.68%±8.15%), compared to hMDM1 and hMDM2 (**Figure 24C**). In summary, it can be stated that PD-1 blockade-mediated effects on *Lm*-induced T-cell proliferation and parasite killing were most distinct in the hMDDC:$PBLs^{PHA}$ co-culture followed by the hMDM1 and hMDM2 co-culture with PHA-treated PBLs.

4.14 PD-1/PD-L blockade affected *Lm* host cell phenotype

In mice, it has been shown that macrophages and dendritic cells can adapt to changes in the microenvironment, e.g. inflammation, by changing their phenotype (Stout et al., 2005). We asked whether the *Lm* host cell phenotype changes during the 5d co-culture with $PBLs^{PHA}$ and in presence or absence of PD-1 blocking antibody. As already mentioned, hMDM1 were characterized in our lab as $CD14^{+}CD163^{-}$, whereas hMDM2 are $CD14^{++}CD163^{+}$ and hMDDC are $CD14^{-}CD1a^{+}$ (Crauwels, 2015).

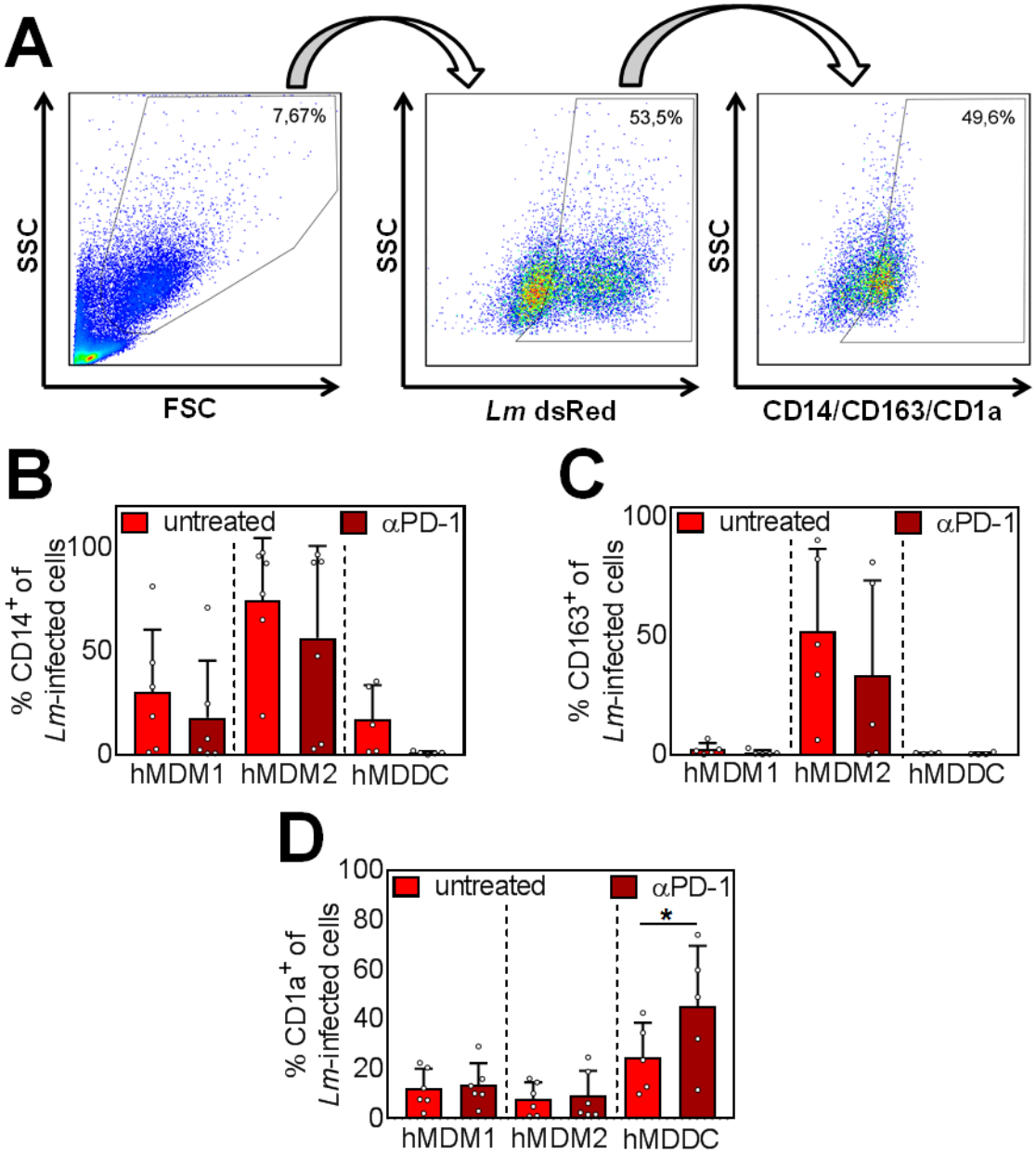

Figure 25: Expression of *Lm* host cell phenotype-specific markers after PBLs^{PHA} co-culture and PD-1 blockade.

hMDM1, hMDM2 or hMDDC were infected with *Lm* dsRED (MOI=10) for 24h at 37°C; 5%CO_2. After washing extracellular parasites away, infected cells were co-cultivated with autologous PBLs^{PHA} for 5d at 37°C, 5%CO_2 in presence or absence of nivolumab (αPD-1). Cells were harvested, immunostained (CD14, CD163 and CD1a) and analyzed by flow cytometry. **(A)** hMDM1, hMDM2 or hMDDC were gated first via their FSC/SSC properties. From these cells, only the *Lm* dsRED positive cells were gated. At last percentage of CD14$^+$, CD163$^+$ or CD1a$^+$ cells of *Lm*-infected cells was measured by means of the corresponding isotype control. **(B, C, D)** Data is presented as mean percentage ± SD. Statistics were calculated using a student's t test, P<0.05 was considered significant (* = P<0.05). Three independent experiments were performed (N = 5 - 6).

After 5d co-culture we determined the expression of CD14, CD163 and CD1a on the *Lm* infected hMDM1, hMDM2 and hMDDC. When gating on the total cell number instead of infected only, we obtained comparable results **(data not shown)**. Because we did not stain with a proliferation dye in this experiment, we could not rule out lymphocytes that might be in the FSC/SSC gate of hMDM or hMDDC. Thus, we gated on the infected cells which in this case are most likely composed of myeloid cells **(Figure 25A)**. In comparison to the untreated control, less *Lm*-infected cells expressed CD14 after PD-1 blockade in the hMDM1 (30.22±30.19%; 17.92±27.59%), hMDM2 (74.63±30.06%; 56.45±44.45%) or hMDDC (17.29±16.39%; 0.97±0.73%) co-culture **(Figure 25B)**. CD163 expression was only detectable on infected cells in the hMDM2 co-culture (51.74±34.70%), but tended to be reduced when PD-1 was blocked (33.39±39.80%) **(Figure 25C)**. PD-1 blockade did not significantly change percentage of CD1a$^+$ cells among the infected cells in the hMDM1 (13.54±8.76%; 12.08±7.99%) or hMDM2 (9.24±10.05%; 7.94±6.66%) co-culture compared to the untreated control **(Figure 25D)**. In contrast, the percentage of CD1a$^+$ cells significantly increased due to PD-1 blockade in the hMDDC co-culture compared to the untreated control (45.34±24.32%; 24.69±13.98%). This data suggests that PD-1 blockade tends to reduce macrophage-specific markers and to increase the expression of the marker CD1a on dendritic cells. As proposed for the RESTORE assay, downregulation of CD14 and CD163 on macrophages might be an inflammation-induced effect. Monocyte-derived dendritic cells consist of inflammatory CD1a$^+$CD14$^-$ and tolerogenic CD1a$^-$ CD14^{low} dendritic cells (Gogolak et al., 2007). Our data shows that in the

PBLs^{PHA} assay, PD-1 blockade shifts the *Lm*-infected hMDDCs towards an inflammatory dendritic cell phenotype.

4.15 PD-1/PD-L blockade increased release of pro-inflammatory cytokines

The pro-inflammatory cytokines TNFα and IFNγ play a critical role in shaping the immune response against *Leishmania* infection (Pirmez et al., 1993). IL-10 is a counteracting anti-inflammatory cytokine that is involved in leishmaniasis disease development and parasite persistence (Vries and Waal Malefyt, 1995). Thus, we analyzed TNFα, IFNγ and IL-10 protein levels in the co-culture supernatants by ELISA. PD-1 blockade significantly increased TNFα levels in the infected hMDM1 samples compared to untreated (216.60±114.90 pg/mL; 88.57±52.52 pg/mL) **(Figure 26A)**. In addition, a slight increase of TNFα was observed in the non-infected hMDM1 samples after PD-1 blockade compared to the untreated sample (199.40±170.60 pg/mL; 131.70±142.00 pg/mL). Increased levels of IFNγ were detected after PD-1 blockade in the infected hMDM1 samples compared to infection alone (80.61±59.73 pg/mL; 16.95±25.68 pg/mL). IFNγ was almost undetectable in the non-infected hMDM1 samples. IL-10 levels detected in the supernatants of the non-infected hMDM1 samples were low and did not differ between untreated (14.52±8.68 pg/mL) and αPD-1-treated (15.87±0.75 pg/mL). *Lm* infection tended to increase release of IL-10 (48.56±28.53 pg/mL), which did not significantly differ in the presence of αPD-1 (40.83±22.82 pg/mL). TNFα levels in the hMDM2 samples were similar to the hMDM1 samples (non-infected: 109.50±97.68 pg/mL; αPD-1: 158.80±105.20 pg/mL; *Lm*: 81.12±65.31 pg/mL; *Lm* + αPD-1: 163.40±107.40 pg/mL) **(Figure 26B)**. In contrast to hMDM1, IFNγ was barely detectable in the PD-1-blocked infected hMDM2 sample (17.62±24.18 pg/mL). IL-10 release was low and did not significantly differ between all four conditions (non-infected: 26.59±22.05 pg/mL; αPD-1: 27.46±16.65 pg/mL; *Lm*: 25.07±10.95 pg/mL; *Lm* + αPD-1: 26.01±4.59 pg/mL)**.**

Regarding *Lm*-infected hMDDC, PD-1 blockade significantly increased TNFα levels in the supernatants (374.50±156.60 pg/mL; 167.20±89.77 pg/mL) **(Figure 26C)**. As observed in the hMDM1 and hMDM2 co-cultures, TNFα tended to increase in the non-infected hMDDC samples after PD-1 blockade compared to the untreated sample (233.00±223.20 pg/mL; 152.90±129.50 pg/mL).

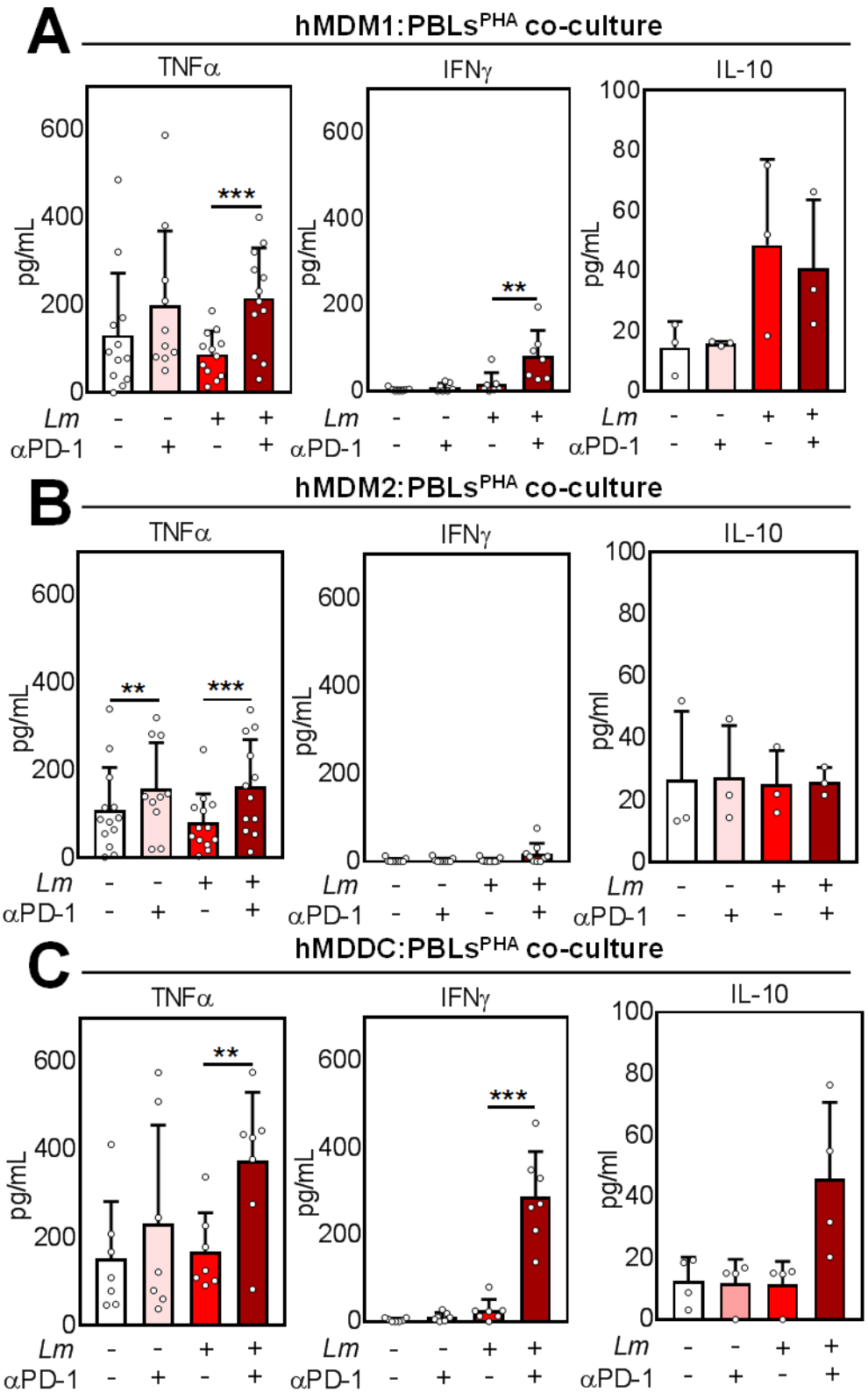

Figure 26: PD-1 blockade increased release of pro-inflammatory cytokines.

Supernatants from the **(A)** hMDM1, **(B)** hMDM2 or **(C)** hMDDC co-culture experiments (**see Figure 24**) were harvested, frozen (-80°C) and thawed. IFNγ, TNFα and IL-10 were measured in the co-culture supernatants by ELISA as described in the methods section. Data is presented as mean pg/mL ± SD. For statistics, a parametric paired t-test was performed, $P<0.05$ is

considered statistically significant, *P<0.05, **P<0.01, ***P<0.001). At least two independent experiments were performed (N = 3 - 14).

IFNγ levels in the supernatant of the *Lm*-infected hMDDC samples were low (25.58±25.54 pg/mL), but strongly enhanced by PD-1 blockade (288.40±103.20 pg/mL). IL-10 release was low and did not significantly differ in all conditions (non-infected: 12.44±7.87 pg/mL; αPD-1: 11.75±7.88 pg/mL; *Lm*: 11.37±7.58 pg/mL), except the *Lm*-infected αPD-1 treated sample, where IL-10 release was slightly elevated (45.85±24.91 pg/mL).
This data suggests that PD-1 blockade-mediated effects on T-cell proliferation and *Lm* infection rate may be mediated by TNFα and IFNγ.

4.16 PD-1/PD-L blockade-mediated effects are partly TNFα-dependent

To assess whether cytokine release correlates with T-cell proliferation or *Lm* infection rate, we performed a correlative analysis. To this end, we focused on *Lm*-infected hMDDC, because these host cells displayed the strongest effects mediated by PD-1 blockade in the co-culture experiment **(Figure 24C, Figure 26C)**. We only analyzed datasets of infected samples in presence and absence of nivolumab (Figure 27**A**). TNFα release correlated with T-cell proliferation (**r = 0.90**) and tended to correlate inversely with infection rate (**r = -0.63**). There was a positive correlation between IFNγ release and T-cell proliferation (**r = 0.83**) but again a slightly inverse correlation between IFNγ release and infection rate (**r =-0.79**). To investigate a causal connection between increased TNFα/IFNγ release and T-cell proliferation/parasite survival, we neutralized TNFα and IFNγ in the co-culture by treatment with blocking antibodies. Neutralization of IFNγ in the infected sample had no significant effect on T-cell proliferation (Figure 27**B**). Neutralization of TNFα tended to reduce T-cell proliferation compared to *Lm* infection only (2.48%±0.80%; 5.02%±2.36% respectively). Simultaneous neutralization of both cytokines reduced T-cell proliferation significantly (2.89%±1.74%) compared to the untreated control and to a similar extent as TNFα neutralization alone. As expected, PD-1 blockade increased T-cell proliferation (26.18%±18.11%). Neutralization of IFNγ did not decrease PD-1 blockade-induced T-cell proliferation (20.29%±15.08%), whereas anti-TNFα treatment had a significant reducing effect (9.37%±7.72%).

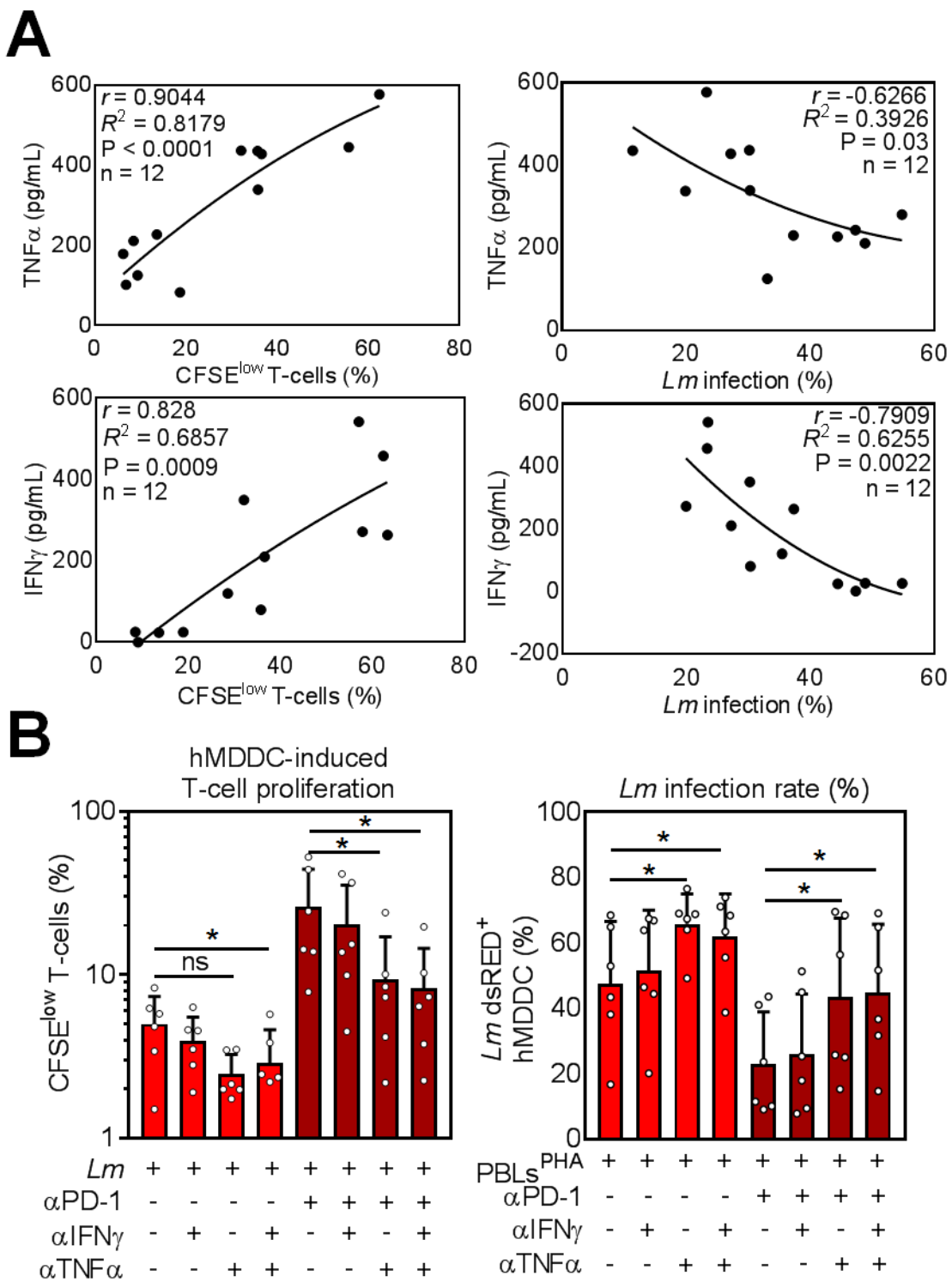

Figure 27: Neutralization of TNFα but not IFNγ partially reversed PD-1 blockade-mediated effects.

(A) TNFα- and IFNγ-release correlated with T-cell proliferation. All *Lm*-infected hMDDC samples (MOI=10) co-cultured with PBLs^{PHA} in presence or absence of anti-PD-1 (αPD-1) were considered (TNFα and IFNγ: n = 12) and Pearson correlation coefficients (r), the coefficient of determination (R^2) plus the significance level (P) were calculated for the indicated datasets. r ≥ 0.7 = positive correlation; r ≤ -0.7 = inverse correlation. **(B)** CFSE-labeled autologous PBLs^{PHA}

were co-cultivated with *Lm*-infected hMDDC, nivolumab (αPD-1), IFNγ neutralizing antibody (αIFNγ) and TNFα neutralizing antibody (αTNFα) as indicated. After 5d, cells were harvested and analyzed by flow cytometry (hMDM/hMDDC gated via their FSC/SSC properties, T-cells additionally via CD3). Data is presented as mean percentage of $CFSE^{low}$ proliferating T-cells ± SD or *Lm* dsRED-infected hMDDC ± SD, respectively. For statistics, a parametric paired t-test was performed, P<0.05 is considered statistically significant, *P<0.05, **P<0.01). At least three independent experiments were performed (N = 5-6).

Simultaneous neutralization of both cytokines did not further enhance this effect (8.30%±6.25%). In the absence of anti-PD-1 antibody, *Lm* infection rate (47.42%±19.11%) was not increased in the IFNγ neutralized sample (51.55%±18.48%). Interestingly, TNFα neutralization highly increased parasite survival (65.85%±9.31%), which was not further enhanced by additional neutralization of IFNγ (61.87%±13.05%). Infection rate in hMDDC decreased in the presence of anti-PD-1 (23.12%±15.78%). Neutralizing single or both cytokines revealed the same effect, as observed for the samples without nivolumab. Again, only TNFα neutralization significantly increased parasite survival (43.40%±24.17%) (Figure 27**B**). Treatment with an isotype control antibody instead of the TNFα and IFNγ blocking antibodies did not alter proliferation or parasite survival (**data not shown**). Even though the correlative analysis pointed towards a role for IFNγ in T-cell proliferation and parasite killing, only neutralization of TNFα partially reversed PD-1 blockade-mediated effects. However, TNFα neutralization already improved parasite survival in the absence of PD-1 blockade, indicating that TNFα might act independently of PD-1.

4.17 Parasite killing is partially mediated by a secreted soluble factor in the PD-1 blocked samples

Parasite killing in the hMDDC:$PBLs^{PHA}$ co-culture is partly mediated by TNFα. In the following experiment we were interested whether the supernatant of the co-culture is sufficient to reduce parasite survival in *Lm*-infected hMDDC or whether cell-cell contact between hMDDC and T-cells is required. Therefore, we cultivated *Lm* dsRED-infected hMDDC with complete medium (CM) or autologous supernatants of the hMDDC co-culture (1-4). We tested supernatants from non-infected (1, Ctrl), non-infected + anti-PD-1 blocking antibody (2, Ctrl + αPD-1), *Lm*-infected (3, *Lm*) and *Lm*-infected + anti-PD-1

blocking antibody (4, *Lm* + αPD-1). After 24h and 120h incubation, cells were harvested and *Lm* infection rate was determined by flow cytometry **(Figure 28)**. After 24h, no significant differences between CM (40.52%±10.05) and each of the supernatants (1: 42.58%±11.19; 2: 40.58%±9.40; 3: 41.80%±8.92; 4: 46.68%±10.31) were observed with regard to *Lm* infection rate. After 120h, infection rate was higher in all samples due to proliferation and transformation of the parasite inside the host cell.

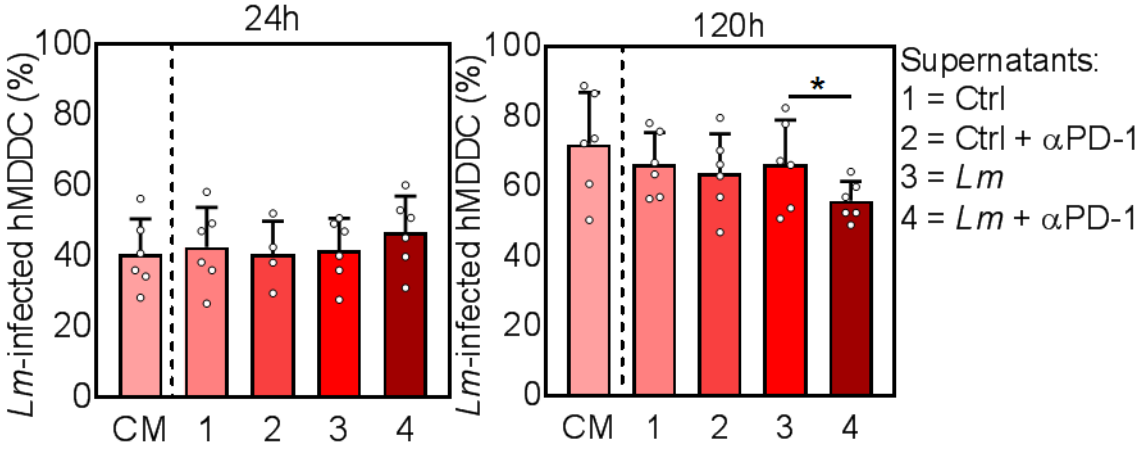

Figure 28: Effect of hMDDC:PBLs^{PHA} supernatants on *Lm*-infected hMDDC.

hMDDC were infected with *Lm* dsRED (MOI=10) for 24 h, 37°C, 5% CO_2. After washing extracellular parasites away, infected cells were further cultivated in complete medium (CM) or autologous supernatants from the hMDDC:PBLs^{PHA} co-culture as depicted in the figure (1-4). After 24h (left graph) and 120h (right graph) incubation at 37 °C, cells were harvested and analyzed by flow cytometry. *Lm*-infected hMDDC were gated via their FSC/SSC properties and dsRED. Data is presented as mean percentage ± SD. Statistics were calculated using a parametric paired t-test, $P < 0.05$ was considered statistically significant (*=$P<0.05$). Three independent experiments were performed (N = 6).

Again, no significant differences between the effects of hMDDC cultivation in CM (71.98%±14.78) or the supernatants from co-cultures with (3: 66.30%±12.61) or without (1: 66.17%±9.15) *Lm* infection or PD-1 blockade only (2: 63.75%±11.23) were observed with regard to *Lm* infection rate. Intriguingly, *Lm* infection rate in hMDDC was lower in the presence of supernatant from the *Lm*-infected PD-1-blocked sample (55.75%±5.60) compared to the supernatant from infection only (3). In all supernatants, the color of the culture medium pH indicator, phenol red, was reddish shortly before harvest of the cells for flow cytometry. This indicates that the observed effects on *Lm* infection rate were not due to a possible lack of nutrients in the medium or starvation of the cells as the medium would acidify in this case and its color would turn yellow. We concluded

that the reduced parasite survival in the PD-1 blocked samples is in part mediated by an uncharacterized soluble factor that is secreted into the co-culture under these conditions.

4.18 Maturation markers of hMDDC were increased upon PD-1 blockade

After phagocytosis of foreign antigens, dendritic cells start to maturate. During this process, expression of several surface molecules is induced, which are important for antigen presentation and T-cell activation. In the following, we investigated whether PD-1 blockade impacts expression of maturation markers on dendritic cells. Therefore, we cultivated *Lm*-infected and non-infected hMDDC separately or in co-culture with autologous $PBLs^{PHA}$ and nivolumab. After 5d incubation, surface expression of MHC class II (HLA-DR), CD80, CD83, CD86 and CD40 was analyzed by flow cytometry. Additionally the viability of the cells was checked using the apoptosis dyes Annexin and PI **(Figure 29)**. (Non-) infected hMDDC showed similar surface expression of HLA-DR in absence or presence of $PBLs^{PHA}$ (hMDDC: 15.52±15.81 RFI; *Lm*-infected hMDDC: 14.75±13.12 RFI; hMDDC:$PBLs^{PHA}$: 13.78±12.01 RFI; *Lm*-infected hMDDC:$PBLs^{PHA}$: 16.79±16.06 RFI) **(Figure 29A)**. PD-1 blockade in the absence of infection had no significant impact on HLA-DR expression (16.50±15.69 RFI), but HLA-DR expression tended to be higher in the PD-1 blocked infected sample (24.86±28.27 RFI) compared to the other conditions. CD80 expression in the absence of $PBLs^{PHA}$ did not differ between the infected (1.62±0.13 RFI) and non-infected sample (1.59±0.38 RFI) **(Figure 29B)**. In the presence of $PBLs^{PHA}$, CD80 expression tended to progressively increase in the four conditions from uninfected ± PD-1 blockade (hMDDC:$PBLs^{PHA}$: 2.06±0.36 RFI; hMDDC:$PBLs^{PHA}$ + αPD-1: 2.75±1.26 RFI) to infected ± PD-1 blockade (*Lm*-infected hMDDC:$PBLs^{PHA}$: 2.95±1.41 RFI; *Lm*-infected hMDDC:$PBLs^{PHA}$ + αPD-1: 4.52±2.82 RFI). The expression of CD83 increased in a similar pattern as observed for CD80 (hMDDC: 1.32±0.37 RFI; *Lm*-infected hMDDC: 1.26±0.18 RFI; hMDDC:$PBLs^{PHA}$: 1.53±0.32 RFI; hMDDC:$PBLs^{PHA}$ + αPD-1: 2.14±0.79 RFI) **(Figure 29C)**. In the presence of $PBLs^{PHA}$, CD83 expression was significantly higher in the *Lm*-infected sample after PD-1 blockade (2.80±0.76 RFI) compared to untreated (1.93±0.72 RFI).

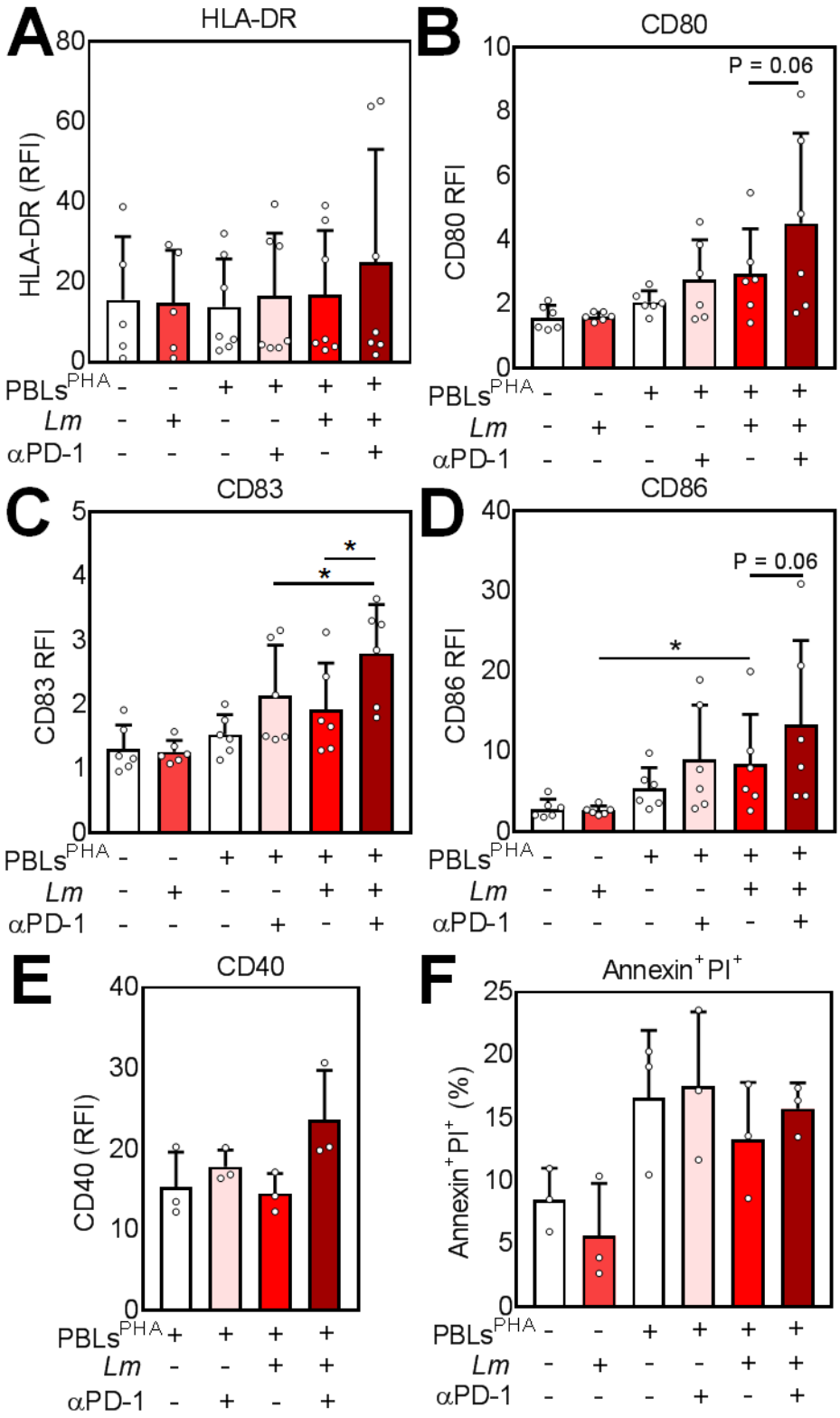

Figure 29: Expression of maturation markers on hMDDC in the hMDDC:PBLs^{PHA} co-culture.

(Non-) *Lm*-infected hMDDC (MOI=10) were cultivated alone or together with CFSE-labeled PBLs^{PHA} and blocked with nivolumab (αPD-1). After five days, cells were harvested, stained for **(A)** HLA-DR, **(B)** CD80, **(C)** CD83, **(D)** CD86, **(E)** CD40 or **(F)** Annexin/PI followed by flow cytometric analysis. hMDDC were gated via their FSC/SSC properties and the indicated

markers. Residual proliferating T-cells were removed by first gating on the $CFSE^{hi}$ cells. Data is presented mean RFI of hMDDC ± SD, respectively. For statistics, a parametric paired t-test was performed, $P<0.05$ is considered statistically significant (*$P<0.05$). At least two independent experiments were performed (N = 3 - 7).

CD86 expression in the absence of $PBLs^{PHA}$ was comparable between infected (2.65±0.58 RFI) and non-infected samples (2.86±1.19 RFI) **(Figure 29D)**. The presence of $PBLs^{PHA}$ significantly increased expression of CD86 on *Lm*-infected hMDDC (8.40±6.25 RFI) compared to *Lm*-infected hMDDC without PBLs co-culture. In this context, PD-1 blockade increased expression of CD86 even further (13.36±10.50 RFI), although the differences were not statistically significant. CD40 expression on hMDDC was only determined in the presence of $PBLs^{PHA}$ **(Figure 29E)**. Whereas CD40 expression was not significantly different between non-infected (15.31±4.33 RFI), nivolumab-treated non-infected (17.80±2.08 RFI) and the infected sample (14.51±2.46 RFI), a slightly higher expression of CD40 was observed in the nivolumab-treated infected sample (23.60±6.16 RFI). As control, we analyzed the viability of hMDDC in this assay setup by using the apoptosis dyes Annexin/PI **(Figure 29F)**. In the absence of $PBLs^{PHA}$, a low percentage of apoptotic cells was measured within the hMDDC gate (hMDDC: 8.52%±2.51%; *Lm*-infected hMDDC: 5.67%±4.15%). In presence of $PBLs^{PHA}$, the percentage of apoptotic cells within the hMDDC gate was slightly increased (hMDDC:$PBLs^{PHA}$: 16.63%±5.35%; hMDDC:$PBLs^{PHA}$ + αPD-1: 17.50%±5.96%; *Lm*-infected hMDDC:$PBLs^{PHA}$: 13.31%±4.54%; *Lm*-infected hMDDC:$PBLs^{PHA}$ + αPD-1: 15.77%±2.03%). Compared to the respective uninfected controls, the infected samples tended to show higher viability. PD-1 blockade did not significantly change hMDDC viability.

To summarize, we examined that PD-1 blockade in presence of *Lm* infection and $PBLs^{PHA}$ increased expression of dendritic cell maturation markers and surface molecules required for efficient antigen presentation and T-cell activation. In the following we focused on the T-cell response in more detail.

4.19 PD-1/PD-L blockade specifically increased *Lm*-induced CD4$^+$ T-cell proliferation

We already demonstrated that *Leishmania*-infected human myeloid cells induced a CD4$^+$ central memory T-cell response *in vitro* when using cells of previously uninfected healthy German blood donors (Crauwels et al., 2015; Crauwels, 2015). Because we use PBLs^{PHA} instead of unstimulated PBLs in our model, the response might differ. Thus, we sought to examine the lymphocyte response after PD-1 blockade in more detail. Therefore, we characterized the proliferating CFSE^{low} and the non-proliferating CFSE^{hi} lymphocytes in the hMDDC co-culture **(Figure 30A)**.

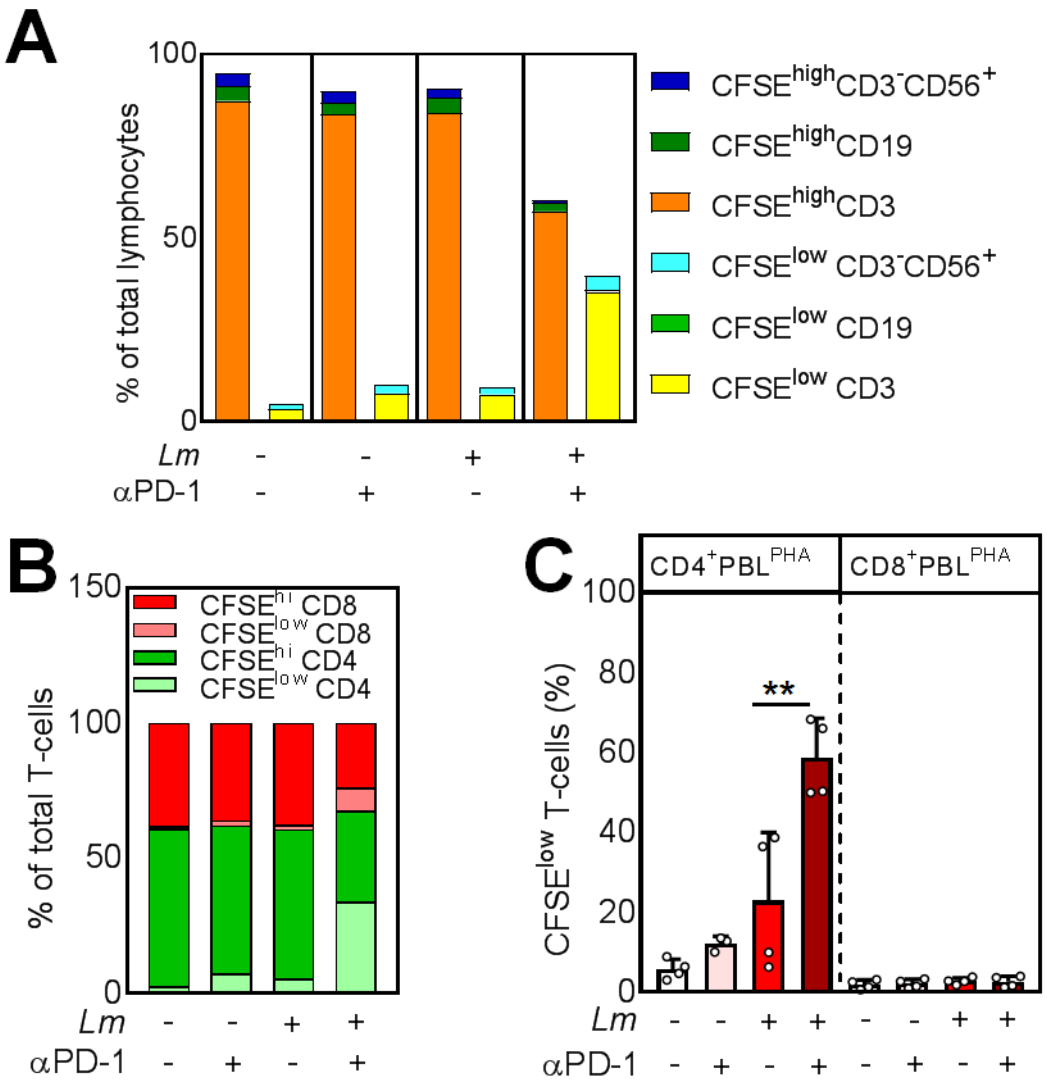

Figure 30: PD-1 blockade specifically enhanced proliferation of CD4$^+$ T-cells.

(A,B) CFSE-labeled autologous PBLs^{PHA} were co-cultivated with *Lm*-infected hMDDC (MOI=10) and nivolumab (αPD-1). After 5d, cells were harvested, fluorescently stained for **(A)** (CD3, CD19, CD56), **(B)** (CD3, CD4, CD8), **(C)** CD3 and analyzed by flow cytometry. T-cells were

gated via their FSC/SSC properties, CFSE and the labeled antibodies. Data is presented as **(A)** percentage of total lymphocytes, **(B)** percentage of total T-cells or **(C)** mean percentage ± SD. At least two independent experiments were performed (N = 4 - 8). **(C)** CFSE-labeled autologous $CD4^+$ or $CD8^+$ $PBLs^{PHA}$ were co-cultivated with *Lm*-infected hMDDC and nivolumab (αPD-1). After 5d, cells were harvested and analyzed by flow cytometry. T-cells were gated via their FSC/SSC properties and CD3. At least two independent experiments were performed (N = 4). Statistics were calculated using the parametric paired t-test; $P<0.05$ is considered statistically significant (*$P<0.05$; **$P<0.01$).

Lymphocytes were mainly composed of $CD3^+$ T-cells ($CFSE^{low}$ CD3: 3.37%±2.31%; $CFSE^{high}$ CD3: 87.31%±4.35%), a few B-cells ($CFSE^{low}$ CD19: 0.10%±0.07%; $CFSE^{high}$ CD19: 4.10±3.26) and NK-cells ($CFSE^{low}$ $CD3^-CD56^+$: 1.60%±1.56%; $CFSE^{high}$ $CD3^-CD56^+$: 3.53±2.71) (uninfected control). Interestingly, in the PD-1-blocked *Lm*-infected sample almost exclusively $CD3^+$ T-cells proliferated (35.37%±18.00% $CFSE^{low}$ $CD3^+$; $CFSE^{low}$ CD19: 0.47%±0.47%; $CFSE^{low}$ $CD3^-CD56^+$: 3.82%±4.49%) **(Figure 30A)**. Proliferating NK-cells were detected in all conditions (uninfected: 1.60%±1.56%; αPD-1: 2.27%±2.58%; *Lm*: 1.95%±1.82%; *Lm* + αPD-1: 3.82%±4.49%) but their overall percentages did not rise to the same extent as for T-cells after PD-1 blockade. Next we analyzed the percentages of helper ($CD4^+$) and cytotoxic ($CD8^+$) T-cells within the $CFSE^{low}$ and $CFSE^{high}$ T-cells **(Figure 30B)**. T-cells were composed of ~60% $CD4^+$ cells and ~40% $CD8^+$ (uninfected control); in the PD-1 blocked *Lm*-infected sample almost exclusively $CD4^+$-T-cells proliferated (33.89%±17.95% $CFSE^{low}$ $CD4^+$; 8.52%±5.73% $CFSE^{low}$ $CD8^+$) **(Figure 30B)**. We confirmed this finding in a co-culture experiment using purified $CD4^+$ $PBLs^{PHA}$ or $CD8^+$ $PBLs^{PHA}$ and detected T-cell proliferation only in the presence of $CD4^+$ $PBLs^{PHA}$ **(Figure 30C)**. Hence, PD-1 blockade mainly enhanced effector functions of $CD4^+$ T-cells.

4.20 Regulatory T-cells were slightly increased by PD-1 checkpoint inhibition

PD-1 blockade might not only target $PD\text{-}1^+CD4^+$ effector T-cells, also regulatory T-cells (Tregs) could be affected by PD-1 blockade. So far, there is conflicting data regarding the effect of PD-1/PD-L checkpoint inhibitors on Tregs (Wang et al., 2009; Peligero et al., 2015; Kagamu et al., 2017). Thus, we analyzed percentage of $CD25^+$ $FOXP3^+$ Tregs within the $CD4^+$ T-cells as depicted in the dot plot **(Figure 31A)**. In the absence of *Lm* infection, only a low percentage of

$CD25^+FOXP3^+$ Tregs was detected (2.44%±1.16%), which significantly increased upon PD-1 blockade (3.79%±1.73%) **(Figure 31B)**. Within the infected samples, this increase was more pronounced (3.18%±2.40%; αPD-1: 5.96%±3.89%).

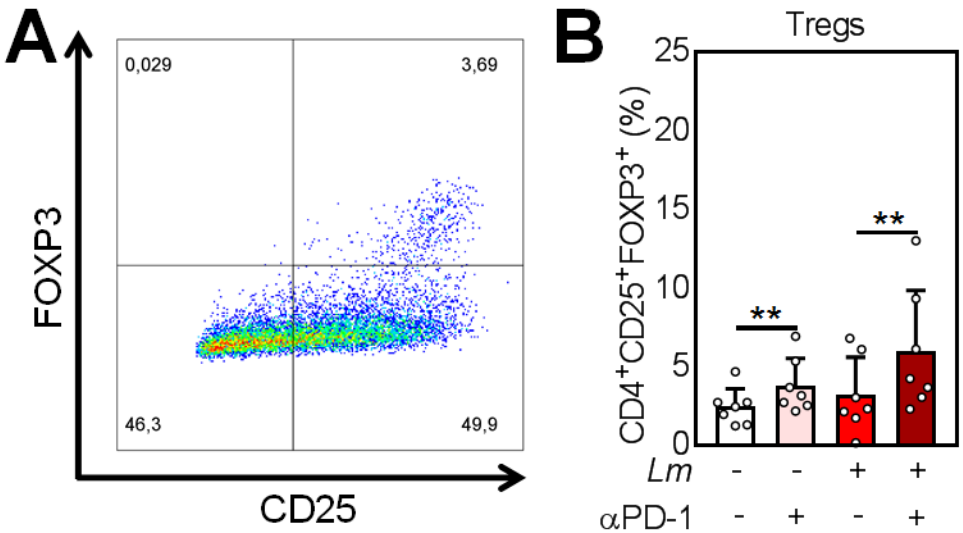

Figure 31: PD-1 blockade slightly increased percentages of regulatory T-cells.

(A, B) Autologous $PBLs^{PHA}$ were co-cultivated with *Lm*-infected hMDDC (MOI=10) and nivolumab (αPD-1). After 5d, cells were harvested and an intranuclear immunostaining (CD4, CD25, and FOXP3) was performed followed by flow cytometric analysis. Regulatory T-cells were gated via their FSC/SSC properties and the labeled antibodies. **(A)** Representative dot plot of CD25 and FOXP3 expression on all $CD4^+$ T-cells. **(B)** Data is presented as mean percentage ± SD. Three independent experiments were performed (N = 7). Statistics were calculated using the parametric paired t-test; $P<0.05$ is considered statistically significant (*$P<0.05$; **$P<0.01$).

This shows that PD-1 blockade slightly increased percentage of regulatory T-cells.

4.21 PD-1 blockade increases T-cell activation marker and proliferation of $CD28^+$ T-cells

Recently it was shown that CD28 but not TCR signaling is inhibited by PD-1 upon interaction with its cognate ligands (Hui et al., 2017). Thus, we wondered whether PD-1 blockade specifically increases the percentage of $CD3^+CD28^+$ T-cells. Compared to the untreated (non-)infected sample (30.93%±21.14%; *Lm*: 43.07%±31.53%), the percentage of $CD3^+CD28^+$ T-cells tended to be higher after PD-1 blockade (41.50%±24.42%; *Lm*: 63.08%±26.50%) **(Figure 32A)**. This is an indicative that specifically $CD28^+$ T-cells proliferate upon PD-1 blockade.

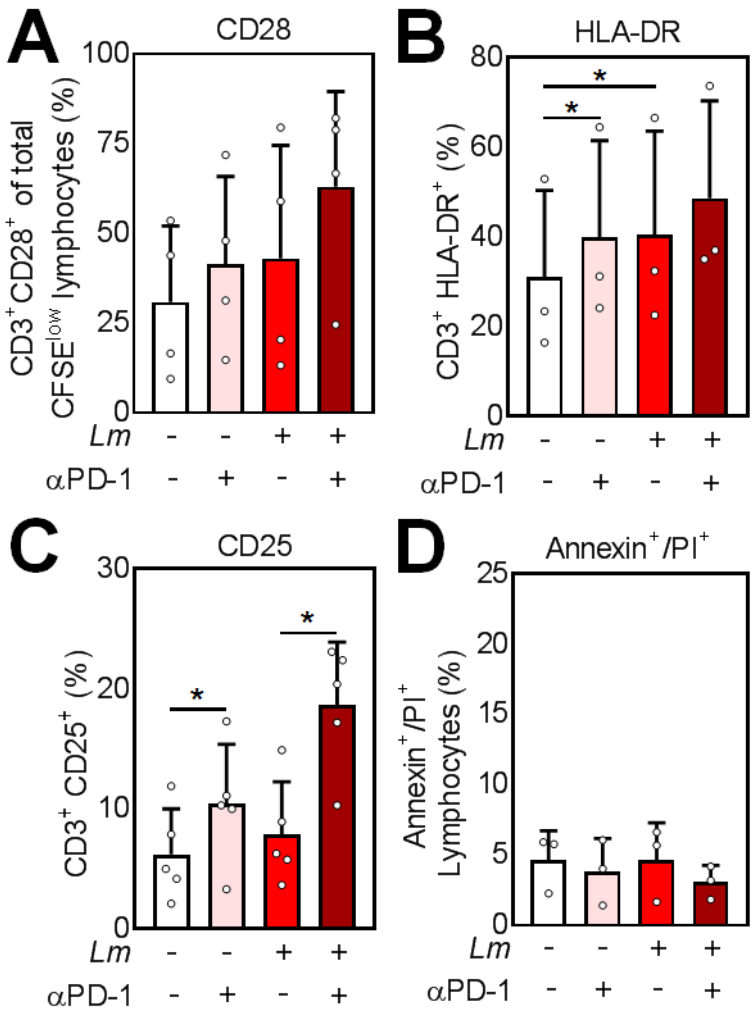

Figure 32: T-cell activation markers were increased upon PD-1 blockade.
(A-D) CFSE-labeled autologous PBLs^{PHA} were co-cultivated with *Lm*-infected hMDDC (MOI=10) and nivolumab (αPD-1). After 5d, cells were harvested, fluorescently labeled with **(A)** (CD3, CD28), **(B)** (CD3, HLA-DR), **(C)** (CD3, CD25), or **(D)** Annexin/PI followed by flow cytometric analysis. T-cells were gated via their FSC/SSC properties, CFSE and the labeled antibodies. Data is presented as mean percentage ± SD. At least two independent experiments were performed (N = 3-5). Statistics were calculated using the parametric paired t-test; $P<0.05$ is considered statistically significant (*$P<0.05$; **$P<0.01$).

Because *Lm*-induced T-cell proliferation was enhanced after PD-1 blockade, we were interested whether T-cell activation markers were also increased. Therefore we analyzed the expression of the T-cell activation markers HLA-DR and CD25 **(Figure 32B, C)**. In the absence of infection, the percentage of HLA-DR$^+$ T-cells was significantly higher after PD-1 blockade (31.00%±19.37%; 40.00%±21.51%) **(Figure 32B)**. *Lm* infection increased the percentage of HLA-DR$^+$ T-cells to a similar extent as PD-1 blockade in the uninfected sample (40.57%±23.08%). In the infected sample, PD-1 blockade tended to increase

the percentage of HLA-DR$^+$ T-cells compared to infection alone (48.63%±21.73%). In the absence of infection, a higher percentage of T-cells expressed the IL-2 receptor CD25 after PD-1 blockade compared to the corresponding untreated sample (10.40%±4.96%; 6.22%±3.80%) **(Figure 32C)**. In presence of *Lm* infection, percentage of CD25 T-cells was not significantly different compared to the uninfected sample (7.91%±4.33%), but PD-1 blockade highly enhanced the number of CD25 expressing T-cells (18.68%±5.21%). By using the apoptosis dyes Annexin/PI, we detected comparable high viability of lymphocytes in all four conditions (4.66%±2.07%; αPD-1: 3.84%±2.33%; *Lm*: 4.66%±2.64%; *Lm* + αPD-1: 3.08%±1.19%) **(Figure 32D)**. In all, this data shows that PD-1 blockade enhances expression of co-stimulatory molecules that are important for an improved T-cell activation.

4.22 PD-1/PD-L blockade shifts *Lm*-induced CD4$^+$ T-cells towards a T_H1 phenotype and increases expression of cytolytic effector molecules

In the classical mouse model of leishmaniasis the induction of a T_H1 response leads to healing, whereas induction of T_H2 cells promotes disease (Sacks and Noben-Trauth, 2002). In human leishmaniasis such a T_H1/T_H2 dichotomy is not evident (Castellano et al., 2009; Nylén and Gautam, 2010). Thus, we examined in our model whether the T_H1-specific transcription-factor Tbet and the T_H2-specific transcription-factor GATA3 are differentially expressed upon PD-1 blockade. The representative pseudocolor plots on the left indicate differential intra-nuclear expression of Tbet and GATA3 in presence or absence of nivolumab in the *Lm*-infected sample **(Figure 33A)**. Compared to the untreated infected sample, a significantly higher number of Tbet$^+$ (13.06%±8.35%; 26.06%±9.46%) and Tbet$^+$/GATA3$^+$ (8.68%±9.22%; 14.41%±11.33%) proliferating CD4$^+$ T-cells was measured in the presence of nivolumab, whereas the percentage of GATA3$^+$ T-cells tended to be lower (18.77±16.68; 12.68±10.54) **(Figure 33B)**. We conclude that PD-1 blockade shifts *Lm*-induced CD4$^+$ T-cells more towards a T_H1- or T_H1/T_H2 phenotype. The higher percentage of T_H1 T-cells might be implicated in the improved parasite killing.

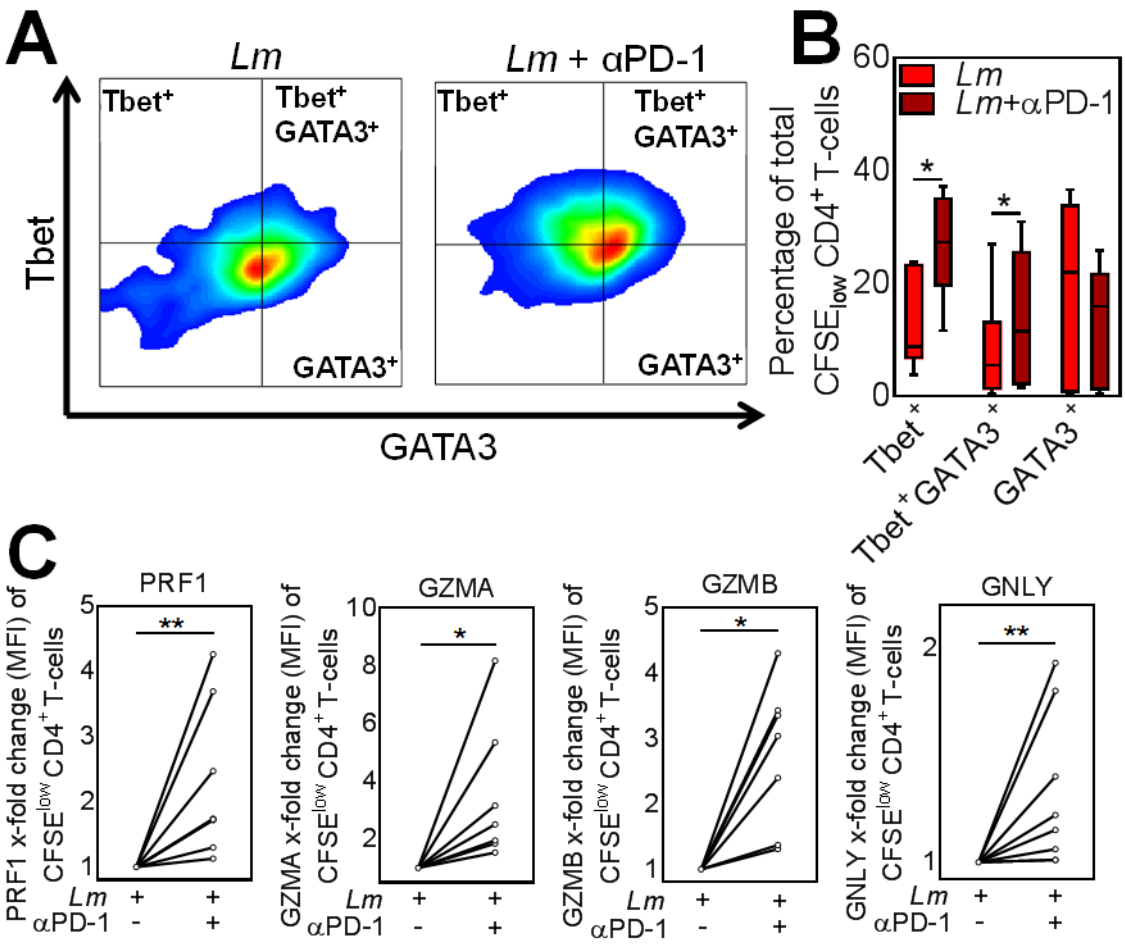

Figure 33: PD-1 blockade shifted proliferating CD4$^+$-T-cells towards a T_H1 or T_H1/T_H2 phenotype and increased expression of cytolytic effector molecules.

(A-C) CFSE-labeled autologous PBLs^{PHA} were co-cultivated with *Lm*-infected hMDDC (MOI=10) and nivolumab (αPD-1). After 5d, cells were harvested, immunostained for **(A-B)** (CD3, CD4, Tbet, GATA3) or **(C)** (CD3, CD4, PRF1, GZMA, GZMB, GNLY) and analyzed by flow cytometry. T-cells were gated via their FSC/SSC properties and the labeled antibodies. **(A)** Representative pseudocolor plot of the *Lm*-infected samples illustrates differential expression of Tbet and GATA3 in presence or absence of αPD-1. Data is presented as **(B)** mean percentage ± SD or **(C)** mean ± SD x-fold change (MFI) relative to the untreated infected sample. At least two independent experiments were performed (N = 4). Statistics were calculated using **(B,C)** the Wilcoxon matched-pairs signed rank test; P<0.05 is considered statistically significant (*P<0.05; **P<0.01).

CD4$^+$ T-cells can release an extensive repertoire of cytolytic effector molecules, used either to help infection control or initiate apoptosis of a target cell (Brown, 2010). To examine, whether PD-1 blockade increases expression of such cytolytic effector molecules, we analyzed intracellular expression of Perforin (PRF1), Granulysin (GNLY), Granzyme A (GZMA) and Granzyme B (GZMB) in CFSE^{low}CD4$^+$-T-cells from the co-culture with hMDDC using flow cytometry

(Figure 33C). Intracellular expression of PRF1 was significantly higher (1.13-fold to 4.26-fold increase) in the proliferating $CD4^+$-T-cells after PD-1 blockade relative to the untreated infected sample. Like for PRF1, we measured a higher GZMA (1.53-fold to 8.17-fold increase), GZMB (1.31-fold to 4.3-fold increase) and GNLY expression (1.01-fold to 1.93-fold increase) in the infected samples when PD-1 was blocked **(Figure 33C)**. To conclude, we determined intracellular PRF1, GNLY, GZMA and GZMB to be increased in the *Lm*-induced proliferating $CD4^+$ T-cells upon PD-1 blockade. This strongly suggests that reduced parasite survival upon PD-1 blockade is mediated in part by PRF1, GZMA, GZMB and GNLY.

4.23 PD-1/PD-L blockade-mediated effects are independent of CD40/CD40L interactions

In the background of chronic infectious diseases like *Toxoplasma gondii*, it was shown that PD-1 blockade-mediated effects on exhausted $CD8^+$ T-cells strongly depend on CD40/CD40L interactions (Bhadra et al., 2013). Mice lacking CD40 were shown to be highly susceptible to *Lm* infection and unable to induce a protective T_H1 response. CD40-CD40L interactions were shown to induce leishmanicidal effector functions in macrophages and dendritic cells (Kamanaka et al., 1996; Grewal and Flavell, 1998). Thus, we decided to investigate whether PD-1 blockade-mediated effects on *Lm* infection and T-cell proliferation are dependent on CD40-CD40L interactions. We already showed that CD40 is highly expressed on hMDDC in the co-culture with $PBLs^{PHA}$, and the expression of this molecule is slightly increased after PD-1 blockade **(Figure 29E)**. Before blocking CD40-CD40L interactions, we first determined CD40 and CD40L expression on T-cells after 5d co-culture with *Lm*-infected hMDDC **(Figure 34A)**. Activated T-cells are reported to express CD40L and to a lesser extent CD40 (Grewal and Flavell, 1998; Bourgeois et al., 2002). We detected a low percentage of $CD40^+$ T-cells in the non-infected sample (6.23%±0.34%), which mildly increased by PD-1 blockade (8.75%±1.38%).

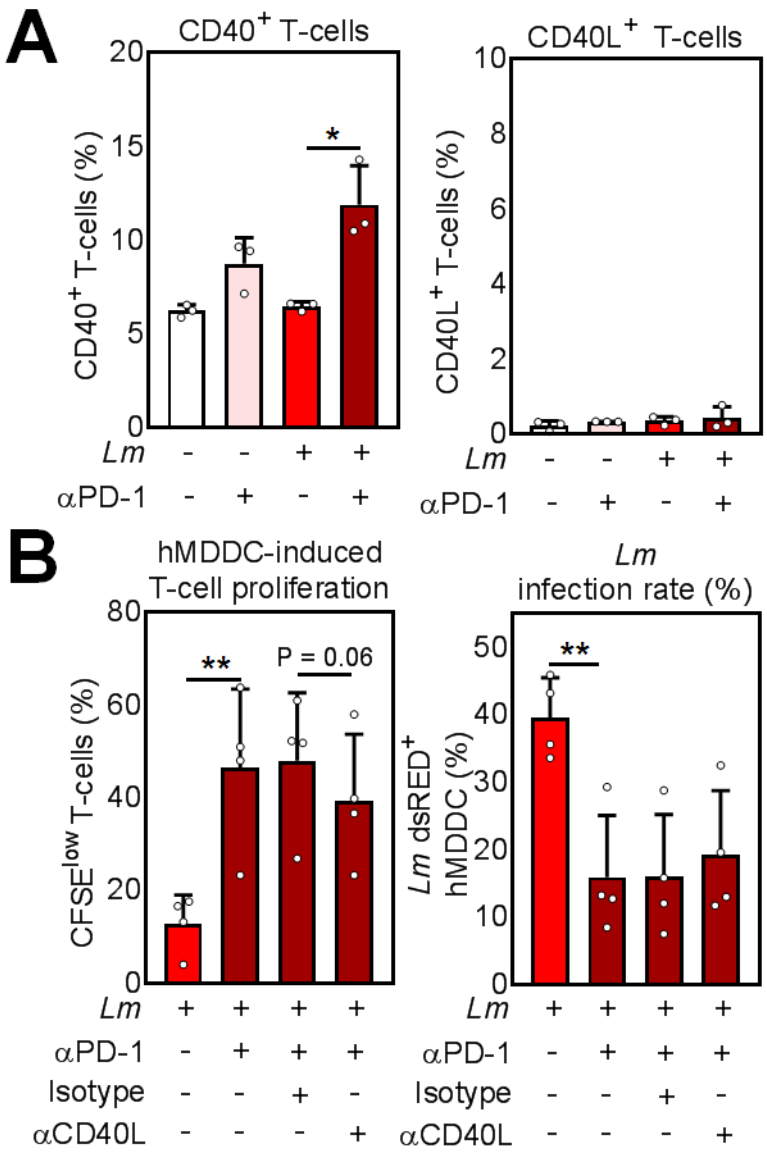

Figure 34: Effects of PD-1 blockade were marginally influenced by CD40/CD40L interactions.

(A-B) CFSE-labeled autologous PBLs^{PHA} were co-cultivated with *Lm*-infected hMDDC (MOI=10), nivolumab (αPD-1) **(B)** and 20 µg/ml CD40L neutralizing antibodies (αCD40L) or corresponding Isotype control (Isotype). After 5d, cells were harvested, immunostained for **(A)** (CD3, CD40 and CD40L) or **(B)** directly analyzed by flow cytometry. **(A-B)** T-cells were gated via their FSC/SSC properties, **(B)** CFSE and the labeled antibodies. hMDDC were gated via their FSC/SSC properties, CFSE and *Lm* dsRED. Data is presented as **(A-B)** mean percentage ± SD. At least two independent experiments were performed (N = 3-4). Statistics were calculated using the parametric paired t-test; $P<0.05$ is considered statistically significant (**$P<0.01$).

Percentages of CD40$^+$ T-cells were comparable between the infected (6.48%±0.23%) and non-infected sample. Interestingly, the number of CD40$^+$ T-cells significantly increased by PD-1 blockade in the infected sample

(11.90%±2.09%) compared to infection alone **(Figure 34A)**. CD40L was not detectable on the surface of T-cells irrespective of the treatment after 5d in co-culture. CD40L expression on $CD4^+$ T-cells reaches its maximal expression 6-8h after antigen stimulation followed by a gradual loss (van Kooten and Banchereau, 2000). In preliminary experiments using two different CD40L antibodies, we did not detect CD40L on T-cells co-cultured for 6h with *Lm*-infected hMDDC **(data not shown)**. Because CD40L has also cytokine-like properties and exists in several soluble isoforms (van Kooten and Banchereau, 2000), we blocked the CD40/CD40L interaction in our assay by using a neutralizing CD40L antibody **(Figure 34B)**. We did not use CD40 blocking antibodies, because most commercially available antibody clones have agonistic properties (Pound et al., 1999). In the presence of *Lm* infection, PD-1 blockade strongly induced T-cell proliferation (46.48%±16.89%). PD-1 blockade-induced T-cell proliferation was not significantly affected by the isotype control antibody (47.95%±14.65%). Compared to the isotype control antibody, CD40L neutralization marginally reduced PD-1 blockade-induced T-cell proliferation (39.40%±14.25%). As already demonstrated, *Lm*-infection rate of hMDDC was significantly dampened after PD-1 blockade (15.92%±9.17%). Compared to the PD-1 blocked sample, treatment with an Isotype control did not significantly change infection rate (16.02%±9.18%). CD40L neutralization tended to increase parasite survival (19.20%±9.52%). Although we saw marginal effects of CD40L neutralization on PD-1 blockade-mediated effects, we concluded that PD-1 blockade-mediated effects in our primary human cell model of leishmaniasis are independent of CD40/CD40L interactions.

5 Discussion

In this thesis the impact of PD-1/PD-L axis, an important negative regulator of T-cell responses, was investigated in *Lm* infection of primary human myeloid and lymphoid cells. Therefore, three different *in vitro* co-culture assays were established and tested for their suitability to modulate PD-1/PD-L interactions by using PD-1 checkpoint inhibitors **(Figure 35; 1.)**. The therapeutic PD-1 checkpoint inhibitor nivolumab did not significantly alter *Lm*-induced T-cell proliferation and *Lm* infection rate compared to the untreated samples in a T-cell assay consisting of autologous PBLs together with *Lm*-infected hMDM1, hMDM2 or hMDDC (Protocol by Crauwels, 2015). Thus, we examined whether PD-1 blockade impacts *Lm* infection rate in myeloid cells and *Lm*-induced T-cell proliferation in an *in vitro* assay, which mimics tissue-like conditions and renders T-cells more responsive to their cognate antigen (modified RESTORE-Assay by Römer et al., 2011). Although PD-1 and its ligands were detectable in this assay, we didn't observe significant differences in T-cell proliferation due to PD-1 checkpoint blockade **(Figure 35; 1.)**.

PD-1/PD-L interactions are highly prominent during chronic inflammation and persistent antigen stimulation, which can lead to dysfunctional or exhausted T-cells. To mimic this situation in our experiments, we applied PHA-pre-stimulated PBLs ($PBLs^{PHA}$) in co-culture with infected hMDM1, hMDM2 or hMDDC. We demonstrated that T-cells of $PBLs^{PHA}$ express high levels of T-cell exhaustion markers, proliferate less upon *Lm* antigen encounter and dampen *Lm* infection rate less efficiently compared to non-pre-stimulated PBLs *in vitro*.

PD-1 checkpoint inhibition with the humanized IgG1 (G&P Biosciences) or the fully-human IgG4 (BMS nivolumab) anti-PD-1 mAb enhanced *Lm*-induced T-cell proliferation and reduced parasite burden in the $PBLs^{PHA}$ assay in a similar manner **(Figure 35; 2.)**. Focusing on the therapeutic IgG4 PD-1 checkpoint inhibitor nivolumab, we found that effector functions of PHA-pre-stimulated T-cells could be restored by PD-1 checkpoint blockade, whereas the magnitude of T-cell proliferation, parasite killing and pro-inflammatory cytokine release was highest in the co-culture with *Lm*-infected hMDDC followed by hMDM1 and hMDM2 **(Figure 35; 3.)**. PD-1 checkpoint inhibition tended to reduce expression of macrophage-specific markers and enhanced dendritic cell-specific markers including maturation markers. Thus, we focused on the hMDDC:$PBLs^{PHA}$ co-

culture, where we found PD-1 checkpoint blockade-mediated effects to be partly TNFα and not IFNγ dependent. Furthermore, PD-1 blockade specifically enhanced proliferation of $CD4^+$ T-cells, increased expression of the T_H1-specific transcription factor Tbet, T-cell activation markers and cytolytic effector proteins, which might be implicated in enhanced parasite killing **(Figure 35; 4.)**.

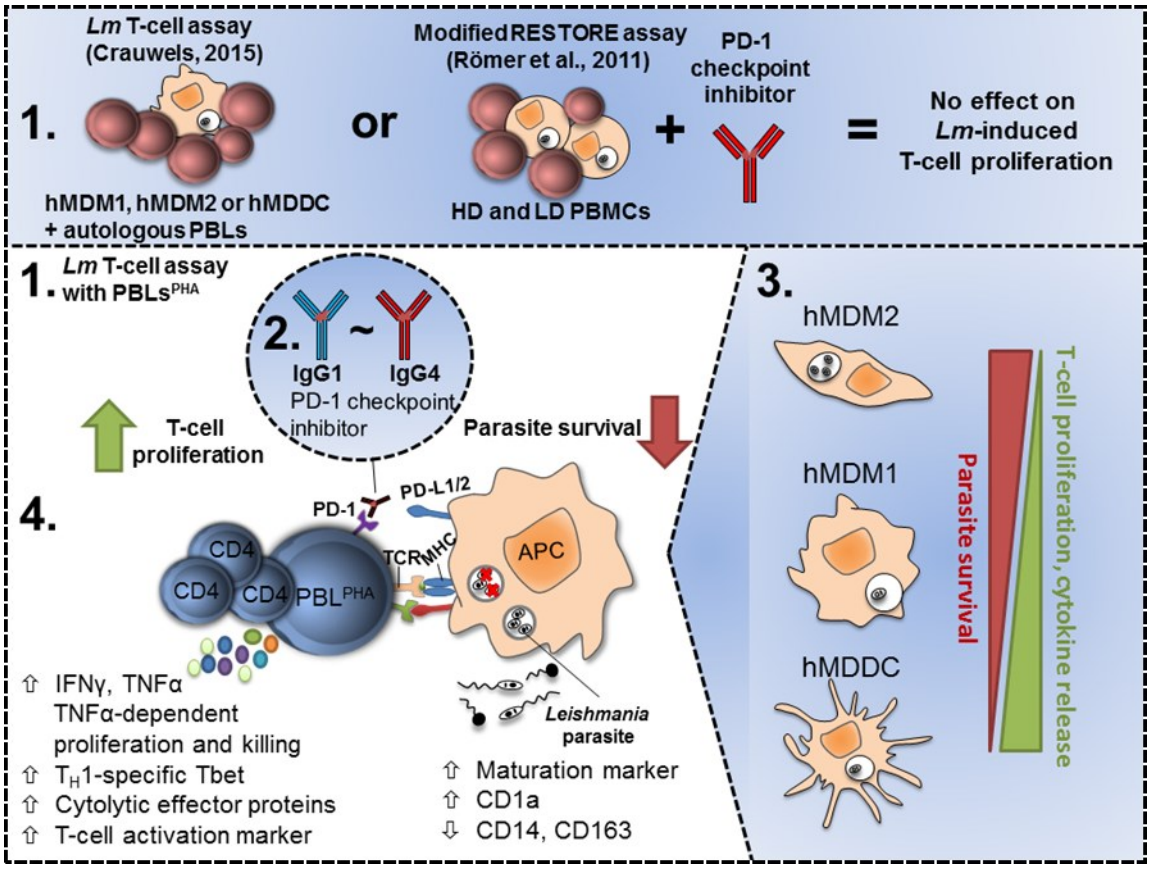

Figure 35: Summary of the obtained research data in this thesis.

1.) Three *Lm*-specific T-cell assays with T-cell proliferation and parasite load as read outs were established. PD-1 checkpoint blockade had no effect on T-cell proliferation in the *Lm* T-cell assay by Crauwels (2015) or the modified RESTORE assay. But PD-1 checkpoint inhibition increased T-cell proliferation and decreased *Lm* infection in the *Lm* T-cell assay with $PBLs^{PHA}$. **2.)** By using the latter approach, two different subclasses (IgG1 and IgG4) of PD-1 checkpoint inhibitors increased T-cell proliferation and reduced parasite survival in a similar manner. **3.)** Effects mediated by PD-1 checkpoint blockade on *Lm*-induced T-cell proliferation, cytokine release and parasite killing were highest in the $PBLs^{PHA}$ co-culture with hMDDC followed by hMDM1 and hMDM2 **4.)** Focusing on the hMDDC:$PBLs^{PHA}$ co-culture, we found PD-1 checkpoint blockade mediated effects to be TNFα-dependent. Furthermore, the T_H1-specific transcription factor Tbet was increased as well as cytolytic effector proteins and T-cell activation markers. In addition PD-1 checkpoint blockade increased maturation marker on hMDDC and the dendritic cell marker CD1a, whereas macrophage specific markers (CD14, CD163) were reduced.

5.1 *Leishmania* infection of human monocyte-derived phagocytic cells enhances their expression of PD-L and augments PD-1 levels on co-cultured T-cells

The function of the co-inhibitory PD-1/PD-L pathway has been extensively investigated in the field of chronic infections, cancer or autoimmunity (Sharpe et al., 2007; Iwai et al., 2017). However, a role of this regulatory pathway in acute or early infection is less established and differs between pathogens (Brown et al., 2010). Early after *Leishmania* infection, macrophages or dendritic cells play an important role in the induction of T-cell responses (Liu and Uzonna, 2012). How the PD-1/PD-L axis influences this process with regard to different professional antigen presenting cells is not clear.

Here, we demonstrated both PD-1 ligands to be expressed on hMDM1, hMDM2 and hMDDC. PD-1 ligands are in general upregulated by signals that lead to activation of macrophages and dendritic cells, e.g. TLR ligands or cytokines (Yamazaki et al., 2002; Loke and Allison, 2003). In coherence, both PD-1 ligands were strongly upregulated on hMDM1, hMDM2 and hMDDC using recombinant human IFNγ. PD-1 ligand expression data of *Leishmania*-infected macrophages and dendritic cells is scarce. In *L. mexicana*-infected wild type mice, immunohistochemistry methods proved PD-L1 and PD-L2 expression in cutaneous lesions (Liang et al., 2006). Flow cytometric analysis revealed that *in vitro* infection (MOI=10, 24h) of peritoneal macrophages from BALB/C mice with *L. mexicana* slightly reduced surface PD-L1 levels and tended to increase PD-L2 levels (Martínez Salazar et al., 2014). By using human primary cells, we found that *Lm* infection increased PD-L1 surface expression both on hMDM1 and hMDM2. PD-L2 levels were significantly increased only on *Lm*-infected hMDM1. Correspondingly, Loke and colleagues showed that PD-L2 is preferentially inducible on inflammatory mouse macrophages (Loke and Allison, 2003), but HIV-infection significantly increased both PD-1 ligands also on anti-inflammatory hMDM2 (Rodríguez-García et al., 2011). PD-L1 and PD-L2 surface expression on hMDDC was not altered by *Lm* infection but basal PD-1 ligand expression was higher compared to both hMDM. Ohradanova-Reic and colleagues showed PD-L2 (CD273) expression to be highest in hMDDC, followed by hMDM1 and hMDM2 (Ohradanova-Repic et al., 2016).

Previously, we reported that *Lm*-infected hMDM1, hMDM2 or hMDDC generated from monocytes of *Leishmania*-naïve German blood donors induce a

MHC class II-dependent T-cell response in autologous *in vitro* co-cultures (Crauwels, 2015). This early T-cell response reduced parasite load in the infected host cells.

We found *Lm* infected hMDM1, hMDM2 or hMDDC to significantly increase the number of PD-1^+ T-cells in a co-culture with autologous PBLs compared to the uninfected control. PD-1 expression is induced on T-cells by antigen-dependent and -independent stimuli, presumably to adjust the resulting T-cell response with its function as a co-inhibitory receptor (Agata et al., 1996; Kinter et al., 2008). Although we detected PD-1 on T-cells and its ligands on the *Lm* host cells, PD-1/PD-L blockade with nivolumab had no significant effect on *Lm*-induced T-cell proliferation or *Lm* infection rate. A reason for this could be that PD-1/PD-L signaling in this setting might be overridden by dominant co-stimulatory signals. For instance, exogenous IL-2 addition or CD28 co-stimulation can override PD-1/PD-L-mediated inhibition (Freeman et al., 2000; Carter et al., 2002). Furthermore, gene expression profiles of PD-1^{hi} vs. PD-1^{low} $CD8^+$ T-cells of healthy donors did not reveal any PD-1-related functional impairment. Rather it was pointed out, that the PD-1 expressing cells represent ordinary effector memory T-cells (Duraiswamy et al., 2011). Thus, we concluded that in the co-culture assay by Crauwels et al. (2015), *Lm*-induced T-cells were not functionally impaired, and increased PD-1 expression was related to T-cell activation.

Upon infection, myeloid and lymphoid cells from the peripheral blood infiltrate the cell-dense skin and differentiate to specific specialized cell types due to environmental factors e.g. cell-cell contacts or inflammation (Ginhoux and Jung, 2014; Varol et al., 2015). Römer and colleagues showed *in vitro* that T-cells and monocytes responded with higher reactivity to an immunogenic stimulus, when they were pre-cultured under high cell density compared to low cell density conditions (Römer et al., 2011). We used a modified protocol of the RESTORE-Assay by Römer et al. (2011) to investigated whether PD-1/PD-L interactions might influence *Lm* infection and the T-cell response under tissue-like conditions. More PD-1^+ T-cells and increased T-cell proliferation were detected upon *Lm* infection, when using high density (HD) pre-cultured PBMCs compared to low density (LD) pre-cultured PBMCs. In addition, *Lm*-infected host cells expressed both PD-1 ligands and had a more pro-inflammatory phenotype

when they were HD pre-cultured. Again, PD-1 blockade had no effect on *Lm*-induced T-cell proliferation. Interestingly we detected a significantly reduced *Lm* infection rate for both LD and HD PBMCs in presence of the PD-1 checkpoint inhibitor nivolumab but this could not be correlated to increased T-cell proliferation. One reason could be that PD-1/PD-L blockade increases expression of pro-inflammatory cytokines without T-cell expansion, thereby reducing parasite load in the host cells. However, this scenario is very unlikely. Experiments with human primary T-cells showed that T-cell proliferation is more sensitive to PD-1/PD-L-mediated inhibition than e.g. IFNγ release or cytotoxicity (Wei et al., 2013). Since a corresponding isotype control antibody was missing in these experiments, we could not rule out parasite killing to be Fc-mediated.
In conclusion, PD-1 and its ligands were expressed in the modified *Lm* RESTORE assay, but nivolumab treatment did not alter *Lm*-induced T-cell proliferation. Interestingly, there was a significant reducing effect of nivolumab on parasite survival, which could not be correlated to an increased T-cell response. PD-1 checkpoint inhibition in the *Lm* RESTORE-assay was not further studied by virtue of a more promising approach.

5.2 PD-1/PD-L axis inhibits T-cell response and leishmanicidal effector functions in an *in vitro* approach mimicking chronic stimulation

PD-1/PD-L interactions are not prominent during the early T-cell priming phase, but they regulate the T-cell response during the effector phase (Ribas, 2012). During chronic infections and cancer, PD-1/PD-L interactions play an important role in gradual deterioration of T-cell effector functions ultimately leading to T-cell dysfunction or exhaustion. Chronic antigen stimulation and high inflammation progressively induce upregulation of several co-inhibitory molecules on exhausted T-cells, e.g. PD-1, PD-L1 and LAG-3 (Wherry, 2011).
To investigate PD-1/PD-L interactions within the context of exhausted T-cells and *Lm* infected host cells, we used a newly established *in vitro* model. In this model, we mimicked exhausted T-cells by stimulating PBLs with phytohemagglutinin (PHA) prior to co-cultivation with autologous *Lm*-infected host cells. PHA is a mitogen used for polyclonal activation and expansion of T-cells (Lindahl-Kiessling, 1972). Furthermore, it is reported to lead to functionally impaired T-lymphocytes in contrast to stimulation by CD3/CD28 (Duarte et al., 2002). We confirmed PHA-stimulated T-cells to express high levels of inhibitory

PD-1, PD-L1, LAG-3, TIM-3 and 2B4, and thus, to resemble exhausted T-cells. T-cell exhaustion is not only characterized by expression of inhibitory surface molecules; also soluble factors, molecular alterations as well as regulatory cells play a role (Speiser, 2012). Hence, to fully demonstrate that T-cells of PBLs^{PHA} are indeed functionally exhausted, genomic profiling would be required.

Comparison of autologous PBLs and PBLs^{PHA} in an autologous co-culture with *Lm*-infected hMDM1 revealed that T-cells of PBLs^{PHA} proliferate less and parasite survival in hMDM1 is higher compared to T-cells of the co-culture with PBLs. This strongly suggests PHA-pre-stimulated T-cells to be functionally impaired. It is also possible that, due to the strong pre-stimulation with PHA, *Lm* responding T-cells could be lost e.g. by activation-induced death and therefore, there is less T-cell proliferation. In future studies, a clear distinction between functional impairment and loss of *Lm* responding T-cells could be achieved by performing a tetramer staining with suitable HLA class II tetramers. A broadly conserved immunodominant *Leishmania* antigen for establishment of such HLA class II tetramers might be PEPCK (Phosphoenolpyruvat carboxykinase), as it was successfully used in vaccination studies of mice and human (Mou et al., 2015).

Taken together, we showed that PHA-pre-stimulation of PBLs is an approach to generate exhausted-like T-cells *in vitro*. Using those cells in a co-culture approach with *Lm*-infected host cells could mimic the persistent antigen-stimulation that occurs during chronic infectious diseases, including leishmaniasis.

5.3 The phenotype of the *Lm*-infected host cell phenotype dictates the magnitude of nivolumab-mediated effects in the co-culture with PBLs^{PHA}

By using our newly established assay with mimicked T-cell exhaustion, we found both anti-PD-1 antibodies, the research grade humanized IgG1 and the therapeutic fully-human IgG4 nivolumab, to enhance T-cell effector functions and reduce parasite survival. Both blocking antibodies yielded similar results. This indicates that the PBLs^{PHA} assay is not sensitive enough to observe significant Fc-dependent differences of PD-1 checkpoint inhibitors. According to the manufacturer, the humanized IgG1 is not glyco-engineered and should be capable of inducing ADCC or CDC. One reason, why we did not observe

significant differences could be that there are too few NK-cells to induce ADCC against PD-1$^+$ T-cells. In the hMDDC:PBLs^{PHA} co-culture we observed only a small percentage of CD3$^-$ CD56$^+$ NK-cells. Thus, we focused only on the therapeutic anti-PD-1 IgG4 nivolumab in all follow-up experiments.

Interestingly, we found nivolumab-mediated effects to depend on the phenotype of the host cell that was initially infected with *Lm*. Our data suggests *Lm*-infected anti-inflammatory hMDM2 not to be target of PD-1/PD-L-mediated inhibition, whereas PD-1/PD-L interactions strongly inhibit T-cell effector functions on *Lm*-infected hMDDC. This might be caused by a higher expression of both PD-1 ligands on hMDDC compared to hMDM2. Furthermore, antigen-presenting dendritic cells are much more potent in inducing T-cell responses compared to macrophages. Arnold and colleagues compared differently polarized human monocyte-derived macrophages and dendritic cells in their ability to induce autologous T-cells by using PPD (mycobacterial purified protein derivate) as recall antigen or KLH (keyhole limpet haemocyanin) as a primary antigen for naïve T-cell responses. In this context, dendritic cells (hMDDC) induced the highest levels of T-cell proliferation to both antigens, whereas LPS+IFNγ-treated macrophages (comparable to hMDM1) and IL-4-treated macrophages (comparable to hMDM2) were less effective in inducing antigen-specific T-cell responses (Arnold et al., 2015).

5.4 Nivolumab treatment enhances the *Lm*-induced CD4$^+$ T-cell response and parasite in a partially TNFα-dependent manner

Focusing on hMDDC, we could partially reverse effects of PD-1 blockade by neutralization of soluble TNFα. Elevated levels of TNFα and a concomitant decrease of parasite load after PD-1/PD-L blockade had previously been demonstrated in the canine model of visceral leishmaniasis (Chiku et al., 2016).

Furthermore, we found that neutralization of IFNγ, which was induced after PD-1 blockade in the hMDDC samples, had no significant effect on T-cell proliferation or parasite load. IFNγ is reported to mediate resistance to *Lm* in mice by inducing inducible nitric oxide synthase (iNOS) expression (Sacks and Noben-Trauth, 2002). In human myeloid cells, iNOS (or NOS2) expression and function is controversially debated (Schneemann et al., 1993; Bogdan, 2001). *In vitro* generated human myeloid cells are unable to express functional iNOS (NOS2) because the essential iNOS co-factor BH4 is missing (Schneemann et

al., 1993). Therefore, IFNγ might not have a leishmanicidal effect in our *in vitro* model. In contrast to mice, reactive oxygen species (ROS) play an important role in parasite control during human leishmaniasis. IFNγ was shown to induce reactive oxygen species (ROS) in *Leishmania*-infected human monocytes, which dampened overall parasite load (Novais et al., 2014). Furthermore, ROS-dependent parasite control was rather evident in monocytes from CL patients than in monocytes from healthy individuals (Carneiro et al., 2016). Thus, it could be that IFNγ-induced ROS production in *Lm*-infected hMDDC was too low reveal significant effects of IFNγ neutralization on infection rate in our *in vitro* model. The general increased survival of T-cells upon IFNγ might be another reason for why we did not observe significant differences in T-cell proliferation. However, IFNγ does not increase the number of antigen-specific T-cell divisions. This was previously shown e.g. for murine OVA-specific $CD4^+$-T-cells (Reed et al., 2008).

In our *in vitro* model, preferentially $CD4^+$-T-cells proliferated upon *Lm* infection and nivolumab treatment. In the classical mouse model of *Lm*, induction of T_H1 response leads to resistance whereas the induction of a T_H2 response promotes disease (Sacks and Noben-Trauth, 2002). Human cutaneous leishmaniasis patients with moderate disease symptoms show a balanced T_H1/T_H2 response, whereas an imbalance of T_H1/T_H2 is associated with increased disease severity (Scorza et al., 2017). Experiments with blood of prostate and advanced melanoma cancer patients revealed that PD-1 blockade augments T_H1 responses und suppresses T_H2 responses (Dulos et al., 2012). By analyzing the intranuclear expression of the T_H1-specific Tbet and T_H2-specific GATA3, we found PD-1 blockade to shift *Lm*-induced $CD4^+$ T-cells more towards a T_H1 or T_H1/T_H2 phenotype, respectively. Thus, the higher abundance of T_H1 T-cells and their effector functions may be implicated in reduction of *Lm* infection.

The transcription factor Tbet does not only control IFNγ production and T_H1 linage, it can also bind to perforin and granzyme B promotor regions to induce expression of cytolytic effector proteins in $CD4^+$ T-cells (Glimcher et al., 2004; Hua et al., 2013). Specific killing of intracellular parasites in a concerted action of perforin, granzymes and granulysin (expressed by T-cells) with minimal collateral damage to the host cell was demonstrated in transgenic mouse

models (Dotiwala et al., 2016). PD-1 blockade is described to increase perforin, granzyme B and granulysin expression in T-cells of tuberculosis- and cancer patients (Rao et al., 2017). Focusing on *Lm*-induced $CD4^+$ T-cells, we detected increased intracellular levels of perforin, granzyme A and B, and granulysin after PD-1 blockade. This was not accompanied by an increased host cell death as shown by Annexin/PI staining. This suggests that cytolytic molecules might contribute to the reduction of *Lm* in hMDDC without significant cytotoxicity of host cells.

5.5 PD-1 checkpoint inhibition: a treatment option for leishmaniasis?

Altogether, our data suggests how the PD-1/PD-L axis can modulate *Lm* host cells and $CD4^+$ T-cells in patients suffering from chronic forms of leishmaniasis. So far, most research groups focus on $CD8^+$ T-cell exhaustion, which was observed in diffuse cutaneous (Hernández-Ruiz et al., 2010) and visceral human leishmaniasis (Gautam et al., 2014). In case of the cutaneous forms of human leishmaniasis, $CD8^+$ T-cells have a dual role (Stäger and Rafati, 2012) but their contribution in resolving primary cutaneous *Leishmania* infection might be negligible (Wang et al., 1993; Huber et al., 1998). $CD4^+$ T-cells activate leishmanicidal functions of infected macrophages and dendritic cells. In our experiments infected hMDDC benefit the most from PD-1 blockade, as this strongly enhanced $CD4^+$ T-cell effector functions and parasite killing. Additionally we found increased levels of maturation markers on *Lm*-infected hMDDC after PD-1 blockade. To induce a strong cell-mediated immunity e.g. after vaccination, adequate maturation of dendritic cells is important. In animal models, it was demonstrated that vaccination against leishmaniasis using LPG from *L. mexicana* induced PD-1/PD-L2 expression on several immune cells in a dose-dependent fashion (Martínez Salazar et al., 2014). Blocking the PD-1/PD-L interaction could be a valuable approach to enhance efficacy of leishmaniasis vaccine candidates. Dendritic cell-based immunotherapy in combination with antimonials has been shown to significantly reduce parasite burden in experimental models of VL (Ghosh et al., 2003; Singh and Sundar, 2014). This approach might also further benefit from PD-1 checkpoint inhibitors.

However, though in many infection models (including leishmaniasis animal models) a beneficial effect of PD-1/PD-L checkpoint inhibition was demonstrated, PD-1 blockade was also shown to exacerbate disease in

tuberculosis and accelerate death of infected animals (Sable, 2013). In addition, PD-L1 knockout and PD-L2 knockout mice showed different susceptibility to *Lm*, indicating an non-redundant role of the PD-1 ligands in PD-1 signaling (Liang et al., 2006). These and other factors have to be considered when thinking about using PD-1 checkpoint inhibitors for treatment of leishmaniasis. Moreover, for treatment of highly inflammatory manifestations of leishmaniasis like MCL, PD-1 blockade in combination with pain killers (inhibitors of cyclooxygenases and prostaglandin synthesis, e.g. aspirin or celecoxib) might be an interesting approach. Both aspirin and celecoxib were demonstrated to synergize with PD-1 checkpoint inhibition in melanoma mouse models (Zelenay et al., 2015). Administration of an alginate hydrogel preparation containing celecoxib and anti-PD-1 blocking antibody into an tumor-bearing mouse model stabilized the anti-inflammatory properties of celecoxib (less IL-1β, IL-6) and enhanced tumoricidal effects of anti-PD-1 (Li et al., 2016). The latter approach could reduce side effects and the effective dose of PD-1 checkpoint inhibitors. This would reduce costs, which makes it more likely to be considered for therapy of the still neglected disease leishmaniasis.

Collectively, the present work provides new insights regarding the PD-1/PD-L signaling axis in *Lm* infection of primary human cells and its consequence for adaptive immunity. However, there are limitations to our data produced in the *in vitro* human primary cell model mimicking T-cell exhaustion. Thus, further experiments, e.g. using material obtained from chronic leishmaniasis patients or healed persons, and different approaches are required to fully understand the mechanisms behind PD-1/PD-L-mediated effects on leishmaniasis and a possible use of PD-1 checkpoint inhibitors as therapeutics.

6 References

Agata, Y., Kawasaki, A., Nishimura, H., Ishida, Y., Tsubata, T., Yagita, H., and Honjo, T. (1996). Expression of the PD-1 antigen on the surface of stimulated mouse T and B lymphocytes. International immunology *8*, 765-772.

Alsaab, H.O., Sau, S., Alzhrani, R., Tatiparti, K., Bhise, K., Kashaw, S.K., and Iyer, A.K. (2017). PD-1 and PD-L1 Checkpoint Signaling Inhibition for Cancer Immunotherapy. Mechanism, Combinations, and Clinical Outcome. Frontiers in pharmacology *8*, 561.

Arnold, C.E., Gordon, P., Barker, R.N., and Wilson, H.M. (2015). The activation status of human macrophages presenting antigen determines the efficiency of Th17 responses. Immunobiology *220*, 10-19.

Bagirova, M., Allahverdiyev, A.M., Abamor, E.S., Ullah, I., Cosar, G., Aydogdu, M., Senturk, H., and Ergenoglu, B. (2016). Overview of dendritic cell-based vaccine development for leishmaniasis. Parasite immunology *38*, 651-662.

Banchereau, J., and Palucka, A.K. (2005). Dendritic cells as therapeutic vaccines against cancer. Nature reviews. Immunology *5*, 296-306.

Baratta-Masini, A. (2007). Mixed cytokine profile during active cutaneous leishmaniasis and in natural resistance. Front Biosci *12*, 839.

Barber, D.L., Wherry, E.J., Masopust, D., Zhu, B., Allison, J.P., Sharpe, A.H., Freeman, G.J., and Ahmed, R. (2006). Restoring function in exhausted CD8 T cells during chronic viral infection. Nature *439*, 682-687.

Bazil, V., and Strominger, J.L. (1991). Shedding as a mechanism of down-modulation of CD14 on stimulated human monocytes. The Journal of Immunology *147*, 1567-1574.

Beck, A., Wurch, T., Bailly, C., and Corvaia, N. (2010). Strategies and challenges for the next generation of therapeutic antibodies. Nature reviews. Immunology *10*, 345-352.

Bhadra, R., Cobb, D.A., and Khan, I.A. (2013). CD40 Signaling to the Rescue. A CD8 Exhaustion Perspective in Chronic Infectious Diseases. Crit Rev Immunol *33*, 361-378.

Blackburn, S.D., Shin, H., Haining, W.N., Zou, T., Workman, C.J., Polley, A., Betts, M.R., Freeman, G.J., Vignali, D.A.A., and Wherry, E.J. (2009). Coregulation of CD8+ T cell exhaustion by multiple inhibitory receptors during chronic viral infection. Nature immunology *10*, 29-37.

Blank, C., Brown, I., Marks, R., Nishimura, H., Honjo, T., and Gajewski, T.F. (2003). Absence of Programmed Death Receptor 1 Alters Thymic Development and Enhances Generation of CD4/CD8 Double-Negative TCR-Transgenic T Cells. The Journal of Immunology *171*, 4574-4581.

Blank, C., Kuball, J., Voelkl, S., Wiendl, H., Becker, B., Walter, B., Majdic, O., Gajewski, T.F., Theobald, M., and Andreesen, R., et al. (2006). Blockade of PD-L1 (B7-H1) augments human tumor-specific T cell responses in vitro. International journal of cancer *119*, 317-327.

Blattman, J.N., Wherry, E.J., Ha, S.-J., van der Most, R.G., and Ahmed, R. (2009). Impact of epitope escape on PD-1 expression and CD8 T-cell exhaustion during chronic infection. Journal of virology *83*, 4386-4394.

Bogdan, C. (2001). Nitric oxide and the immune response. Nature immunology *2*, 907-916.

Bourgeois, C., Rocha, B., and Tanchot, C. (2002). A role for CD40 expression on CD8+ T cells in the generation of CD8+ T cell memory. Science (New York, N.Y.) *297*, 2060-2063.

Bourreau, E., Collet, M., Prévot, G., Milon, G., Ashimoff, D., Hasagewa, H., Parra-Lopez, C., and Launois, P. (2002). IFN-γ-producing CD45RA+ CD8+ and IL-10-producing CD45RA- CD4+ T cells generated in response to LACK in naive subjects never exposed toLeishmania. Eur. J. Immunol. *32*, 510-520.

Boussiotis, V.A., Chatterjee, P., and Li, L. (2014). Biochemical signaling of PD-1 on T cells and its functional implications. Cancer journal (Sudbury, Mass.) *20*, 265-271.

Brown, D.M. (2010). Cytolytic CD4 cells. Direct mediators in infectious disease and malignancy. Cellular immunology *262*, 89-95.

Brown, J.A., Dorfman, D.M., Ma, F.-R., Sullivan, E.L., Munoz, O., Wood, C.R., Greenfield, E.A., and Freeman, G.J. (2003). Blockade of Programmed Death-1

Ligands on Dendritic Cells Enhances T Cell Activation and Cytokine Production. The Journal of Immunology *170*, 1257-1266.

Brown, K.E., Freeman, G.J., Wherry, E.J., and Sharpe, A.H. (2010). Role of PD-1 in regulating acute infections. Current opinion in immunology *22*, 397-401.

Bruhns, P., Iannascoli, B., England, P., Mancardi, D.A., Fernandez, N., Jorieux, S., and Daëron, M. (2009). Specificity and affinity of human Fcgamma receptors and their polymorphic variants for human IgG subclasses. Blood *113*, 3716-3725.

Carneiro, P.P., Conceição, J., Macedo, M., Magalhães, V., Carvalho, E.M., and Bacellar, O. (2016). The Role of Nitric Oxide and Reactive Oxygen Species in the Killing of Leishmania braziliensis by Monocytes from Patients with Cutaneous Leishmaniasis. PloS one *11*, e0148084.

Carter, L., Fouser, L.A., Jussif, J., Fitz, L., Deng, B., Wood, C.R., Collins, M., Honjo, T., Freeman, G.J., and Carreno, B.M. (2002). PD-1:PD-L inhibitory pathway affects both CD4(+) and CD8(+) T cells and is overcome by IL-2. Eur. J. Immunol. *32*, 634-643.

Castellano, L.R., Filho, D.C., Argiro, L., Dessein, H., Prata, A., Dessein, A., and Rodrigues, V. (2009). Th1/Th2 immune responses are associated with active cutaneous leishmaniasis and clinical cure is associated with strong interferon-gamma production. Human immunology *70*, 383-390.

Caux, C. (1996). CD34+ hematopoietic progenitors from human cord blood differentiate along two independent dendritic cell pathways in response to GM-CSF+TNF alpha. The Journal of experimental medicine *184*, 695-706.

Chiku, V.M., Silva, K.L.O., Almeida, B.F.M. de, Venturin, G.L., Leal, A.A.C., Martini, C.C. de, Rezende Eugênio, F. de, Dos Santos, P.S.P., and Lima, V.M.F. de (2016). PD-1 function in apoptosis of T lymphocytes in canine visceral leishmaniasis. Immunobiology *221*, 879-888.

Chung, N.P.-Y., Chen, Y., Chan, V.S.F., Tam, P.K.H., and Lin, C.-L.S. (2004). Dendritic cells. Sentinels against pathogens. Histology and histopathology *19*, 317-324.

Crauwels, P. (2015). The interaction of Leishmania major parasites with human myeloid cells and its consequence for adaptive immunity. Mainz, Univ., Diss., 2015 (Mainz).

Crauwels, P., Bohn, R., Thomas, M., Gottwalt, S., Jäckel, F., Krämer, S., Bank, E., Tenzer, S., Walther, P., and Bastian, M., et al. (2015). Apoptotic-like Leishmania exploit the host's autophagy machinery to reduce T-cell-mediated parasite elimination. Autophagy *11*, 285-297.

da Silva, R., and Sacks, D.L. (1987). Metacyclogenesis is a major determinant of Leishmania promastigote virulence and attenuation. Infection and immunity *55*, 2802-2806.

Dahan, R., Sega, E., Engelhardt, J., Selby, M., Korman, A.J., and Ravetch, J.V. (2015). FcγRs Modulate the Anti-tumor Activity of Antibodies Targeting the PD-1/PD-L1 Axis. Cancer cell *28*, 285-295.

Dotiwala, F., Mulik, S., Polidoro, R.B., Ansara, J.A., Burleigh, B.A., Walch, M., Gazzinelli, R.T., and Lieberman, J. (2016). Killer lymphocytes use granulysin, perforin and granzymes to kill intracellular parasites. Nature medicine *22*, 210-216.

Duarte, R.F., Chen, F.E., Lowdell, M.W., Potter, M.N., Lamana, M.L., Prentice, H.G., and Madrigal, J.A. (2002). Functional impairment of human T-lymphocytes following PHA-induced expansion and retroviral transduction. Implications for gene therapy. Gene therapy *9*, 1359-1368.

Dulos, J., Carven, G.J., van Boxtel, S.J., Evers, S., Driessen-Engels, L.J.A., Hobo, W., Gorecka, M.A., Haan, A.F.J. de, Mulders, P., and Punt, C.J.A., et al. (2012). PD-1 blockade augments Th1 and Th17 and suppresses Th2 responses in peripheral blood from patients with prostate and advanced melanoma cancer. Journal of immunotherapy (Hagerstown, Md. : 1997) *35*, 169-178.

Duraiswamy, J., Ibegbu, C.C., Masopust, D., Miller, J.D., Araki, K., Doho, G.H., Tata, P., Gupta, S., Zilliox, M.J., and Nakaya, H.I., et al. (2011). Phenotype, function, and gene expression profiles of programmed death-1(hi) CD8 T cells in healthy human adults. Journal of immunology (Baltimore, Md. : 1950) *186*, 4200-4212.

Ehrlich, P. (1906). Collected studies on immunity (John Wiley & Sons).

Esch, K.J., Juelsgaard, R., Martinez, P.A., Jones, D.E., and Petersen, C.A. (2013). Programmed death 1-mediated T cell exhaustion during visceral leishmaniasis impairs phagocyte function. Journal of immunology (Baltimore, Md. : 1950) *191*, 5542-5550.

Ettinger, N.A., and Wilson, M.E. (2008). Macrophage and T-cell gene expression in a model of early infection with the protozoan Leishmania chagasi. PLoS neglected tropical diseases *2*, e252.

Etzerodt, A., Maniecki, M.B., Møller, K., Møller, H.J., and Moestrup, S.K. (2010). Tumor necrosis factor α-converting enzyme (TACE/ADAM17) mediates ectodomain shedding of the scavenger receptor CD163. Journal of leukocyte biology *88*, 1201-1205.

Etzerodt, A., and Moestrup, S.K. (2013). CD163 and inflammation. Biological, diagnostic, and therapeutic aspects. Antioxidants & redox signaling *18*, 2352-2363.

European Medicines Agency (2017). http://www.ema.europa.eu/ema/.

Flies, D.B., and Chen, L. (2007). The new B7s. Playing a pivotal role in tumor immunity. Journal of immunotherapy (Hagerstown, Md. : 1997) *30*, 251-260.

Francisco, L.M., Sage, P.T., and Sharpe, A.H. (2010). The PD-1 pathway in tolerance and autoimmunity. Immunological reviews *236*, 219-242.

Francisco, L.M., Salinas, V.H., Brown, K.E., Vanguri, V.K., Freeman, G.J., Kuchroo, V.K., and Sharpe, A.H. (2009). PD-L1 regulates the development, maintenance, and function of induced regulatory T cells. The Journal of experimental medicine *206*, 3015-3029.

Freeman, G.J. (2008). Structures of PD-1 with its ligands. Sideways and dancing cheek to cheek. Proceedings of the National Academy of Sciences of the United States of America *105*, 10275-10276.

Freeman, G.J., Long, A.J., Iwai, Y., Bourque, K., Chernova, T., Nishimura, H., Fitz, L.J., Malenkovich, N., Okazaki, T., and Byrne, M.C., et al. (2000). Engagement of the PD-1 immunoinhibitory receptor by a novel B7 family member leads to negative regulation of lymphocyte activation. The Journal of experimental medicine *192*, 1027-1034.

Freeman, G.J., Wherry, E.J., Ahmed, R., and Sharpe, A.H. (2006). Reinvigorating exhausted HIV-specific T cells via PD-1-PD-1 ligand blockade. The Journal of experimental medicine *203*, 2223-2227.

Garbi, N., Hämmerling, G.J., Probst, H.-C., and van den Broek, M. (2010). Tonic T cell signalling and T cell tolerance as opposite effects of self-recognition on dendritic cells. Current opinion in immunology *22*, 601-608.

García-Hernández, R., Manzano, J.I., Castanys, S., and Gamarro, F. (2012). Leishmania donovani develops resistance to drug combinations. PLoS neglected tropical diseases *6*, e1974.

Gautam, S., Kumar, R., Singh, N., Singh, A.K., Rai, M., Sacks, D., Sundar, S., and Nylén, S. (2014). CD8 T cell exhaustion in human visceral leishmaniasis. The Journal of infectious diseases *209*, 290-299.

Ghiotto, M., Gauthier, L., Serriari, N., Pastor, S., Truneh, A., Nunès, J.A., and Olive, D. (2010). PD-L1 and PD-L2 differ in their molecular mechanisms of interaction with PD-1. International immunology *22*, 651-660.

Ghosh, M., Pal, C., Ray, M., Maitra, S., Mandal, L., and Bandyopadhyay, S. (2003). Dendritic cell-based immunotherapy combined with antimony-based chemotherapy cures established murine visceral leishmaniasis. Journal of immunology (Baltimore, Md. : 1950) *170*, 5625-5629.

Ginhoux, F., and Jung, S. (2014). Monocytes and macrophages. Developmental pathways and tissue homeostasis. Nature reviews. Immunology *14*, 392-404.

Glimcher, L.H., Townsend, M.J., Sullivan, B.M., and Lord, G.M. (2004). Recent developments in the transcriptional regulation of cytolytic effector cells. Nature reviews. Immunology *4*, 900-911.

Gogolak, P., Rethi, B., Szatmari, I., Lanyi, A., Dezso, B., Nagy, L., and Rajnavolgyi, E. (2007). Differentiation of CD1a- and CD1a+ monocyte-derived dendritic cells is biased by lipid environment and PPARgamma. Blood *109*, 643-652.

Grewal, I.S., and Flavell, R.A. (1998). CD40 and CD154 in cell-mediated immunity. Annual review of immunology *16*, 111-135.

Guilliams, M., Ginhoux, F., Jakubzick, C., Naik, S.H., Onai, N., Schraml, B.U., Segura, E., Tussiwand, R., and Yona, S. (2014). Dendritic cells, monocytes and macrophages. A unified nomenclature based on ontogeny. Nature reviews. Immunology *14*, 571-578.

Guleria, I., Khosroshahi, A., Ansari, M.J., Habicht, A., Azuma, M., Yagita, H., Noelle, R.J., Coyle, A., Mellor, A.L., and Khoury, S.J., et al. (2005). A critical role for the programmed death ligand 1 in fetomaternal tolerance. The Journal of experimental medicine *202*, 231-237.

Hefnawy, A., Berg, M., Dujardin, J.-C., and Muylder, G. de (2017). Exploiting Knowledge on Leishmania Drug Resistance to Support the Quest for New Drugs. Trends in parasitology *33*, 162-174.

Hernández-Ruiz, J., Salaiza-Suazo, N., Carrada, G., Escoto, S., Ruiz-Remigio, A., Rosenstein, Y., Zentella, A., and Becker, I. (2010). CD8 cells of patients with diffuse cutaneous leishmaniasis display functional exhaustion. The latter is reversed, in vitro, by TLR2 agonists. PLoS neglected tropical diseases *4*, e871.

Hodi, F.S., O'Day, S.J., McDermott, D.F., Weber, R.W., Sosman, J.A., Haanen, J.B., Gonzalez, R., Robert, C., Schadendorf, D., and Hassel, J.C., et al. (2010). Improved survival with ipilimumab in patients with metastatic melanoma. The New England journal of medicine *363*, 711-723.

Hoffmann, M., Pantazis, N., Martin, G.E., Hickling, S., Hurst, J., Meyerowitz, J., Willberg, C.B., Robinson, N., Brown, H., and Fisher, M., et al. (2016). Exhaustion of Activated CD8 T Cells Predicts Disease Progression in Primary HIV-1 Infection. PLoS pathogens *12*, e1005661.

Hua, L., Yao, S., Pham, D., Jiang, L., Wright, J., Sawant, D., Dent, A.L., Braciale, T.J., Kaplan, M.H., and Sun, J. (2013). Cytokine-dependent induction of CD4+ T cells with cytotoxic potential during influenza virus infection. Journal of virology *87*, 11884-11893.

Huber, M., Timms, E., Mak, T.W., Röllinghoff, M., and Lohoff, M. (1998). Effective and Long-Lasting Immunity against the Parasite Leishmania major in CD8-Deficient Mice. Infection and immunity *66*, 3968-3970.

Hubo, M., Trinschek, B., Kryczanowsky, F., Tuettenberg, A., Steinbrink, K., and Jonuleit, H. (2013). Costimulatory molecules on immunogenic versus tolerogenic human dendritic cells. Frontiers in immunology *4*, 82.

Hui, E., Cheung, J., Zhu, J., Su, X., Taylor, M.J., Wallweber, H.A., Sasmal, D.K., Huang, J., Kim, J.M., and Mellman, I., et al. (2017). T cell costimulatory receptor CD28 is a primary target for PD-1-mediated inhibition. Science (New York, N.Y.) *355*, 1428-1433.

Ishibashi, M., Tamura, H., Isoda, A., Matsumoto, M., Sasaki, M., Komatsu, N., Handa, H., Imai, Y., Tanaka, J., and Tanosaki, S., et al. (2015). Reverse signaling via B7-H1/PD-1 interaction and clinical characteristics of B7-H1 (PD-L1) expressed on multiple myeloma cells. Clinical Lymphoma Myeloma and Leukemia *15*, e214.

Ishida, Y., Agata, Y., Shibahara, K., and Honjo, T. (1992). Induced expression of PD-1, a novel member of the immunoglobulin gene superfamily, upon programmed cell death. The EMBO Journal *11*, 3887-3895.

Iwai, Y., Hamanishi, J., Chamoto, K., and Honjo, T. (2017). Cancer immunotherapies targeting the PD-1 signaling pathway. Journal of biomedical science *24*, 26.

Iwai, Y., Ishida, M., Tanaka, Y., Okazaki, T., Honjo, T., and Minato, N. (2002). Involvement of PD-L1 on tumor cells in the escape from host immune system and tumor immunotherapy by PD-L1 blockade. Proceedings of the National Academy of Sciences of the United States of America *99*, 12293-12297.

Iwai, Y., Terawaki, S., and Honjo, T. (2005). PD-1 blockade inhibits hematogenous spread of poorly immunogenic tumor cells by enhanced recruitment of effector T cells. International immunology *17*, 133-144.

Jensen, A.T.R., Kemp, K., Theander, T.G., and Handman, E. (2001). Cloning, expression and antigenicity of the L. donovani reductase. Apmis *109*, 461-468.

Joshi, T., Rodriguez, S., Perovic, V., Cockburn, I.A., and Stäger, S. (2009). B7-H1 blockade increases survival of dysfunctional CD8(+) T cells and confers protection against Leishmania donovani infections. PLoS pathogens *5*, e1000431.

Kadri, N., Korpos, E., Gupta, S., Briet, C., Löfbom, L., Yagita, H., Lehuen, A., Boitard, C., Holmberg, D., and Sorokin, L., et al. (2012). CD4(+) type II NKT cells mediate ICOS and programmed death-1-dependent regulation of type 1 diabetes. Journal of immunology (Baltimore, Md. : 1950) *188*, 3138-3149.

Kagamu, H., Yamaguchi, O., Shiono, A., Mouri, A., Miyauchi, S., Utsugi, H., Nishihara, F., Uchida, T., Murayama, Y., and Kobayashi, K. (2017). CD4+ T cells in PBMC to predict the outcome of anti-PD-1 therapy. Journal of Clinical Oncology *35*, 11525.

Kamanaka, M., Yu, P., Yasui, T., Yoshida, K., Kawabe, T., Horii, T., Kishimoto, T., and Kikutani, H. (1996). Protective Role of CD40 in Leishmania major Infection at Two Distinct Phases of Cell-Mediated Immunity. Immunity *4*, 275-281.

Kaye, P., and Scott, P. (2011). Leishmaniasis. Complexity at the host-pathogen interface. Nature reviews. Microbiology *9*, 604-615.

Keir, M.E., Butte, M.J., Freeman, G.J., and Sharpe, A.H. (2008). PD-1 and its ligands in tolerance and immunity. Annual review of immunology *26*, 677-704.

Kemp, M., Hansen, M.B., and Theander, T.G. (1992). Recognition of Leishmania antigens by T lymphocytes from nonexposed individuals. Infection and immunity *60*, 2246-2251.

Kinter, A.L., Godbout, E.J., McNally, J.P., Sereti, I., Roby, G.A., O'Shea, M.A., and Fauci, A.S. (2008). The common gamma-chain cytokines IL-2, IL-7, IL-15, and IL-21 induce the expression of programmed death-1 and its ligands. Journal of immunology (Baltimore, Md. : 1950) *181*, 6738-6746.

Köhler, G., and Milstein, C. (1975). Continuous cultures of fused cells secreting antibody of predefined specificity. Nature *256*, 495-497.

Konishi, J., Yamazaki, K., Azuma, M., Kinoshita, I., Dosaka-Akita, H., and Nishimura, M. (2004). B7-H1 expression on non-small cell lung cancer cells and its relationship with tumor-infiltrating lymphocytes and their PD-1 expression. Clinical cancer research : an official journal of the American Association for Cancer Research *10*, 5094-5100.

Kristjansdottir, H., Steinsson, K., Gunnarsson, I., Gröndal, G., Erlendsson, K., and Alarcón-Riquelme, M.E. (2010). Lower expression levels of the

programmed death 1 receptor on CD4+CD25+ T cells and correlation with the PD-1.3A genotype in patients with systemic lupus erythematosus. Arthritis and rheumatism *62*, 1702-1711.

Kubach, J., Becker, C., Schmitt, E., Steinbrink, K., Huter, E., Tuettenberg, A., and Jonuleit, H. (2005). Dendritic cells. Sentinels of immunity and tolerance. International journal of hematology *81*, 197-203.

Kuipers, H., Muskens, F., Willart, M., Hijdra, D., van Assema, F.B.J., Coyle, A.J., Hoogsteden, H.C., and Lambrecht, B.N. (2006). Contribution of the PD-1 ligands/PD-1 signaling pathway to dendritic cell-mediated CD4+ T cell activation. Eur. J. Immunol. *36*, 2472-2482.

Kumar, R., Chauhan, S.B., Ng, S.S., Sundar, S., and Engwerda, C.R. (2017). Immune Checkpoint Targets for Host-Directed Therapy to Prevent and Treat Leishmaniasis. Frontiers in immunology *8*, 1492.

Larsson, M., Shankar, E.M., Che, K.F., Saeidi, A., Ellegård, R., Barathan, M., Velu, V., and Kamarulzaman, A. (2013). Molecular signatures of T-cell inhibition in HIV-1 infection. Retrovirology *10*, 31.

Latchman, Y., Wood, C.R., Chernova, T., Chaudhary, D., Borde, M., Chernova, I., Iwai, Y., Long, A.J., Brown, J.A., and Nunes, R., et al. (2001). PD-L2 is a second ligand for PD-1 and inhibits T cell activation. Nature immunology *2*, 261-268.

Lázár-Molnár, E., Yan, Q., Cao, E., Ramagopal, U., Nathenson, S.G., and Almo, S.C. (2008). Crystal structure of the complex between programmed death-1 (PD-1) and its ligand PD-L2. Proceedings of the National Academy of Sciences of the United States of America *105*, 10483-10488.

Li, Y., Fang, M., Zhang, J., Wang, J., Song, Y., Shi, J., Li, W., Wu, G., Ren, J., and Wang, Z., et al. (2016). Hydrogel dual delivered celecoxib and anti-PD-1 synergistically improve antitumor immunity. Oncoimmunology *5*, e1074374.

Liang, S.C., Greenwald, R.J., Latchman, Y.E., Rosas, L., Satoskar, A., Freeman, G.J., and Sharpe, A.H. (2006). PD-L1 and PD-L2 have distinct roles in regulating host immunity to cutaneous leishmaniasis. Eur. J. Immunol. *36*, 58-64.

Liang, S.C., Latchman, Y.E., Buhlmann, J.E., Tomczak, M.F., Horwitz, B.H., Freeman, G.J., and Sharpe, A.H. (2003). Regulation of PD-1, PD-L1, and PD-L2 expression during normal and autoimmune responses. Eur. J. Immunol. *33*, 2706-2716.

Lindahl-Kiessling, K. (1972). Mechanism of phytohemagglutinin (PHA) action. V. PHA compared with concanavalin A (Con A). Experimental cell research *70*, 17-26.

Liu, D., and Uzonna, J.E. (2012). The early interaction of Leishmania with macrophages and dendritic cells and its influence on the host immune response. Frontiers in cellular and infection microbiology *2*, 83.

Livak, K.J., and Schmittgen, T.D. (2001). Analysis of relative gene expression data using real-time quantitative PCR and the 2(-Delta Delta C(T)) Method. Methods (San Diego, Calif.) *25*, 402-408.

Loke, P.'n., and Allison, J.P. (2003). PD-L1 and PD-L2 are differentially regulated by Th1 and Th2 cells. Proceedings of the National Academy of Sciences of the United States of America *100*, 5336-5341.

Mandell, G.L., and Douglas, R.G. Mandell, Douglas, and Bennett's principles and practice of infectious diseases (Philadelphia PA: Elsevier Saunders).

Mantovani, A., Sica, A., Sozzani, S., Allavena, P., Vecchi, A., and Locati, M. (2004). The chemokine system in diverse forms of macrophage activation and polarization. Trends in immunology *25*, 677-686.

Martínez Salazar, M.B., Delgado Domínguez, J., Silva Estrada, J., González Bonilla, C., and Becker, I. (2014). Vaccination with Leishmania mexicana LPG induces PD-1 in $CD8^+$ and PD-L2 in macrophages thereby suppressing the immune response. A model to assess vaccine efficacy. Vaccine *32*, 1259-1265.

McLaughlin, P., Grillo-López, A.J., Link, B.K., Levy, R., Czuczman, M.S., Williams, M.E., Heyman, M.R., Bence-Bruckler, I., White, C.A., and Cabanillas, F., et al. (1998). Rituximab chimeric anti-CD20 monoclonal antibody therapy for relapsed indolent lymphoma. Half of patients respond to a four-dose treatment program. Journal of clinical oncology : official journal of the American Society of Clinical Oncology *16*, 2825-2833.

Mino-Kenudson, M. (2016). Programmed cell death ligand-1 (PD-L1) expression by immunohistochemistry. Could it be predictive and/or prognostic in non-small cell lung cancer? Cancer biology & medicine *13*, 157-170.

Monge-Maillo, B., and López-Vélez, R. (2013a). Therapeutic options for old world cutaneous leishmaniasis and new world cutaneous and mucocutaneous leishmaniasis. Drugs *73*, 1889-1920.

Monge-Maillo, B., and López-Vélez, R. (2013b). Therapeutic options for visceral leishmaniasis. Drugs *73*, 1863-1888.

Mou, Z., Li, J., Boussoffara, T., Kishi, H., Hamana, H., Ezzati, P., Hu, C., Yi, W., Liu, D., and Khadem, F., et al. (2015). Identification of broadly conserved cross-species protective Leishmania antigen and its responding CD4+ T cells. Science translational medicine *7*, 310ra167.

Mou, Z., Muleme, H.M., Liu, D., Jia, P., Okwor, I.B., Kuriakose, S.M., Beverley, S.M., and Uzonna, J.E. (2013). Parasite-derived arginase influences secondary anti-Leishmania immunity by regulating programmed cell death-1-mediated CD4+ T cell exhaustion. Journal of immunology (Baltimore, Md. : 1950) *190*, 3380-3389.

Nadler, L.M., Stashenko, P., Hardy, R., Kaplan, W.D., Button, L.N., Kufe, D.W., Antman, K.H., and Schlossman, S.F. (1980). Serotherapy of a patient with a monoclonal antibody directed against a human lymphoma-associated antigen. Cancer research *40*, 3147-3154.

Nimmerjahn, F., Gordan, S., and Lux, A. (2015). FcγR dependent mechanisms of cytotoxic, agonistic, and neutralizing antibody activities. Trends in immunology *36*, 325-336.

Nimmerjahn, F., and Ravetch, J.V. (2008). Fcgamma receptors as regulators of immune responses. Nature reviews. Immunology *8*, 34-47.

Nishijima, T.F., Shachar, S.S., Nyrop, K.A., and Muss, H.B. (2017). Safety and Tolerability of PD-1/PD-L1 Inhibitors Compared with Chemotherapy in Patients with Advanced Cancer. A Meta-Analysis. The oncologist *22*, 470-479.

Nishimura, H., Agata, Y., Kawasaki, A., Sato, M., Imamura, S., Minato, N., Yagita, H., Nakano, T., and Honjo, T. (1996). Developmentally regulated

expression of the PD-1 protein on the surface of double-negative(CD4 – CD8 –) thymocytes. International immunology *8*, 773-780.

Nishimura, H., and Honjo, T. (2001). PD-1. An inhibitory immunoreceptor involved in peripheral tolerance. Trends in immunology *22*, 265-268.

Nishimura, H., Honjo, T., and Minato, N. (2000). Facilitation of β Selection and Modification of Positive Selection in the Thymus of Pd-1–Deficient Mice. The Journal of experimental medicine *191*, 891-898.

Nishimura, H., Nose, M., Hiai, H., Minato, N., and Honjo, T. (1999). Development of lupus-like autoimmune diseases by disruption of the PD-1 gene encoding an ITIM motif-carrying immunoreceptor. Immunity *11*, 141-151.

Novais, F.O., Nguyen, B.T., Beiting, D.P., Carvalho, L.P., Glennie, N.D., Passos, S., Carvalho, E.M., and Scott, P. (2014). Human classical monocytes control the intracellular stage of Leishmania braziliensis by reactive oxygen species. The Journal of infectious diseases *209*, 1288-1296.

Nylén, S., and Gautam, S. (2010). Immunological perspectives of leishmaniasis. Journal of global infectious diseases *2*, 135-146.

Ohradanova-Repic, A., Machacek, C., Fischer, M.B., and Stockinger, H. (2016). Differentiation of human monocytes and derived subsets of macrophages and dendritic cells by the HLDA10 monoclonal antibody panel. Clinical & translational immunology *5*, e55.

Okazaki, T., and Honjo, T. (2006). The PD-1-PD-L pathway in immunological tolerance. Trends in immunology *27*, 195-201.

Parish, C.R. (1999). Fluorescent dyes for lymphocyte migration and proliferation studies. Immunology and cell biology *77*, 499-508.

Park, J.-J., Omiya, R., Matsumura, Y., Sakoda, Y., Kuramasu, A., Augustine, M.M., Yao, S., Tsushima, F., Narazaki, H., and Anand, S., et al. (2010). B7-H1/CD80 interaction is required for the induction and maintenance of peripheral T-cell tolerance. Blood *116*, 1291-1298.

Parry, R.V., Chemnitz, J.M., Frauwirth, K.A., Lanfranco, A.R., Braunstein, I., Kobayashi, S.V., Linsley, P.S., Thompson, C.B., and Riley, J.L. (2005). CTLA-4

and PD-1 receptors inhibit T-cell activation by distinct mechanisms. Molecular and cellular biology *25*, 9543-9553.

Peligero, C., Argilaguet, J., Güerri-Fernandez, R., Torres, B., Ligero, C., Colomer, P., Plana, M., Knobel, H., García, F., and Meyerhans, A. (2015). PD-L1 Blockade Differentially Impacts Regulatory T Cells from HIV-Infected Individuals Depending on Plasma Viremia. PLoS pathogens *11*, e1005270.

Peng, T.-R., Tsai, F.-P., and Wu, T.-W. (2017). Indirect comparison between pembrolizumab and nivolumab for the treatment of non-small cell lung cancer. A meta-analysis of randomized clinical trials. International immunopharmacology *49*, 85-94.

Pillai, R.N., Behera, M., Owonikoko, T.K., Kamphorst, A.O., Pakkala, S., Belani, C.P., Khuri, F.R., Ahmed, R., and Ramalingam, S.S. (2017). Comparison of the toxicity profile of PD-1 versus PD-L1 inhibitors in non-small cell lung cancer. A systematic analysis of the literature. Cancer.

Pirmez, C., Yamamura, M., Uyemura, K., Paes-Oliveira, M., Conceição-Silva, F., and Modlin, R.L. (1993). Cytokine patterns in the pathogenesis of human leishmaniasis. The Journal of clinical investigation *91*, 1390-1395.

Pompeu, M.M., Brodskyn, C., Teixeira, M.J., Clarêncio, J., van Weyenberg, J., Coelho, I.C., Cardoso, S.A., Barral, A., and Barral-Netto, M. (2001). Differences in gamma interferon production in vitro predict the pace of the in vivo response to Leishmania amazonensis in healthy volunteers. Infection and immunity *69*, 7453-7460.

Pound, J.D., Challa, A., Holder, M.J., Armitage, R.J., Dower, S.K., Fanslow, W.C., Kikutani, H., Paulie, S., Gregory, C.D., and Gordon, J. (1999). Minimal cross-linking and epitope requirements for CD40-dependent suppression of apoptosis contrast with those for promotion of the cell cycle and homotypic adhesions in human B cells. International immunology *11*, 11-20.

Probst, H.C., McCoy, K., Okazaki, T., Honjo, T., and van den Broek, M. (2005). Resting dendritic cells induce peripheral CD8+ T cell tolerance through PD-1 and CTLA-4. Nature immunology *6*, 280-286.

Radziewicz, H., Ibegbu, C.C., Fernandez, M.L., Workowski, K.A., Obideen, K., Wehbi, M., Hanson, H.L., Steinberg, J.P., Masopust, D., and Wherry, E.J., et al.

(2007). Liver-infiltrating lymphocytes in chronic human hepatitis C virus infection display an exhausted phenotype with high levels of PD-1 and low levels of CD127 expression. Journal of virology *81*, 2545-2553.

Ramos-Esquivel, A., van der Laat, A., Rojas-Vigott, R., Juárez, M., and Corrales-Rodríguez, L. (2017). Anti-PD-1/anti-PD-L1 immunotherapy versus docetaxel for previously treated advanced non-small cell lung cancer. A systematic review and meta-analysis of randomised clinical trials. ESMO open *2*, e000236.

Rao, M., Valentini, D., Dodoo, E., Zumla, A., and Maeurer, M. (2017). Anti-PD-1/PD-L1 therapy for infectious diseases. Learning from the cancer paradigm. International journal of infectious diseases : IJID : official publication of the International Society for Infectious Diseases *56*, 221-228.

Reed, J.M., Branigan, P.J., and Bamezai, A. (2008). Interferon gamma enhances clonal expansion and survival of CD4+ T cells. Journal of interferon & cytokine research : the official journal of the International Society for Interferon and Cytokine Research *28*, 611-622.

Ribas, A. (2012). Tumor immunotherapy directed at PD-1. The New England journal of medicine *366*, 2517-2519.

Riley, J.L. (2009). PD-1 signaling in primary T cells. Immunological reviews *229*, 114-125.

Ritz, J., and Schlossman, S.F. (1982). Utilization of monoclonal antibodies in the treatment of leukemia and lymphoma. Blood *59*, 1-11.

Rodig, N., Ryan, T., Allen, J.A., Pang, H., Grabie, N., Chernova, T., Greenfield, E.A., Liang, S.C., Sharpe, A.H., and Lichtman, A.H., et al. (2003). Endothelial expression of PD-L1 and PD-L2 down-regulates CD8+ T cell activation and cytolysis. Eur. J. Immunol. *33*, 3117-3126.

Rodrigues, V., Cordeiro-da-Silva, A., Laforge, M., Ouaissi, A., Akharid, K., Silvestre, R., and Estaquier, J. (2014). Impairment of T cell function in parasitic infections. PLoS neglected tropical diseases *8*, e2567.

Rodríguez-García, M., Porichis, F., Jong, O.G. de, Levi, K., Diefenbach, T.J., Lifson, J.D., Freeman, G.J., Walker, B.D., Kaufmann, D.E., and Kavanagh, D.G. (2011). Expression of PD-L1 and PD-L2 on human macrophages is up-

regulated by HIV-1 and differentially modulated by IL-10. Journal of leukocyte biology *89*, 507-515.

Rogers, K.A., and Titus, R.G. (2004). Characterization of the early cellular immune response to Leishmania major using peripheral blood mononuclear cells from Leishmania-naive humans. The American journal of tropical medicine and hygiene *71*, 568-576.

Römer, P.S., Berr, S., Avota, E., Na, S.-Y., Battaglia, M., Berge, I. ten, Einsele, H., and Hünig, T. (2011). Preculture of PBMCs at high cell density increases sensitivity of T-cell responses, revealing cytokine release by CD28 superagonist TGN1412. Blood *118*, 6772-6782.

Russo, D.M., Chakrabarti, P., and Burns, J.M. (1998). Naive human T cells develop into Th1 or Th0 effectors and exhibit cytotoxicity early after stimulation with Leishmania-infected macrophages. The Journal of infectious diseases *177*, 1345-1351.

Sable, S.B. (2013). Programmed death 1 lives up to its reputation in active tuberculosis. The Journal of infectious diseases *208*, 541-543.

Sacks, D., and Noben-Trauth, N. (2002). The immunology of susceptibility and resistance to Leishmania major in mice. Nature reviews. Immunology *2*, 845-858.

Sacks, D.L., and Perkins, P.V. (1984). Identification of an infective stage of Leishmania promastigotes. Science (New York, N.Y.) *223*, 1417-1419.

Sallusto, F. (1994). Efficient presentation of soluble antigen by cultured human dendritic cells is maintained by granulocyte/macrophage colony-stimulating factor plus interleukin 4 and downregulated by tumor necrosis factor alpha. The Journal of experimental medicine *179*, 1109-1118.

Sassi, A., Largueche-Darwaz, B., Collette, A., Six, A., Laouini, D., Cazenave, P.A., and Dellagi, K. (2005). Mechanisms of the Natural Reactivity of Lymphocytes from Noninfected Individuals to Membrane-Associated Leishmania infantum Antigens. The Journal of Immunology *174*, 3598-3607.

Schneemann, M., Schoedon, G., Hofer, S., Blau, N., Guerrero, L., and Schaffner, A. (1993). Nitric oxide synthase is not a constituent of the

antimicrobial armature of human mononuclear phagocytes. The Journal of infectious diseases *167*, 1358-1363.

Scorza, B.M., Carvalho, E.M., and Wilson, M.E. (2017). Cutaneous Manifestations of Human and Murine Leishmaniasis. International journal of molecular sciences *18*.

Serbina, N.V., Salazar-Mather, T.P., Biron, C.A., Kuziel, W.A., and Pamer, E.G. (2003). TNF/iNOS-Producing Dendritic Cells Mediate Innate Immune Defense against Bacterial Infection. Immunity *19*, 59-70.

Sha, S., Agarabi, C., Brorson, K., Lee, D.-Y., and Yoon, S. (2016). N-Glycosylation Design and Control of Therapeutic Monoclonal Antibodies. Trends in biotechnology *34*, 835-846.

Sharpe, A.H., Wherry, E.J., Ahmed, R., and Freeman, G.J. (2007). The function of programmed cell death 1 and its ligands in regulating autoimmunity and infection. Nature immunology *8*, 239-245.

Shen, L., Gao, Y., Liu, Y., Zhang, B., Liu, Q., Wu, J., Fan, L., Ou, Q., Zhang, W., and Shao, L. (2016). PD-1/PD-L pathway inhibits M.tb-specific CD4(+) T-cell functions and phagocytosis of macrophages in active tuberculosis. Scientific reports *6*, 38362.

Singh, O.P., and Sundar, S. (2014). Immunotherapy and targeted therapies in treatment of visceral leishmaniasis. Current status and future prospects. Frontiers in immunology *5*, 296.

Spec, A., Shindo, Y., Burnham, C.-A.D., Wilson, S., Ablordeppey, E.A., Beiter, E.R., Chang, K., Drewry, A.M., and Hotchkiss, R.S. (2016). T cells from patients with Candida sepsis display a suppressive immunophenotype. Critical care (London, England) *20*, 15.

Speiser, D.E. (2012). A molecular profile of T-cell exhaustion in cancer. Oncoimmunology *1*, 369-371.

Stäger, S., and Rafati, S. (2012). CD8(+) T cells in leishmania infections. Friends or foes? Frontiers in immunology *3*, 5.

Stebut, E. von, and Tenzer, S. (2017). Cutaneous leishmaniasis. Distinct functions of dendritic cells and macrophages in the interaction of the host

immune system with Leishmania major. International journal of medical microbiology : IJMM.

Stechmiller, J.K., Childress, B., and Cowan, L. (2005). Arginine supplementation and wound healing. Nutrition in clinical practice : official publication of the American Society for Parenteral and Enteral Nutrition *20*, 52-61.

Steverding, D. (2017). The history of leishmaniasis. Parasites & vectors *10*, 82.

Stout, R.D., Jiang, C., Matta, B., Tietzel, I., Watkins, S.K., and Suttles, J. (2005). Macrophages sequentially change their functional phenotype in response to changes in microenvironmental influences. The Journal of Immunology *175*, 342-349.

Subudhi, S.K., Zhou, P., Yerian, L.M., Chin, R.K., Lo, J.C., Anders, R.A., Sun, Y., Chen, L., Wang, Y., and Alegre, M.-L., et al. (2004). Local expression of B7-H1 promotes organ-specific autoimmunity and transplant rejection. The Journal of clinical investigation *113*, 694-700.

Suntharalingam, G., Perry, M.R., Ward, S., Brett, S.J., Castello-Cortes, A., Brunner, M.D., and Panoskaltsis, N. (2006). Cytokine storm in a phase 1 trial of the anti-CD28 monoclonal antibody TGN1412. The New England journal of medicine *355*, 1018-1028.

Topalian, S.L., Hodi, F.S., Brahmer, J.R., Gettinger, S.N., Smith, D.C., McDermott, D.F., Powderly, J.D., Carvajal, R.D., Sosman, J.A., and Atkins, M.B., et al. (2012). Safety, activity, and immune correlates of anti-PD-1 antibody in cancer. The New England journal of medicine *366*, 2443-2454.

Tripathi, P., Singh, V., and Naik, S. (2007). Immune response to leishmania. Paradox rather than paradigm. FEMS immunology and medical microbiology *51*, 229-242.

U.S. Food & Drug Administration (2017). https://www.fda.gov/Drugs/InformationOnDrugs/ApprovedDrugs/ucm279174.htm.

van Griensven, J., Gadisa, E., Aseffa, A., Hailu, A., Beshah, A.M., and Diro, E. (2016). Treatment of Cutaneous Leishmaniasis Caused by Leishmania

aethiopica. A Systematic Review. PLoS neglected tropical diseases *10*, e0004495.

van Kooten, C., and Banchereau, J. (2000). CD40-CD40 ligand. Journal of leukocyte biology *67*, 2-17.

van Zandbergen, G., Bollinger, A., Wenzel, A., Kamhawi, S., Voll, R., Klinger, M., Müller, A., Hölscher, C., Herrmann, M., and Sacks, D., et al. (2006). Leishmania disease development depends on the presence of apoptotic promastigotes in the virulent inoculum. Proceedings of the National Academy of Sciences of the United States of America *103*, 13837-13842.

van Zandbergen, G., Klinger, M., Mueller, A., Dannenberg, S., Gebert, A., Solbach, W., and Laskay, T. (2004). Cutting Edge. Neutrophil Granulocyte Serves as a Vector for Leishmania Entry into Macrophages. The Journal of Immunology *173*, 6521-6525.

Varol, C., Mildner, A., and Jung, S. (2015). Macrophages. Development and tissue specialization. Annual review of immunology *33*, 643-675.

Veras, E., Kurman, R.J., Wang, T.-L., and Shih, I.-M. (2017). PD-L1 Expression in Human Placentas and Gestational Trophoblastic Diseases. International journal of gynecological pathology : official journal of the International Society of Gynecological Pathologists *36*, 146-153.

Verreck, F.A.W., Boer, T. de, Langenberg, D.M.L., Hoeve, M.A., Kramer, M., Vaisberg, E., Kastelein, R., Kolk, A., Waal-Malefyt, R. de, and Ottenhoff, T.H.M. (2004). Human IL-23-producing type 1 macrophages promote but IL-10-producing type 2 macrophages subvert immunity to (myco)bacteria. Proceedings of the National Academy of Sciences of the United States of America *101*, 4560-4565.

Vidarsson, G., Dekkers, G., and Rispens, T. (2014). IgG subclasses and allotypes. From structure to effector functions. Frontiers in immunology *5*, 520.

Vries, J.E. de and Waal Malefyt, R. de (1995). Interleukin-10 (Berlin, Heidelberg: Springer Berlin Heidelberg).

Walker, L.S.K., and Abbas, A.K. (2002). The enemy within. Keeping self-reactive T cells at bay in the periphery. Nature reviews. Immunology *2*, 11-19.

Wang, C., Thudium, K.B., Han, M., Wang, X.-T., Huang, H., Feingersh, D., Garcia, C., Wu, Y., Kuhne, M., and Srinivasan, M., et al. (2014). In vitro characterization of the anti-PD-1 antibody nivolumab, BMS-936558, and in vivo toxicology in non-human primates. Cancer immunology research *2*, 846-856.

Wang, C.-J., Chou, F.-C., Chu, C.-H., Wu, J.-C., Lin, S.-H., Chang, D.-M., and Sytwu, H.-K. (2008). Protective role of programmed death 1 ligand 1 (PD-L1)in nonobese diabetic mice. The paradox in transgenic models. Diabetes *57*, 1861-1869.

Wang, W., Lau, R., Yu, D., Zhu, W., Korman, A., and Weber, J. (2009). PD1 blockade reverses the suppression of melanoma antigen-specific CTL by CD4+ CD25(Hi) regulatory T cells. International immunology *21*, 1065-1077.

Wang, Z.E., Reiner, S.L., Hatam, F., Heinzel, F.P., Bouvier, J., Turck, C.W., and Locksley, R.M. (1993). Targeted activation of CD8 cells and infection of beta 2-microglobulin-deficient mice fail to confirm a primary protective role for CD8 cells in experimental leishmaniasis. Journal of immunology (Baltimore, Md. : 1950) *151*, 2077-2086.

Webster, R.M. (2014). The immune checkpoint inhibitors. Where are we now? Nature reviews. Drug discovery *13*, 883-884.

Wei, F., Zhong, S., Ma, Z., Kong, H., Medvec, A., Ahmed, R., Freeman, G.J., Krogsgaard, M., and Riley, J.L. (2013). Strength of PD-1 signaling differentially affects T-cell effector functions. Proceedings of the National Academy of Sciences of the United States of America *110*, E2480-9.

Wherry, E.J. (2011). T cell exhaustion. Nature immunology *12*, 492-499.

Wherry, E.J., Ha, S.-J., Kaech, S.M., Haining, W.N., Sarkar, S., Kalia, V., Subramaniam, S., Blattman, J.N., Barber, D.L., and Ahmed, R. (2007). Molecular signature of CD8+ T cell exhaustion during chronic viral infection. Immunity *27*, 670-684.

Wherry, E.J., and Kurachi, M. (2015). Molecular and cellular insights into T cell exhaustion. Nature reviews. Immunology *15*, 486-499.

World Health Organization (2017). Leishmaniasis Fact Sheet. http://www.who.int/mediacentre/factsheets/fs375/en/. 21.07.2017.

Xiao, Y., Yu, S., Zhu, B., Bedoret, D., Bu, X., Francisco, L.M., Hua, P., Duke-Cohan, J.S., Umetsu, D.T., and Sharpe, A.H., et al. (2014). RGMb is a novel binding partner for PD-L2 and its engagement with PD-L2 promotes respiratory tolerance. The Journal of experimental medicine *211*, 943-959.

Yamazaki, T., Akiba, H., Iwai, H., Matsuda, H., Aoki, M., Tanno, Y., Shin, T., Tsuchiya, H., Pardoll, D.M., and Okumura, K., et al. (2002). Expression of Programmed Death 1 Ligands by Murine T Cells and APC. The Journal of Immunology *169*, 5538-5545.

Ye, B., Liu, X., Li, X., Kong, H., Tian, L., and Chen, Y. (2015). T-cell exhaustion in chronic hepatitis B infection. Current knowledge and clinical significance. Cell death & disease *6*, e1694.

Youngnak, P., Kozono, Y., Kozono, H., Iwai, H., Otsuki, N., Jin, H., Omura, K., Yagita, H., Pardoll, D.M., and Chen, L., et al. (2003). Differential binding properties of B7-H1 and B7-DC to programmed death-1. Biochemical and biophysical research communications *307*, 672-677.

Zamani, M.R., Aslani, S., Salmaninejad, A., Javan, M.R., and Rezaei, N. (2016). PD-1/PD-L and autoimmunity. A growing relationship. Cellular immunology *310*, 27-41.

Zelenay, S., van der Veen, A.G., Böttcher, J.P., Snelgrove, K.J., Rogers, N., Acton, S.E., Chakravarty, P., Girotti, M.R., Marais, R., and Quezada, S.A., et al. (2015). Cyclooxygenase-Dependent Tumor Growth through Evasion of Immunity. Cell *162*, 1257-1270.

7 Acronyms and Abbreviations

°C	Degree Celsius
A/I	Activation/Inhibition
ADCC	Antibody-dependent cell-mediated cytotoxicity
ADCL	Anergic diffuse cutaneous leishmaniasis
ADCP	Antibody-dependent cellular phagocytosis
µl	Microliter
µM	Micromolar
µm	Micrometer
APC	Antigen presenting cell
BH4	Tetrahydrobiopterin
BSA	Bovine serum albumin
CD	Cluster of differentiation
CDC	Complement dependent cytolysis
cDNA	Complementary DNA
CFSE	5(6)-Carboxyfluorescein diacetate N-succinimidyl ester
CL	Cutaneous leishmaniasis
cm	Centimeter
CT	Cycle threshold
CTL	Cytotoxic potential
CTLA-4	Cytotoxic T-lymphocyte-associated protein 4
d	Day/s
DCL	Diffuse cutaneous leishmaniasis
DL	Disseminated leishmaniasis
DMSO	Dimethylsulfoxid
DNA	Deoxyribonucleic acid
dNTP	Deoxy-nucleotide tri-phosphate
DTH	Delayed-type Hypersensitivity
EDTA	Ethylene-diamine-tetraacetic acid
ELISA	Enzyme-linked Immunosorbent Assay
EMA	European Medicines Agency
EpCAM	Epithelial cell adhesion molecule
Fab	Fragment antigen binding
FAS	First apoptosis signal

FAS-L	First apoptosis signal ligand
FACS	Fluorescence activated cell sorting
Fc	Fragment crystallizable
FcγR	Fc-gamma receptor
FCS	Fetal Calf Serum
FDA	U. S. Food and Drug Administration
FOXP3	Forkhead-Box-Protein P3
FSC	Forward scatter
g	Gramm
g	Gravitational force
GAPDH	Glycerinaldehyd-3-phosphat-Dehydrogenase
GITR	Glucocorticoid-induced TNFR-related protein
GM-CSF	Granulocyte macrophage colony-stimulating factor
GMP	Good Manufacturing Practice
GNLY	Granulysin
GZMA	Granzyme A
GZMB	Granzyme B
h	Hour/s
HBV	Hepatitis B virus
HCV	Hepatitis C virus
HD	High density
HEPES	4-(2-hydroxyethyl)-1-piperazineethanesulfonic acid
HER-2	human epidermal growth factor receptor 2
HIV	Human immunodeficiency virus
HLA-DR	Human Leukocyte Antigen – antigen D Related
hMDM	Human monocyte-derived macrophage
hMDM1 (M1)	Pro-inflammatory human monocyte-derived macrophage
hMDM2 (M2)	Anti-inflammatory human monocyte-derived macrophage
hMDDC (DC/s)	Human monocyte-derived dendritic cell/s
IFN-γ	Interferon γ
IC	Immune complex
IDO	Indolamin-2,3-Dioxygenase
IgG	Immunoglobulin G
IL	Interleukin

IL-1R	Interleukin-1 receptor
ITSM	Immunoreceptor Tyrosine-Based Switch Motif
ITIM	Immunoreceptor Tyrosine-Based Inhibitory Motif
kDa	Kilo Dalton
KLH	Keyhole limpet haemocyanin
KIR	Killer cell immunoglobulin-like receptors
L.	*Leishmania*
Lae	*Leishmania aethiopica*
LAG-3	Lymphocyte-activation gene 3
LCL	Localized cutaneous leishmaniasis
LCMV	Lymphocytic choriomeningitis virus
LD	Low density
LEAF	Low Endotoxin Azide-Free
Lm	*Leishmania major*
LPS	Lipopolysaccharide
LPG	Lipophosphoglycan
LSM	Leucocyte separation medium 1077
mAb/s	Monoclonal antibody/antibodies
MACS	Magnetic activated cell sorting
MCL	Mucocutaneous leishmaniasis
M-CSF	Macrophage colony-stimulating factor
MFs (MΦ)	Macrophage/s
MFI	Mean fluorescence intensity
MHC	Major histocompatibility complex
min	Minute/s
ml	Milliliter
mM	Millimolar
mm	Millimeter
MOI	Multiplicity of infection
ng	Nanogramm
NK	Natural killer
NO	Nitric oxide
NSCLC	Non-small-cell lung carcinoma
OVA	Ovalbumin

OX40	Tumor necrosis factor receptor superfamily, member 4
p.i.	Post infection
PBLs	Peripheral Blood Lymphocytes
$PBLs^{PHA}$	PHA-pre-stimulated PBLs
PBMC/s	Peripheral Blood Mononuclear Cell/s
PBS	Phosphate buffered saline
PD-1	Programmed-Death 1
PD-L1 (B7H1)	Programmed-Death 1 ligand 1 (B7 homolog 1)
PD-L2 (B7DC)	Programmed-Death 1 ligand 2
PFA	Paraformaldehyde
pg	Picogramm
PHA	Phytohemagglutinin
PI3K	Phosphatidylinositol 3 kinase
PI3P	Phosphatidylinositol-3-phosphate
PKCθ	Protein kinase C theta
PKDL	Post Kala-Azar dermal leishmaniasis
PMN	Polymorphonuclear neutrophil granulocytes
PPD	Mycobacterial purified protein derivate
PRF1	Perforin
qRT-PCR	Quantitative Real-Time Polymerase Chain Reaction
RESTORE	RESetting T cells to Original REactivity
RFI	Relative fluorescence intensity
RGMb	Repulsive guidance molecule B
RNA	Ribonucleic Acid
ROS	Reactive oxygen species
RT	Room temperature (22°C)
RUNX1	Runt-related transcription factor 1
SD	Standard deviation
sec	Second/s
SHP2	Src Homology Phosphatase 2
SNP	Single Nucleotide Polymorphism
SSC	Side scatter
TAE	Tris-acetate-EDTA
Tbet	T-box transcription factor TBX21

TCR	T cell receptor
T_H	T-helper
TIM-3	T-cell immunoglobulin and mucin-domain containing-3
TLR	Toll-like receptor
TNF-α	Tumor necrosis factor α
Treg	Regulatory T-cells
Tris	Tris(hydroxylmethyl)-aminomethan
V	Volt
v/v	Volume per volume
VL	Visceral leishmaniasis
w/v	Weight per volume
WHO	World health organization
WT	Wildtype
x	Times
ZAP70	Zeta-chain-associated protein kinase 70

8 Figures list

9 Table list

10 Declaration of authorship

I hereby certify that I have written the present dissertation with the topic

PD-1 checkpoint inhibition in *Leishmania* infection of primary human cells

independently, using no other aids then those I have cited. I have clearly mentioned the source of the passages that are taken word for word or paraphrased from other works.

The presented thesis has not been submitted in this or any other form to another faculty or examination institution.

Eidesstattliche Versicherung

Hiermit versichere ich, dass ich die vorgelegte Dissertation mit dem Titel

PD-1 checkpoint inhibition in *Leishmania* infection of primary human cells

selbstständig verfasst habe und keine anderen als die angegebenen Quellen und Hilfsmittel verwendet habe. Die Stellen der Dissertation, die anderen Werken und Veröffentlichungen dem Wortlaut oder dem Sinn nach entnommen wurden, sind durch Quellenangaben gekennzeichnet.

Diese Dissertation wurde in der jetzigen oder in ähnlicher Form noch an keiner anderen Hochschule eingereicht und hat noch keinen sonstigen Prüfungszwecken gedient.

Langen, 31.01.2018

Christodoulos Filippis

11 Acknowledgements

12 Curriculum vitae